THERMO-HYDRO-MECHANICAL COUPLED MODELING:

MULTIPLE FRACTURE MODEL, BMT2
COUPLED STRESS-FLOW MODEL, TC1

DECOVALEX – PHASE 1

Prepared for

Nuclear Regulatory Commission
Contract NRC-02-88-005

Prepared by

Center for Nuclear Waste Regulatory Analyses
San Antonio, Texas

April 1992

9312060009 920430
PDR WASTE
WM-11 PDR

CNWRA 92-005

THERMO-HYDRO-MECHANICAL COUPLED MODELING:

MULTIPLE FRACTURE MODEL, BMT2
COUPLED STRESS-FLOW MODEL, TC1

DECOVALEX - PHASE 1

Prepared for

Nuclear Regulatory Commission
Contract NRC-02-88-005

Prepared by

Mikko P. Ahola
Sui-Min (Simon) Hsiung
Loren J. Lorig
Asadul H. Chowdhury

Center for Nuclear Waste Regulatory Analyses
San Antonio, Texas

April 1992

010008

TABLE OF CONTENTS

LIST OF FIGURES iv
LIST OF TABLES vi
ACKNOWLEDGMENTS viii

1 INTRODUCTION 1
1.1 DECOVALEX ORGANIZATION 1
1.2 DECOVALEX PROBLEMS: PHASE I 2
1.3 COMPUTER PROGRAMS FOR THM PROCESSES 4

2 BRIEF MATHEMATICAL BACKGROUND TO THE CODE . . 5
2.1 ROCK JOINT REPRESENTATION 8
2.2 ROCK JOINT BEHAVIOR 9
2.3 BLOCK DEFORMABILITY 13
2.4 HYDROMECHANICAL COUPLING 13
2.5 THERMOMECHANICAL COUPLING 15
2.6 PERFORMING COUPLED ANALYSES 17

3 CODE DESCRIPTION 20

4 COMMENTS ON THE GIVEN SPECIFICATIONS OF BMT AND TC PROBLEMS 22
4.1 MULTIPLE FRACTURE MODEL, BMT2 22
4.2 COUPLED STRESS-FLOW MODEL, TC1 22

5 COMPUTER HARDWARE AND TIME 26

6 RESULTS 27
6.1 MULTIPLE FRACTURE MODEL, BMT2 27
6.2 COUPLED STRESS-FLOW MODEL, TC1 33

7 DISCUSSION OF THE RESULTS 48
7.1 MULTIPLE FRACTURE MODEL, BMT2 48
7.2 COUPLED STRESS-FLOW MODEL, TC1 51

8 RECOMMENDATIONS 53
8.1 MULTIPLE FRACTURE MODEL, BMT2 53
8.2 COUPLED STRESS-FLOW MODEL, TC1 53

9 REFERENCES 55

TABLE OF CONTENTS (Cont'd)

APPENDIX A: TABULAR OUTPUT FROM UDEC FOR THE BMT2 AND TC1 PROBLEMS A-1

APPENDIX B: UDEC INPUT FILES FOR THE BMT2 AND TC1 PROBLEMS B-1

LIST OF TABLES

Table	Title	Page
A.1.1	TEMPERATURE AT MONITORING POINTS 1-41 FOR BMT2	A-1
A.1.2	NORMAL STRESSES AT ROCK BLOCK CENTERS FOR BMT2	A-3
A.1.3	HYDRAULIC HEAD AT MONITORING POINTS 1-41 FOR BMT2	A-4
A.1.4	FLUID VELOCITY AT MONITORING POINTS 42-48 FOR BMT2	A-6
A.1.5	FLUID VELOCITY AT MONITORING POINTS 49-55 FOR BMT2	A-7
A.1.6	DISPLACEMENT COMPONENTS AT MONITORING POINTS 1-41 FOR BMT2	A-8
A.2.1	UDEC RESULTS FOR NORMAL LOADING INCREMENT #1 CORRESPONDING TO A NORMAL STRESS OF 5.0 MPa FOR TC1	A-14
A.2.2	UDEC RESULTS FOR NORMAL LOADING INCREMENT #2 CORRESPONDING TO A NORMAL STRESS OF 15.0 MPa FOR TC1	A-15
A.2.3	UDEC RESULTS FOR NORMAL LOADING INCREMENT #3 CORRESPONDING TO A NORMAL STRESS OF 25.0 MPA FOR TC1	A-16
A.2.4	UDEC RESULTS FOR NORMAL UNLOADING INCREMENT #4 CORRESPONDING TO A NORMAL STRESS OF 15.0 MPa FOR TC1	A-17
A.2.5	UDEC RESULTS FOR NORMAL UNLOADING INCREMENT #5 CORRESPONDING TO A NORMAL STRESS OF 5.0 MPa FOR TC1	A-18
A.2.6	UDEC RESULTS FOR NORMAL UNLOADING INCREMENT #6 CORRESPONDING TO A NORMAL STRESS OF 0.0 MPa FOR TC1	A-19
A.2.7	UDEC RESULTS FOR SHEAR LOADING INCREMENT #1 CORRESPONDING TO A JOINT SHEAR DISPLACEMENT OF 0.5 MM IN THE FORWARD DIRECTION FOR TC1	A-20
A.2.8	UDEC RESULTS FOR SHEAR LOADING INCREMENT #2 CORRESPONDING TO A JOINT SHEAR DISPLACEMENT OF 0.8 MM IN THE FORWARD DIRECTION FOR TC1	A-21

LIST OF TABLES (Cont'd)

Table	Title	Page
A.2.9	UDEC RESULTS FOR SHEAR LOADING INCREMENT #3 CORRESPONDING TO A JOINT SHEAR DISPLACEMENT OF 2.0 MM IN THE FORWARD DIRECTION FOR TC1	A-22
A.2.10	UDEC RESULTS FOR SHEAR LOADING INCREMENT #4 CORRESPONDING TO A JOINT SHEAR DISPLACEMENT OF 4.0 MM IN THE FORWARD DIRECTION FOR TC1	A-23
A.2.11	UDEC RESULTS FOR SHEAR LOADING INCREMENT #5 CORRESPONDING TO A JOINT SHEAR DISPLACEMENT OF 2.0 MM IN THE REVERSE DIRECTION FOR TC1	A-24
A.2.12	UDEC RESULTS FOR SHEAR LOADING INCREMENT #6 CORRESPONDING TO A JOINT SHEAR DISPLACEMENT IN THE REVERSE DIRECTION BACK TO THE INITIAL STARTING LOCATION FOR TC1	A-25

ACKNOWLEDGEMENTS

The authors would like to thank Randall D. Manteufel and Wesley C. Patrick for their technical reviews of this document. In addition, the authors would like to thank Jacob Philip of the Nuclear Regulatory Commission (NRC) for his contribution in initial meetings on the discussions of the bench-mark and test case problems for the DEvelopment of COupled models and their VALidation against EXperiments in nuclear waste isolation (DECOVALEX) Phase I modeling studies and for providing coordination between the Center for Nuclear Waste Regulatory Analyses (CNWRA) research team and the DECOVALEX Secretariat. The authors are also thankful to Ms. Pam Smith for skillful typing of the report and to Ms. Cathy Garcia for help in organizing the figures.

This report was prepared to document work performed by the Center for Nuclear Waste Regulatory Analyses (CNWRA) for the NRC under Contract No. NRC-02-88-005. The activities reported here were performed on behalf of the NRC Office of Nuclear Regulatory Research, Division of Regulatory Applications. The report is an independent product of the CNWRA and does not necessarily reflect the views or regulatory position of the NRC.

1 INTRODUCTION

Despite the similarity between an underground mine and a mined geologic repository system, some substantial differences exist in the analysis and design practice of underground openings of these two types of facilities. This is because the considerations for repository design such as the nature of repository environment, the performance objectives, the time scale required for effective waste isolation, and the legal and regulatory environment in which waste isolation is to be engineered and managed are different from the underground mine design considerations.

The response of the rock mass in a high-level nuclear waste geologic repository is a coupled phenomenon involving thermal (T), hydrological (H), mechanical (M), and chemical (C) processes. This implies that one process affects the initiation and progress of another and, therefore, the rock mass response in a repository environment cannot be predicted by considering each process independently (Tsang, 1991). Therefore, it is necessary to take into account thermally induced mechanical, hydrological, and chemical phenomena and the couplings among them that may occur within the fractured host rock and surrounding strata. The importance of various couplings will depend upon the thermal loading of the repository, the design of the engineered barriers, properties of the geologic medium, and the scale at which these phenomena are of interest. It is necessary to develop appropriate conceptual models and computer codes describing the coupled phenomena.

The capability of modeling coupled thermal-hydrological-mechanical-chemical (THMC) processes is at a very early stage of development in comparison with geosphere transport modeling. Considerable work is needed before codes can be developed that are capable of modeling coupled THMC processes (Noorishad et al., 1984; Tsang, 1991; Mangold et al., 1991). Another problem is the lack of applicable test cases for validation purposes.

1.1 DECOVALEX ORGANIZATION

To increase understanding of three processes, thermo-hydro-mechanical (THM), for rock mass stability and radionuclide release and transport from a repository to the biosphere and how they can be described by mathematical models, the Swedish Nuclear Power Inspectorate (SKI) has organized an international cooperative project for the DECOVALEX. DECOVALEX is being structured and conducted similar to the INTRACOIN, HYDROCOIN, and INTRAVAL cooperatives that have previously been undertaken by SKI to better understand the various analytical and numerical methods being used to describe groundwater flow and transport of radioactive nuclides. In the DECOVALEX project, modeling will be used to develop and design validation tests of THM coupled processes. DECOVALEX is expected to lead to development and validation of coupled THM models which are believed to be critical to the licensing of a high-level nuclear waste repository.

At the time of this writing, nine organizations have joined DECOVALEX as Funding Organizations. They are: NRC (USA), Agence Nationale Pour la Gestion des Dechets Radioactifs (ANDRA) (France), Atomic Energy of Canada Ltd (AECL) (Canada), Commission

of Atomic Energy/Institute of Nuclear Protection and Safety (CEA/IPSN) (France), NIREX Ltd. (NIREX) (UK), Power Reactor and Nuclear Fuel Development Corp. (PNC) (Japan), SKI (Sweden), Swedish Nuclear Fuel & Waste Management Co. (SKB) (Sweden), and Finnish Center for Radiation and Nuclear Safety (STUK) (Finland). Each Funding Organization, also called a Party, is a managing organization in radioactive waste disposal and supports one or more Research Teams. The tasks of the Research Teams are to perform coupled analysis of some or all the problems selected by the DECOVALEX Steering Committee and report their results to their sponsoring Funding Organizations and the DECOVALEX Project Secretariat. The CNWRA, NRC's Federally Funded Research and Development Center (FFRDC), is a NRC sponsored Research Team. The organization of DECOVALEX is given in Figure 1.

1.2 DECOVALEX PROBLEMS: PHASE I

During the first Steering Committee meeting of DECOVALEX in Paris, France on October 28, 1991, two bench-mark tests (BMT) and one test case (TC) problem were selected for modeling in the first phase of DECOVALEX. These were selected from several potential bench-mark tests and test case problems that were discussed during the two DECOVALEX organizational meetings that preceded the first Steering Committee meeting. These three problems are briefly discussed below.

- Far Field THM Model, BMT1. This BMT is designed to simulate the THM processes in a large rock mass within a repository located at a depth of about 500 meters. The model is two-dimensional, measures 3000 m X 1000 m and contains two sets of intersecting fractures. A nonuniform hydraulic head acts at the ground surface and zero flux is imposed on the bottom and lateral boundaries. The heat flux from the repository is assumed to decay exponentially with time. The model has been prepared by M. Durin of CEA/DMT and H. Baroudi of INERIS, France. Detailed specifications of this problem are given in DECOVALEX Doc 91/103 (1991).

- Multiple Fracture Model, BMT2. This BMT consist of an assemblage of nine blocks, separated by two sets of discontinuities (planar fractures). The model measures 0.75 m X 0.50 m and is confined along all boundaries. The rock mass is subjected to in-situ stress and thermal loading as well as a hydraulic gradient. No-flow and adiabatic conditions are imposed at the top and bottom of the model. The heat flux acting along a section of one of the lateral boundaries will include expansion of the rock mass and cause shearing in the model. This Multiple Fracture Model has been prepared by T. Chan and K. Khair of AECL, Applied Geoscience Branch, Pinawa, Manitoba Canada. DECOVALEX Doc 91/104 (1991) contains the specifications of this problem.

- Coupled Stress-Flow Model, TC1. To obtain the experimental data needed to quantify the effects of joint deformation and joint conductivity, an apparatus has been designed and built by the Norwegian Geotechnical Institute (NGI), Oslo,

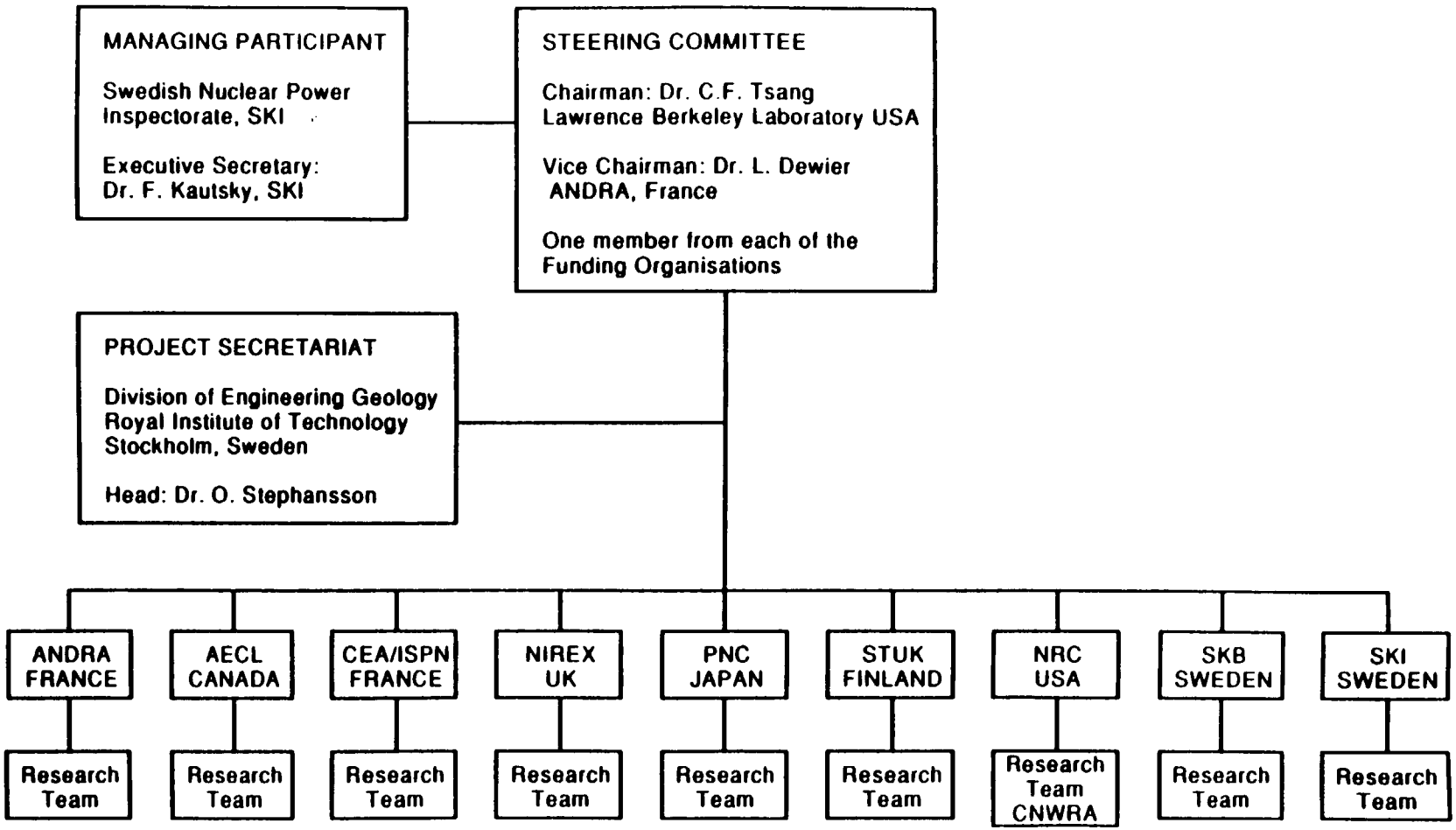

Figure 1. The organization of DECOVALEX

Norway. With this apparatus, joints can be closed and sheared under controlled conditions while fluids can be flushed through the joint. Deformations, flow rates, and stresses are recorded simultaneously. The boundary stresses applied by flat jacks are intended to result in a nearly pure normal stress when the same pressure is applied in the flat jacks. An increasing shear stress occurs when differential pressure is applied. The proposed Coupled Stress-Flow Model has input data derived from recent Stripa studies. The options of linear and nonlinear joint deformability are given and different loading conditions are specified. The Coupled Stress-Flow Model has been prepared by N. Barton of NGI. The specifications of this problem are given in DECOVALEX Doc 91/105 (1991).

1.3 COMPUTER PROGRAMS FOR THM PROCESSES

Currently there are very few codes capable of computing coupled three-dimensional THM problems in fractured rock masses with discrete or simulated representations of the fracture surfaces. Some of the two- and three-dimensional computer programs with various degrees of THM coupled modeling capabilities that are being used or considered by DECOVALEX Research Teams from several countries include: ROCMAS I, II (Noorishad and Tsang, 1989), GENASYS (Wijesinghe, 1989), THAMES 3D (Ohnishi, 1990), FEHMS (Kelkar et al., 1990), UDEC (Board, 1989), 3DEC (Hart et al., 1988), DDA (Shi, 1990), JOBFEM (Stille et al., 1982), and JRTEMP (Halonen, 1989). The CNWRA Research Team has selected the Universal Distinct Element Code (UDEC) for DECOVALEX Phase 1 analysis. This selection is based on the findings of the code qualification study of the CNWRA Seismic Rock Mechanics Research project (Brady, et. al, 1990a) and the degree of THM coupled modeling capability of UDEC.

The CNWRA Research Team has conducted THM coupled analysis on two problems in the first phase of DECOVALEX. These two problems are the Multiple Fracture Model, BMT2 and the Coupled Stress-Flow Model, TC1. These problems have been analyzed using the distinct element computer program UDEC. This report presents the analysis results of these two problems in a format suggested by the DECOVALEX Project Secretariat.

2 BRIEF MATHEMATICAL BACKGROUND TO THE CODE

The state-of-the-art of the behavior of fractured rocks under various coupled processes has been reported by Tsang (1991). The computer code UDEC can be used to model the thermo-hydro-mechanical processes with fluid flow through only fractures i.e., in cases where the rock matrix may be assumed to be impermeable.

Numerous references describe the theoretical background and numerical formulation used in UDEC. One of the most comprehensive descriptions is given by Board (1989). The description of the mechanical and hydromechanical code formulation presented here is adapted from Hart (1991), and that of the thermomechanical code formulation is adapted from Board (1989).

In the distinct element method, a rock mass is represented as an assemblage of discrete blocks. Joints are viewed as interfaces between distinct bodies (i.e., the discontinuity is treated as a boundary condition rather than a special element in the model). The contact forces and displacements at the interfaces of a stressed assembly of blocks are found through a series of calculations which trace the movements of blocks. Movements result from the propagation through the block system of a disturbance applied at the boundary. This is a dynamic process in which the speed of propagation is a function of the physical properties of the discrete system. The dynamic behavior is described numerically by using a time-stepping algorithm in which the size of the timestep is selected such that velocities and accelerations can be assumed constant within the timestep. The distinct element method is based on the concept that the timestep is sufficiently small that during a single step disturbances cannot propagate from one discrete element in the model further than its immediate neighbors. This solution scheme is identical to that used by the explicit finite difference method for continuum numerical analysis. The timestep restriction applies to both contacts and blocks. For rigid blocks, the block mass and interface stiffness between blocks define the timestep limitation; for deformable blocks, the zone size is used, and the stiffness of the system includes contributions from both the intact rock modulus and the stiffness at the contacts.

The calculations performed in the distinct element method alternate between application of a force-displacement law at the contacts and Newton's second law of motion at the blocks. The force-displacement law is used to find contact forces from displacements. Newton's second law gives the motion of the blocks resulting from the forces acting on them. If the blocks are deformable, motion is calculated at the gridpoints of the triangular finite-difference (constant-strain) elements within the blocks. Then, the application of the block material constitutive relations gives new stresses within the elements. Figure 2 shows schematically the calculation cycle for the distinct element method.

This numerical formulation conserves momentum and energy by satisfying Newton's laws of motion exactly. Although some error may be introduced in the computer programs by the numerical integration process, this error may be made arbitrarily small by the use of suitable timesteps and high precision coordinates.

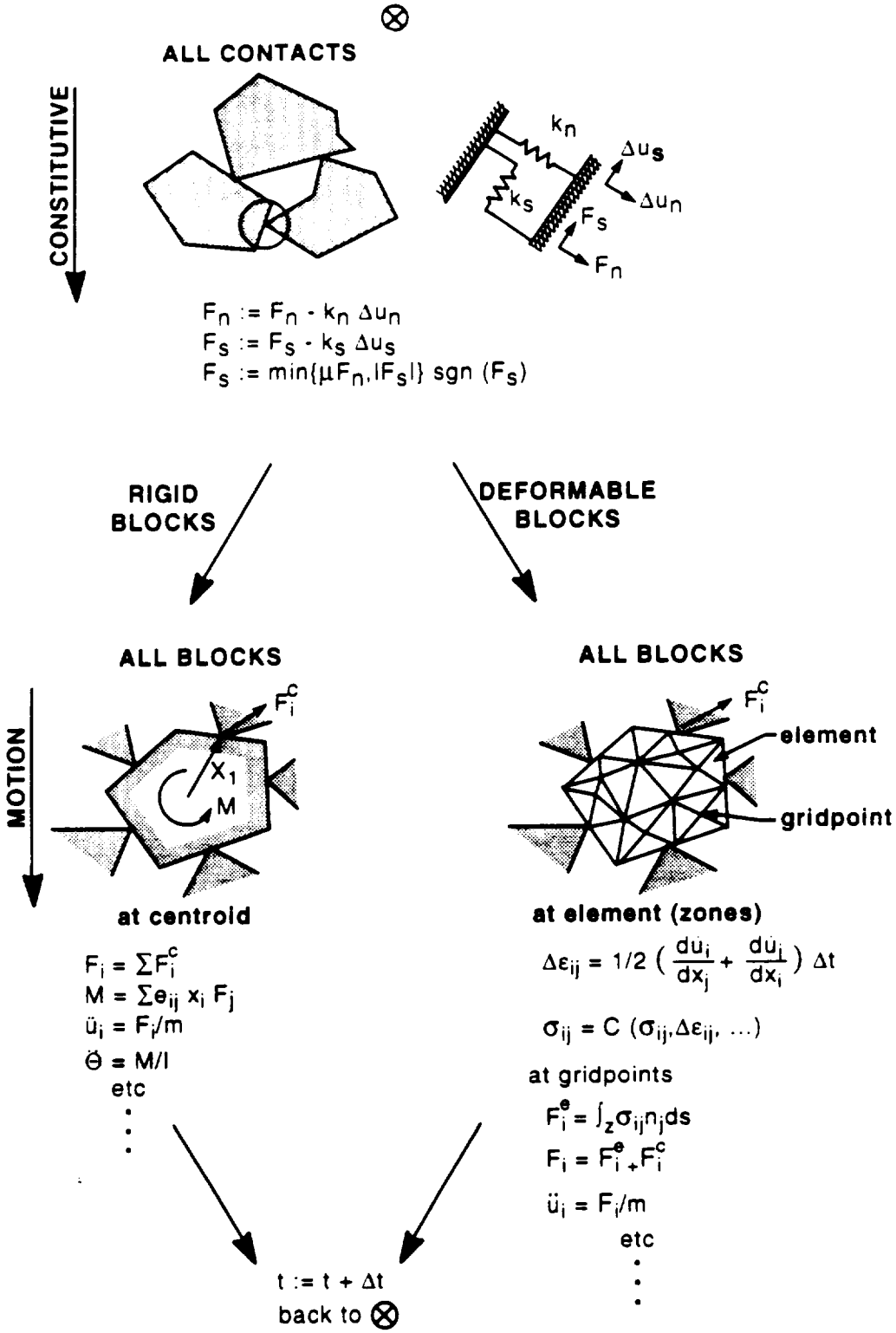

Figure 2. Calculation cycle for the distinct element method (symbols defined in the appendix) [Hart, 1991]

NOMENCLATURE FOR FIGURE 2

Contacts:

F_n, F_s	normal and shear forces
Δu_n, Δu_s	increment normal, shear displacements
k_n, k_s	normal, shear stiffness
μ	friction coefficient

Rigid Blocks:

F_i	block force vector
F_i^c	contact force vector
I	moment of inertia
M	block moment
$\ddot{u}_i$	translational acceleration
x_i	position vector
Θ	angular acceleration
e_{ij}	permutation tensor
m	block mass

Deformable Blocks:

C( )	functional form of constitutive law
F_i^c	contact force vector
F_i^e	gridpoint force vector
u_i	gridpoint velocity vector
$\Delta\epsilon_{ij}$	incremental strain in zone
T_{ij}	stress tensor in zone
Δt	timestep
m	zone mass
n_j	unit outward normal vector
ds	incremental segment

2.1 ROCK JOINT REPRESENTATION

A rock joint is represented numerically as a contact surface (composed of individual point contacts) formed between two block edges. In general, for each pair of blocks that touch (or is separated by a small enough gap), data elements are created to represent point contacts. In UDEC, adjacent blocks can touch along a common edge segment or at discrete points where a corner meets an edge or another corner. For rigid blocks, a contact in UDEC is created at each corner interacting with a corner or edge of an opposing block (Figure 3). If the blocks are deformable (internally discretized into finite difference elements), point contacts are created at all gridpoints located on the block edge in contact. Thus, the number of contact points can be increased as a function of the internal zoning of the adjacent blocks.

A specific problem with contact schemes is the unrealistic response that can result when block interaction occurs close to or at opposing block corners. Numerically, blocks may become locked or hung-up. This is a result of the modeling assumption that block corners are sharp or have infinite strength. In reality, crushing of the corners would occur as a result of a stress concentration. Explicit modeling of this effect is impractical. However, a realistic representation can be achieved by rounding the corners so that blocks can smoothly slide past one another when two opposing corners interact. Corner rounding is used in UDEC by specifying a circular arc for each block corner. The arc is defined by the distance from the true apex to the point of tangency with the adjoining edges. By specifying this distance rather than a constant radius, the truncation of sharp corners is not severe.

In UDEC, the point of contact between a corner and an edge is located at the intersection between the edge and the normal taken from the center of the radius of the circular arc at the corner to the edge [Figure 4(a)]. If two corners are in contact, the point of contact is the intersection between the line joining the two opposing centers of radii and the circular arcs [Figure 4(b)]. The directions of normal and shear force acting at a contact are defined with respect to the direction of the contact normal (Figure 4). Contacts along the edge of a deformable block are represented by corners with very large rounding lengths.

Corner rounding only applies to the contact mechanics calculation in UDEC. All other calculations and properties such as block and zone mass are based on the entire block. Corner rounding can introduce inaccuracy in the solution if the rounding is too large. If the rounding length is kept to approximately one percent (1 percent) of the representative block edge length in the model, good accuracy is achieved.

Contact points in UDEC are updated automatically as block motion occurs. The algorithms to perform this updating must be computationally efficient, particularly for dynamic analysis, in which large displacements may require deleting and adding hundreds of contacts during the dynamic simulation. UDEC takes advantage of a network of "domains" created by the two-dimensional block assembly. Domains are the regions of space between blocks which are defined by the contact points (e.g., D1 and D2 in Figure 5). During one timestep, new contacts can be formed only between corners and edges within the same domain, so local updates

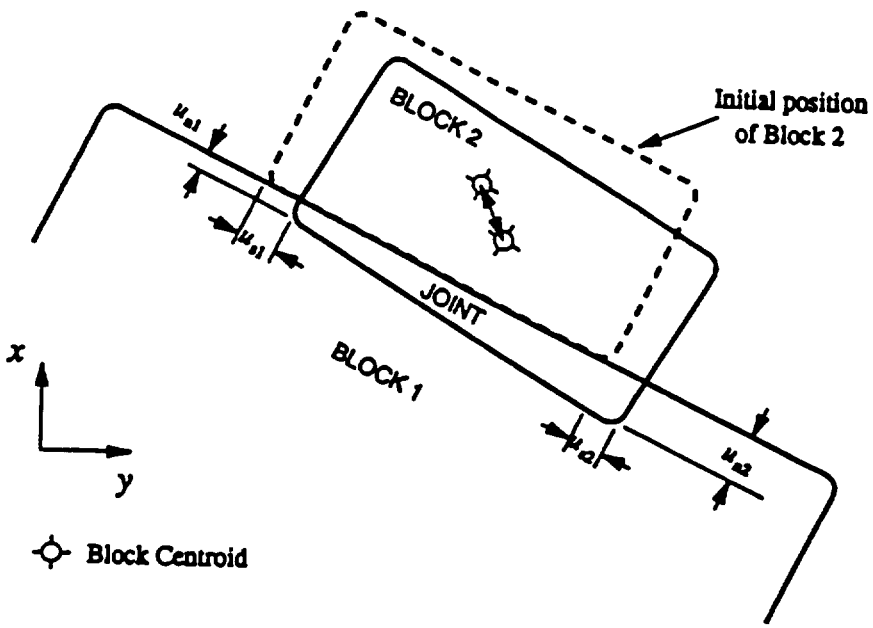

Figure 3. Contacts between two rigid blocks in UDEC (block overlap is exaggerated)

can be executed efficiently whenever some prescribed measure of motion is reached within the domain. The main disadvantage of this scheme is that it cannot be used for very loose systems because the domain structure becomes ill-defined.

2.2 ROCK JOINT BEHAVIOR

Numerically, a joint is a special contact type which is classified as an edge-to-edge contact. In UDEC, a joint is recognized when a domain is defined by two point contacts. The joint is assumed to extend between the two contacts and be divided in half with each half-length supporting its own contact stress (Figure 5). Incremental normal and shear displacements are calculated for each point contact and associated length (i.e., L1, L2 and L3 in Figure 5).

UDEC uses several joint behavior relations to describe the mechanical response at the interface. The basic joint model used in the code captures several of the features which are representative of the physical response of joints. In the normal direction, the stress-displacement relation is assumed to be linear and governed by the stiffness k_n such that

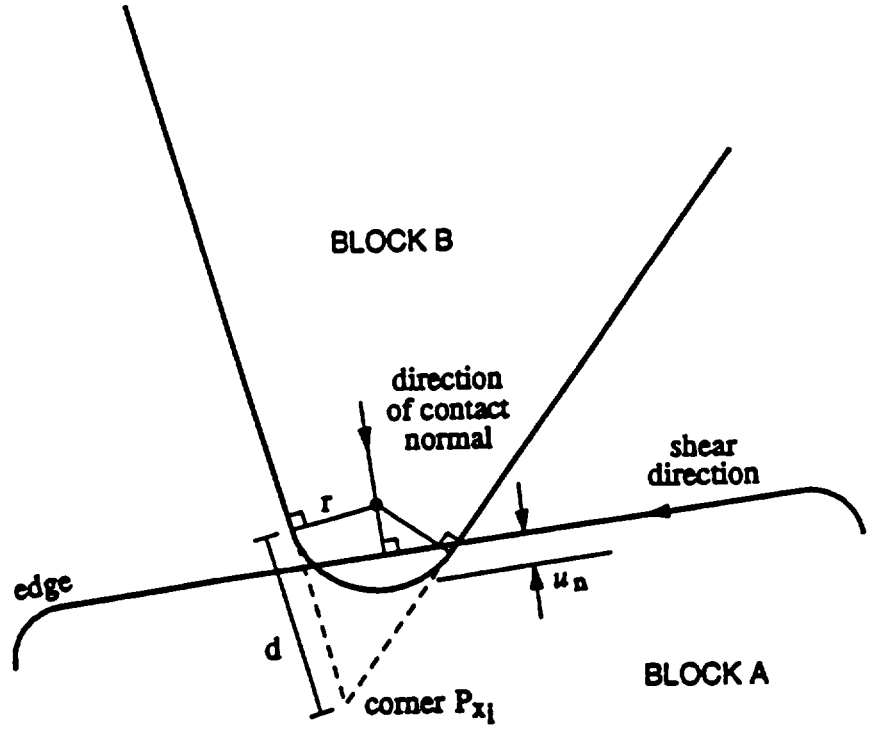

(a)

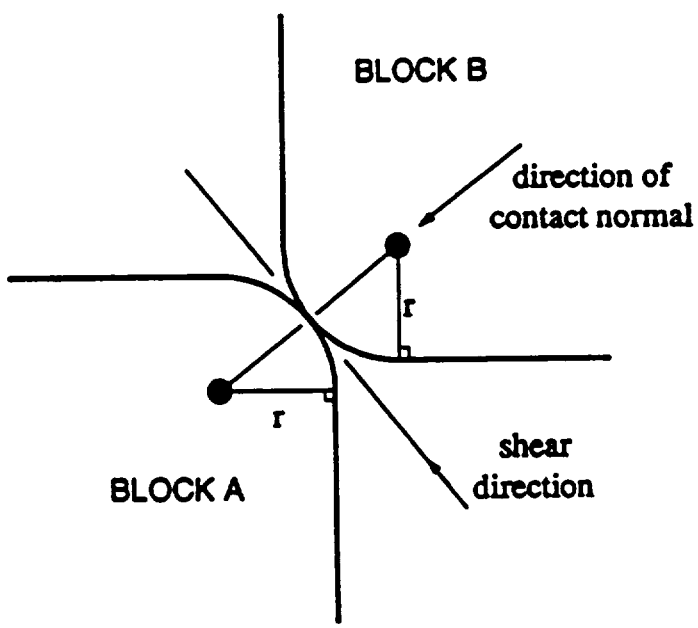

(b)

Figure 4. Definition of contact normal in UDEC: (a) detail of rounded corner-to-edge contact (rounding length exaggerated); (b) smooth interaction of corner-to-corner contact

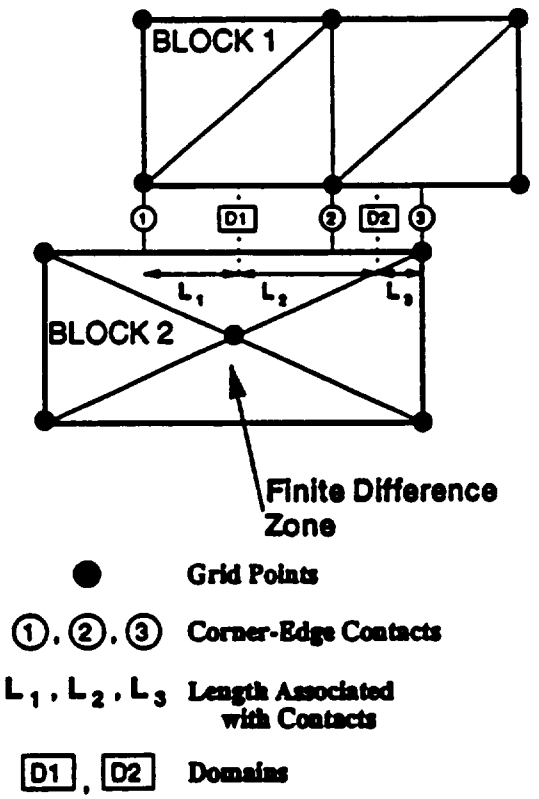

Figure 5. Contacts and domains between two deformable blocks [Hart, 1991]

$$\sigma_n = \; = k_n \, u_n \tag{1}$$

where σ_n is the effective normal stress, and u_n is the normal displacement.

There is also a limiting tensile strength, T, for the joint. If the tensile strength is exceeded (i.e., if $\sigma_n < -T$), then $\sigma_n = 0$. Similarly, in shear, the response is controlled by a constant shear stiffness, k_s. The shear stress, τ_s, is limited by a combination of cohesive (C) and frictional (ϕ) strength. Thus, if

$$|\tau_s| \le C + \sigma_n \tan \phi = \tau_{max} \tag{2}$$

then

$$\tau_s = k_s \, u_s^e \tag{3}$$

or else, if

$$|\tau_s| \ge \tau_{max} \tag{4}$$

then

$$\tau_s = \text{sign}\,(u_s)\; \tau_{max} \tag{5}$$

where u_s^e is the elastic component of the shear displacement, and u_s is the total shear displacement.

This model is described as the Coulomb slip model. In addition, joint dilation may occur at the onset of slip (nonelastic sliding) of the joint. Dilation is governed in the Coulomb slip model by a specified dilation angle γ. The accumulated dilation is generally limited by either a high normal stress level or by a large accumulated shear displacement which exceeds a limiting value U_{cs}. The limitation on dilation corresponds to the observation that crushing of asperities at high normal stress or large shearing would eventually prevent the joint from dilating.

In the Coulomb model, the dilation is restricted such that if $|\tau_S| \le \tau_{max}$, then $\gamma = 0$, and if $|\tau_S| = \tau_{max}$ and $u_s \ge U_{cs}$, then $\gamma = 0$.

The Coulomb model can approximate a displacement-weakening response which is often observed in physical joints. This is accomplished by setting both the tensile strength, T, and cohesion, C, to zero whenever either the tensile or shear strength is exceeded.

A more comprehensive displacement-weakening model is also available in UDEC. This model, the continuously-yielding joint model (Cundall and Lemos, 1990) is intended to simulate the intrinsic mechanism of progressive damage of the joint under shear.

UDEC also includes an empirical joint model described by Barton et al. (1985). In this joint model, the effect of surface roughness on joint deformation and strength is described in terms of empirical relations between normal stress and closure, mobilized roughness and normalized shear displacements, and a nonlinear strength criterion.

2.3 BLOCK DEFORMABILITY

In UDEC, each block can be automatically discretized into triangular constant-strain elements. These elements may follow an arbitrary, nonlinear constitutive law (e.g., Mohr-Coulomb failure criterion with nonassociated flow rule). Other nonlinear plasticity models recently added to UDEC include a ubiquitous joint model and strain-softening models for both shear and volumetric (collapse) yield. The complexity of deformation of the blocks depends on the number of elements into which the blocks are divided.

2.4 HYDROMECHANICAL COUPLING

UDEC has the capability to model the flow of a fluid through the fractures of a system of impermeable blocks. A fully-coupled mechanical-hydraulic analysis is performed in which fracture conductivity is dependent on mechanical deformation and, conversely, joint water pressures affect the mechanical behavior. Joint apertures and water pressures are updated at every timestep.

The fluid logic takes advantage of the domain network logic used in UDEC to monitor changes in contacts. The domains are considered to be fluid volumes which fluctuate as a function of contact normal displacement at the two ends of the domain. Each contact is assigned a conducting (hydraulic) aperture, a, which is related to normal displacement by

$$a = a_o + u_n \tag{6}$$

where a_o is the aperture at zero normal stress, and u_n is the joint normal displacement (positive denoting opening).

A minimum residual value, a_{res}, is assumed at higher confining stresses. This allows for some fluid conductivity always to be maintained, in keeping with experimental observation.

Joint dilation will modify the basic relation, and is assumed to be irrecoverable. A maximum contact aperture is also defined which limits the magnitude of the conductivity when the joint opens.

Flow in planar rock fractures is idealized as a case of laminar viscous flow between parallel plates. In this model, the flow rate per unit width, q, if given by

$$q = C\, a^3 \left[\frac{\Delta p}{L}\right] \tag{7}$$

$$C = \frac{1}{12\mu} \tag{8}$$

where C is the fluid flow joint property which is assumed to remain constant,

μ is the dynamic viscosity of the fluid,

Δp is the change in pressure across a contact between adjacent domains, and

L is the length assigned to the contact.

The rate of fluid flow thus is assumed to be dependent upon the cubic power of the aperture.

The domain pressures are updated by taking into account the net flow into the domain and changes in domain volume due to incremental motion of the surrounding blocks. The new domain pressure is

$$p = p_0 + K_W\, Q \left[\frac{\Delta t}{V}\right] - K_W \left[\frac{\Delta V}{V_M}\right] \tag{9}$$

where p_0 is the domain pressure in the preceding timestep,

Q is the sum of flow rates into the domain from all surrounding contacts,

K_w is the bulk modulus of the fluid, and

$$\Delta V = V - V_0,\ V_m = \frac{V + V_0}{2} \tag{10}$$

where V and V_0 are the domain volumes at the present and previous timesteps.

The domain pressures are resolved into forces exerted by the fluid at the contacts and are added to the mechanical contact forces and external loads to be applied at the block boundaries.

Thus, total stresses will result inside the impermeable blocks, while effective normal stresses are obtained for the mechanical contacts.

Lemos and Lorig (1990) describe the following limitations of the current procedure as well as an adaptive procedure for determining steady-state condition. For transient flow analysis, the numerical stability requirements may be rather severe, and may make some analyses very time-consuming or impractical, especially if large contact apertures and very small domain areas are present. A scheme that can be used to enhance computational efficiency consists in assigning to domains at the intersection of the joints part of the volume of the joints meeting at the point, and correspondingly reducing the volume of the joint domains. Furthermore, the fluid filling a joint also increases the apparent joint stiffness by K_w/a, thus possibly requiring a reduction of the timestep used in the mechanical calculation.

In many studies, only the final steady-state condition is of interest. In this case, several simplifications are possible which make the present algorithm very efficient for many practical problems. The steady-state condition does not involve the domain volumes. Thus, these can be scaled to improve the convergence to the solution. A scheme that was found to produce good results consists in assigning to a given domain a volume V that, inserted in the timestep expression above, leads to the same timestep for all domains (Lemos and Lorig, 1990). The contribution of the change in domain volume to the pressure variation can also be neglected, thus eliminating the influence of the fluid stiffness in the mechanical timestep. Furthermore, as the steady-state condition is approached, the pressure variation in each fluid step becomes very small, allowing the execution of several fluid steps for each mechanical step without loss of accuracy. An adaptive procedure was implemented in UDEC which "triggers" the update of the mechanical quantities, whenever the maximum increment of pressure in any domain exceeds some prescribed tolerance (for example, 1 percent of the maximum pressure).

2.5 THERMOMECHANICAL COUPLING

The heat transfer in UDEC is based on conductive transfer within the medium with the provision for temperature, flux, convective or radiative boundaries. The standard equations for transient heat conduction can be found in many texts, such as Karlekar and Desmond (1982), and are reviewed here. The basic equation of conduction heat transfer is Fourier's law, which can be written in one dimension as

$$Q_x = - k_x \frac{\partial T}{\partial x} \tag{11}$$

where Q_x = flux in the x-direction (W/m^2), and

k_x = thermal conductivity in the x-direction (W/m °C).

A similar equation can be written for Q_y. Also, for any mass, the change in temperature can be written as

$$\frac{\partial T}{\partial t} = \frac{Q_{net}}{c_p M} \tag{12}$$

where Q_{net} = net heat flow into mass (W),

c_p = specific heat (J/kg °C), and

M = mass (kg).

These two equations form the basis of the governing heat flow logic in UDEC. Eq. (12) can be written as

$$\frac{\partial T}{\partial t} = \frac{1}{c_p \rho} \left[\frac{\partial Q_x}{\partial x} + \frac{\partial Q_y}{\partial y} \right] \tag{13}$$

where ρ is the mass density.

Combining this with Eq. (11),

$$\begin{aligned} \frac{\partial T}{\partial t} &= \frac{1}{c_p \rho} \frac{\partial}{\partial x} \left[k_x \frac{\partial T}{\partial x} \right] + \frac{\partial}{\partial y} \left[k_y \frac{\partial T}{\partial y} \right] \\ &= \frac{1}{\rho c_p} \left[k_x \frac{\partial^2 T}{\partial x^2} + k_y \frac{\partial^2 T}{\partial y^2} \right] \end{aligned} \tag{14}$$

if k_x and k_y are constant. This is the standard two-dimensional heat diffusion equation.

Temperature changes cause stress changes for fully-deformable blocks according to the equation

$$\Delta \sigma_{ij} = - \delta_{ij} K \beta \Delta T \tag{15}$$

where σ_{ij} = change in ij stress component,

δ_{ij} = Kronecker delta function,

$$\begin{bmatrix} 1 & 0 \\ 0 & 1 \end{bmatrix}$$

K = bulk modulus (N/m^2),
ß = volumetric thermal expansion coefficient ß (1/°C), and
ΔT = temperature change.

Note that ß = 3α, where α = linear thermal expansion coefficient.

Equation (15) assumes a constant temperature in each triangular zone which is interpolated from the surrounding gridpoints. The incremental change in stress is added to the zone stress state prior to application of the constitutive law.

The mechanical changes can also cause temperature changes as energy is dissipated in the system. This coupling is not modeled in UDEC because the heat produced in usually negligible for quasi-static problems.

2.6 PERFORMING COUPLED ANALYSES

In performing coupled analyses, it is important to be clear about the relative time scales associated with heat flow, fluid flow and mechanical loading. Mechanical effects occur almost instantaneously in the real world, in the order of milliseconds. Fluid flow effects in jointed rock usually take somewhat longer, on the order of seconds, hours or even days, depending on joint permeability. However, heat flow is a much longer-term process, taking place over months and years.

As discussed previously, UDEC is an explicit code, which means that it takes "timesteps" to solve a problem. Thus, although mechanical effects take place almost instantaneously, UDEC takes a finite number of steps to reach mechanical equilibrium. However, there is no true time period associated with these steps; they are merely an internal mechanism for the code to attain equilibrium. An alternative way in which to think of these mechanical steps is to imagine that each step represents a microsecond or less of time, so that, even if many steps are taken, almost no time elapses.

The procedure for running a coupled thermomechanical simulation is shown in Figure 6. The fundamental requirement in performing the simulation is that temperature increases between successive thermal timesteps cause only "small" out-of-balance forces in blocks. Out-of-balance forces are "small" if they do not adversely affect the solution. For nonlinear problems, some experimentation may be necessary to obtain a sense of what "small" means in the particular problem being solved. This is performed by trying different allowable temperature increases when running the problem. An important point to note is that the same temperature

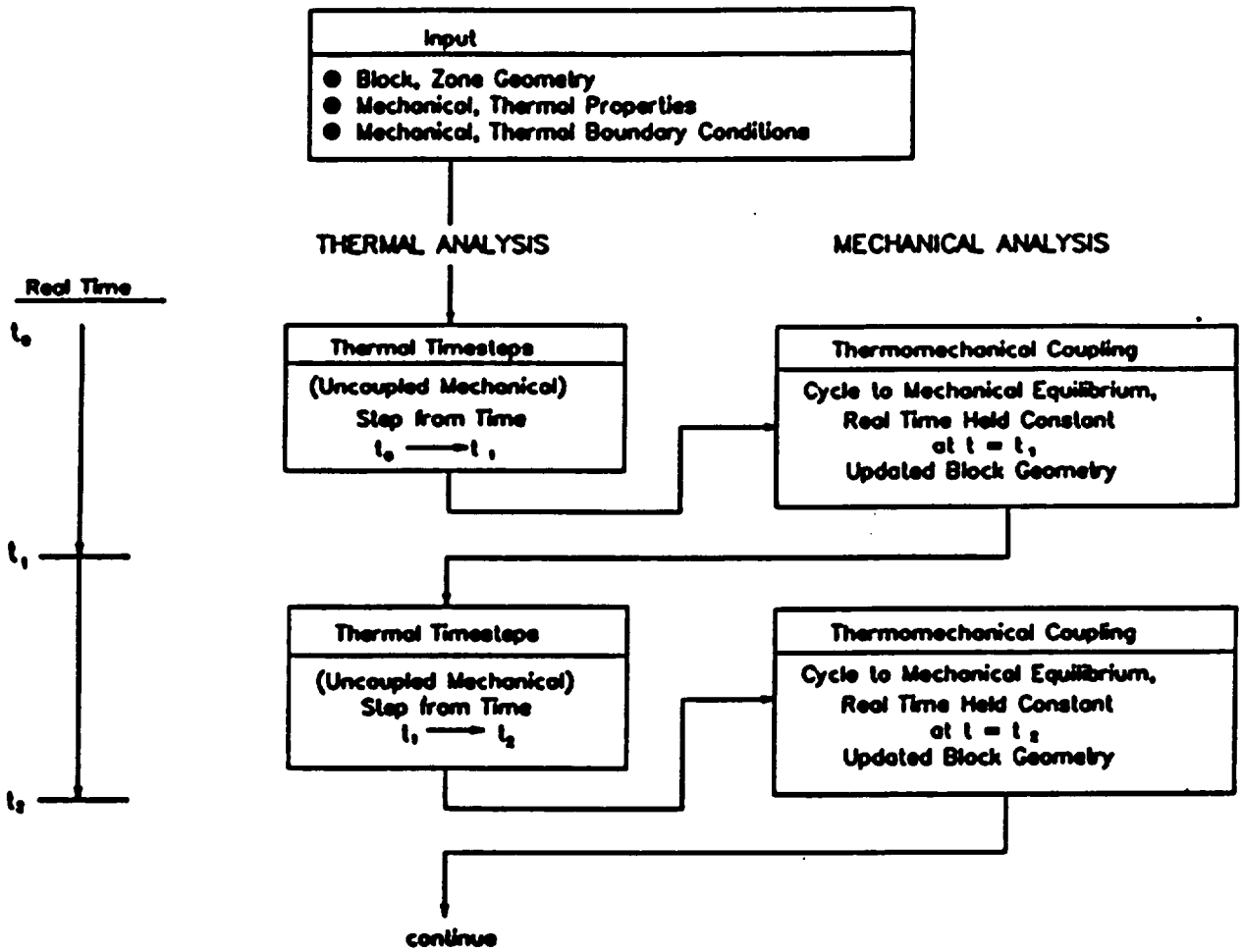

Figure 6. Method of running a coupled thermomechanical simulation with UDEC (Board, 1989)

increase is not necessarily acceptable to all times in a problem. While the system is far from yield (i.e., inelastic behavior), large temperature changes may be acceptable but, near yield, only relatively small increases can be tolerated.

In many studies involving coupled thermal, hydrological and mechanical analyses, only the steady-state condition at specified times are of interest. For these problems, the adaptive hydromechanical coupling scheme described at the end of Section 2.4 can be used. If this procedure is used to determine the steady-state fluid flow condition, then again, no true time period is associated with the fluid flow steps and the procedure for running a coupled simulation is similar to that shown in Figure 6.

The three main differences would be that:

- hydrologic properties and boundary conditions would be specified under "input";
- mechanical analysis would be replaced by hydromechanical analysis; and
- mechanical equilibrium would be replaced by mechanical and hydrologic equilibrium.

This method of performing coupled analysis results in the following interactions.

- Temperature change is not affected by fluid flow (convective heat transfer).
- Pore pressure in fractures is not affected by temperature change.
- Mechanical stress is affected by temperature change.
- Temperature is not affected by volume change.
- Mechanical stress is affected by pore pressure.
- Pore pressure is not affected by aperture change.
- Thermal conductivity is constant.

3 CODE DESCRIPTION

Formulation and development of the distinct element method has progressed for over 20 years, beginning with the initial presentation by Cundall (1971). The method was created originally as a two-dimensional representation of a jointed rock mass, but has been extended to applications in particle flow research (Walton, 1980), studies on micromechanics of granular media (Cundall and Strack, 1983), and crack development in rocks and concrete (Plesha and Aifantis, 1983; Lorig and Cundall, 1987). The most recent two-dimensional program, UDEC was developed in 1980 (Cundall, 1980; Lemos et al., 1985) to combine into one code the formulation to represent both rigid and deformable blocks separated by discontinuities. In 1983, work was begun on the development of a three-dimensional version of the method. This work is embodied in a computer program entitled 3DEC (Cundall, 1988; Hart et al., 1988). The chronology of development of the distinct element method, and UDEC in particular, is shown in Figure 7.

Over the years, the performance of UDEC has been verified for specific problems through numerous studies (Board, 1989; Brady et al., 1990a,b; Lemos and Lorig, 1990; Itasca, 1991). These verification studies have shown reasonable agreement with analytical solutions and/or results obtained using other codes.

UDEC has also been used to analyze the results of field tests (Brady et al., 1985; Hart et al., 1985) and to predict the results of laboratory tests. UDEC models of jointed rock problems involving response to storage of high-level nuclear waste have been made by many investigators (e.g., Johansson et al., 1991a,b; Board, 1989; Christianson, 1989; Lorig and Dasgupta, 1989).

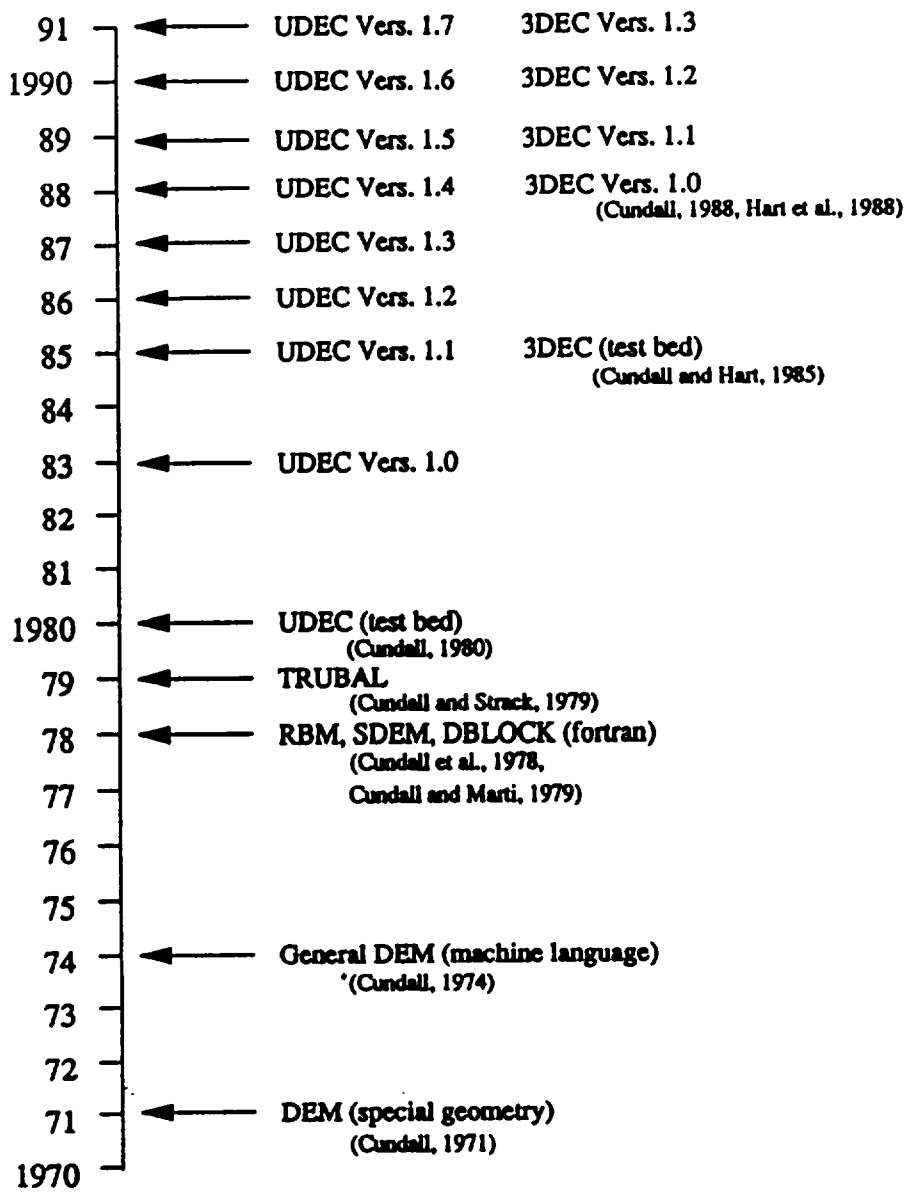

Figure 7. Chronology of the distinct element method

4 COMMENTS ON THE GIVEN SPECIFICATIONS OF BMT AND TC PROBLEMS

4.1 MULTIPLE FRACTURE MODEL, BMT2

In general, this problem appears to be fairly well specified. Comments regarding this problem as specified in DECOVALEX Doc 91/104 (1991) are as follows.

- This problem is attractive because it includes aspects of phenomenological coupling which are important in studies for high-level nuclear waste repositories. This type of problem is analogous to an in-situ block test and, therefore, represents a good problem for code validation.

- The problem specifications suggest that forced convective heat transfer in the joints should be explicitly modeled. At present, UDEC does not have this capability, and it is worthwhile considering whether this capability is important. In-situ heated block tests completed to date suggest that conductive heat transfer is dominant and sufficient to describe temperature fields in jointed rock (Zimmerman et al., 1986 and Voegele et al., 1981). However, the joint apertures in these block tests were significantly less than the apertures specified for this problem.

- The residual hydraulic aperture for the Coulomb-Friction joint model (CF model) is not given. A maximum fracture closure of 230 microns was specified for the Barton-Bandis model (BB model). This value was used for the CF model, resulting in a residual hydraulic aperture of 70 microns.

4.2 COUPLED STRESS-FLOW MODEL, TC1

Comments regarding the specifications given in DECOVALEX Doc 91/105 (1991) for this problem are as follows.

- The specified normal stiffness (1 GPa/m) for the steel-epoxy interface (I4), is too low. The specified maximum normal stress (25 MPa) applied at the boundary produces a normal displacement of 25 mm, which is 2.5 times greater than the steel thickness. In order to overcome this difficulty, the normal stiffness for the steel-epoxy interface was increased from 1 GPa/m to 100 GPa/m. A similar problem arises at the epoxy-epoxy interface (I5). The normal stiffness for this interface was similarly increased by two orders of magnitude, from 0.1 GPa/m to 10 GPa/m.

- On page 16, it is stated that "the displacement needed to mobilize peak shear strength of the rock joint is slightly above 0.8 mm." This statement is true for

values of JRC greater than 5. In this problem, JRC is less than 5 and, hence, the displacement needed to mobilize the peak shear strength is 2*0.84 mm = 1.68 mm.

- Reference for the Barton-Bandis type of joint model (see page 11) is not provided. The joint model used in this exercise is described by Barton (1982) and Barton et al. (1985).

- On page 11 it states "Each Research Team has therefore to decide whether plane strain or plane stress conditions should be used in a two-dimensional model." However, no information about end conditions is provided. Specification of end conditions would allow proper determination of whether plane strain or plane stress conditions are appropriate. Based on the relatively thin sample thickness (i.e., 100 mm) and probable lack of end restraint, a plane stress analysis was assumed.

- Page 12 provides the relation to be used between hydraulic aperture, e, and mechanical aperture, b. This relation is defined by Barton et al. (1985). However, this reference is not provided. It is believed that, in this relation, b must be specified in microns. The small scale roughness coefficient for the joint, JRC_o used in the relation is not specified. The value of $JRC_o = 1.95$ was used as shown below. The relation also specifies that the hydraulic aperture be less than or equal to the mechanical aperture. If $JRC_o = 1.95$, then

$$e = 0.19b^2$$

Therefore, the hydraulic aperture will equal the mechanical aperture for mechanical apertures greater than about 5 microns. In this problem, mechanical apertures are greater than 5 microns; therefore, the mechanical and hydraulic apertures are always taken to be equal.

- On page 12 it states that "gravity works in the vertical direction (downwards)." The subscript "v" in Figure 4 suggests that gravity acts in the plane of analysis. This contradicts the assumptions for Option 1, in which gravity is neglected. Gravity was neglected in the analysis presented here.

- Values for JRC_o and JCS_o were not provided. In the analysis presented here, these values were back-calculated based on joint length. The following values were used in the analysis presented here:

$$JRC_o = 1.95$$
$$JCS_o = 156.21$$

- The boundary conditions for the upper block for sequence B are not defined. It is impossible to specify stress boundary conditions to produce specific amounts of joint shear displacement after the joint reaches peak shear strength. Therefore, displacement boundary conditions were estimated for the analysis presented here. However, two difficulties arise when attempting to do this.

  First, the problem specification states that joint normal stress should be kept constant during shearing (see page 15). This means that joint dilation resulting from shear must be accounted for in the boundary conditions. For the results shown in this report, it was assumed that a dilation angle of 0.5 degrees would result from shearing of the joint under constant normal stress. This value was determined based on use of a joint exerciser (i.e., spread sheet) assuming a joint normal stress of 25 MPa.

  The second problem that arises is that the location of specified shear displacement (i.e., 0, 0.5 m, 0.8 mm, etc.) is not given. Before joint slip occurs, boundary displacements in the shear direction are not the same as joint shear displacement. Displacements before slip occurs are larger at the boundary than at the joint. Also, shear displacement varies slightly along the joint. Trial and error was involved to prescribe boundary conditions of a specified amount on the joint.

- The problem specification implies that normal stress along the length of the rock joint is constant (see page 20). However, the normal stress varies considerably along the length of the joint. The highest normal stresses are obtained at the ends of the rock joint. The lowest values of normal stress are at the middle of the joint length. This result is exactly what is expected, since the epoxy-epoxy interface at the joint ends has a much lower normal stiffness than the rock joint.

  For the given geometry, the normal stress concentration at the ends of the rock joint are primarily a function of the ratio of normal stiffnesses for the rock joint and epoxy interface. In order to limit the normal stress concentration, and at least attempt to approach a condition of constant normal stress, the normal stiffness of the rock joint was limited to a normal stiffness of 500 GPa/m. This value of normal stiffness is the same value specified for Option 1. The joint aperture in the Barton-Bandis model in UDEC is calculated from the joint normal stress using a hyperbolic stress displacement function. The use of a stiffness limit in the normal direction, therefore, does not affect apertures. The stiffness limit will result in a slightly greater displacement of the blocks on either side of the joint. The magnitude of this additional displacement is usually several orders of magnitude less than the displacements due to elastic compression of the block.

Using a maximum normal stiffness of 500 MPa/m for the rock joint and 10 GPa/m for the epoxy interface still results in a threefold difference between the midpoint and end point rock joint normal stress.

The output specifications for the model ask for the "average" normal stress across the joint. The concept of an "average" normal stress may be misleading in the problem, since the maximum stresses may be of importance in determining flow characteristics and shear deformations.

- The initial joint aperture was not specified for Option 2. An initial aperture is calculated from the Barton-Bandis model assuming parameters previously given and assuming a rock compressive strength of 240 MPa. The resultant initial unstressed aperture is 81 microns. Initial closure at the beginning of the fourth normal load cycle is 30 microns. Consequently, the initial unstressed aperture at the beginning of the normal loading sequence is 51 microns.

5 COMPUTER HARDWARE AND TIME

Both the Multiple Fracture Model (BMT2) and the Coupled Stress Flow Model (TC1) were run using UDEC installed on a Sun IPX Sparcstation. For the Coupled Stress Flow Model, the computer time required to simulate both loading sequences A and B was 7.7 hours. For this analysis, output files were created after each loading increment for both normal loading and shear loading. Enough time steps were specified after each normal or shear loading increment to ensure mechanical and fluid flow equilibrium. The computer time required to run the Multiple Fracture Model was 1.5 hours. For this analysis, output files were created after each of the specified output time periods after thermal loading was initiated. Listings of the input files for both analyses are given in Appendix B.

6 RESULTS

6.1 MULTIPLE FRACTURE MODEL, BMT2

Results of the two-dimensional, plane strain Multiple Fracture Model analysis using UDEC are presented. Only Case A, involving fluid flow through the fractures, was simulated (DECOVALEX Doc 91/104,1991). Matrix flow, as specified for Cases B and C in DECOVALEX Doc 91/104 (1991) could not be analyzed with the present UDEC capabilities. The bench-mark test consisted of an assemblage of nine blocks, separated by two sets of planar fractures, one set being horizontal and the other vertical (Figure 8(a)). The dimensions of the model were 0.75 by 0.5 m in the horizontal and vertical directions, respectively. Figure 8a also shows the location of the 41 specified monitoring points. Points 1-9 are located at the block centroids while points 10-41 are located at the block corners on either side of the joints. Figure 8b shows the discretization of the model into finite difference zones. The maximum edge length for the triangular zones was specified at 0.07 m throughout the model. The rock was subjected to total in-situ compressive stresses of 4.0 MPa in both the horizontal and vertical directions. The mechanical boundary conditions consisted of zero normal displacements around the four edges of the model (i.e. boundaries were rollered). The rock matrix was assumed to be linear elastic, while the joint constitutive relations followed the Coulomb-Friction model. Material properties for the rock matrix as well as the joint properties for the Coulomb-Friction model are given in DECOVALEX Doc 91/104 (1991).

The hydraulic boundary conditions consisted of a fixed pressure of 10.0 kPa on the left model boundary and a fixed pressure of 11.0 kPa along the right model boundary. Both the top and bottom boundaries were assumed to be impermeable. The initial fluid pressure through the model was specified to be 10.0 kPa. The initial aperture for the joints under the in situ conditions was specified at 300 microns. For the thermal analyses, an initial temperature distribution of 15°C was assumed throughout the model. This initial temperature distribution was assumed not to induce thermal stresses within the blocks. The thermal boundary conditions consisted of fixing the temperature along the right side of the model at 15°C. A constant flux of 60 W/m^2 was applied to the lower left model boundary over a length of 0.2 m as shown in Figure 8(a). All other portions of the model boundary were assumed to be adiabatic. Due to the small thermal loading, it was expected that little shear deformation would take place.

The problem specification required running the problem to steady-state flow conditions before applying the thermal load. At steady-state, the flow rate per unit depth through each horizontal joint was determined from UDEC to be 2.668E-06 m^2/sec. No flow occurs through the vertical joints, as would be expected from symmetry conditions. The analytic solution for the flow rate through the horizontal joints [Eq. (7), Section 2.4] gives a steady-state flow rate of 2.669E-06 m^2/sec, which agrees with the result from UDEC. After the steady-state flow was reached, all the block displacements and rotations as well as joint shear displacements were set equal to zero at the start of thermal loading.

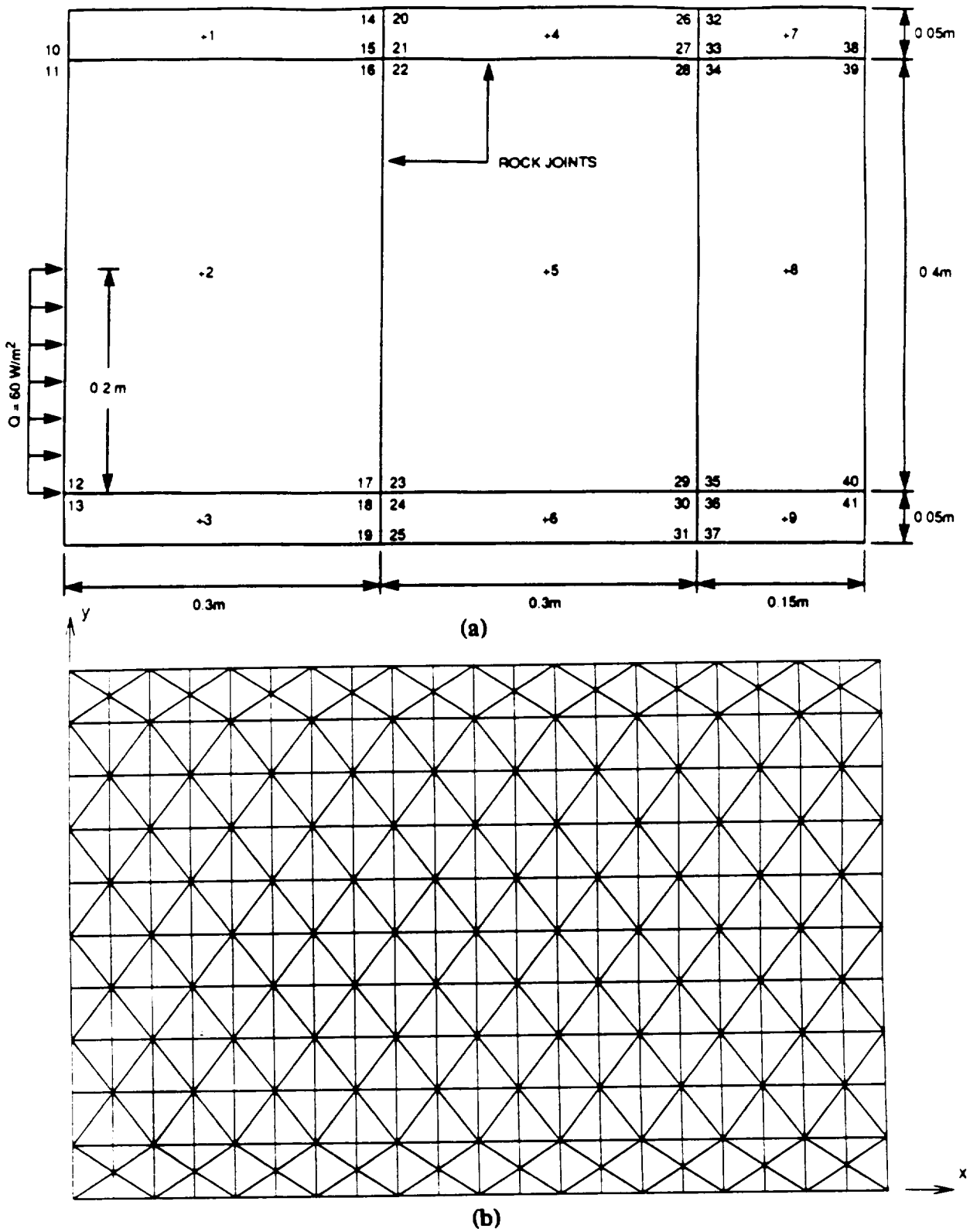

Figure 8. (a) Block geometry for BMT2, showing location of 41 monitoring points; (b) zone discretization of fully deformable blocks for BMT2

Tables A.1.1 through A.1.6 show the numerical values of the temperatures, stresses, hydraulic heads, flow velocities, and displacements taken at times of 0, 10, 10^2, 10^3, 10^4, 10^5, 10^6, and 10^7 seconds after the thermal loading was applied. Table A.1.1 shows that the maximum temperature rise of the 41 monitoring points is only 6.2 °C, and occurs at points 12 and 13. Figures 9 and 10 show plots of temperature at the various monitoring points versus time. The two figures show that a steady-state temperature distribution within the model is reached after approximately 10^6 seconds. The temperature rise results in only small thermally induced stresses. As shown in Table A.1.2, the maximum thermally induced stress of the 9 monitoring points located at the block centroids is approximately 0.2 MPa at point 2. Similarly, very little change in the hydraulic head is experienced, as indicated in Table A.1.3. Aperture closures of approximately 17 microns occur at several points along the lower horizontal fracture at the end of the thermal simulation. Tables A.1.4 and A.1.5 show fluid velocities at seven points along each the upper and lower horizontal fractures, respectively. The average velocity of the seven monitoring points along the lower joint upon reaching steady-state flow is calculated to be -8.902E-3 m/sec. After steady-state thermal loading is reached, the average velocity of the same seven monitoring points is -8.385E-3, a reduction of approximately 6 percent. Table A.1.6 shows the displacements of the 41 monitoring points at each of the specified output times. The maximum displacements in the x and y directions upon reaching steady-state thermal loading are on the order of 10E-5 m. Plots of the temperature contours and gridpoint displacement vectors at the end of thermal loading are shown in Figures 11a and b.

It should be noted, that each of the specified output times listed above represents a steady-state flow situation. The approach taken with UDEC in conducting the analysis was to initially run the thermal analysis out to some period of time. At this point, the temperature field would be known throughout the model. Next, the mechanical and fluid flow cycling would be initiated until steady-state equilibrium was reached with the temperature distribution at this period in time. As discussed in Section 2.4, this mechanical and fluid flow cycling does not represent the real problem time. It is only the cycling time necessary to reach calculational equilibrium with the thermal loading, while the real time is held constant. Since both the temperature gradients as a result of the applied heat flux and the maximum temperature differences throughout the model were small, it was felt sufficient to run the thermal analysis directly to each of the above listed output times, before initiating the mechanical and fluid flow cycling. Thus, time histories for stresses, gridpoint displacements, hydraulic head, and fluid velocities would consist of only those points which represent the steady-state solution as listed in Tables A.1.2-A.1.6 for the times 0, 10, 10^2, 10^3, 10^4, 10^5, 10^6, and 10^7 seconds. Since most of these parameters change very little, these time histories were not plotted.

UDEC does not have the capability to simulate heat transfer due to fluid convection as discussed in Section 2. Thus, the results presented in this analysis only took into account conduction through the rock as the sole mode of heat transfer. Due to the relatively large initial aperture (300 μm), and the fact that an average initial fluid velocity of 8.902E-03 m/sec results in a travel time for fluid through the model of approximately 85 seconds, it is most likely that some of the heat would be carried out by convection within the horizontal fractures.

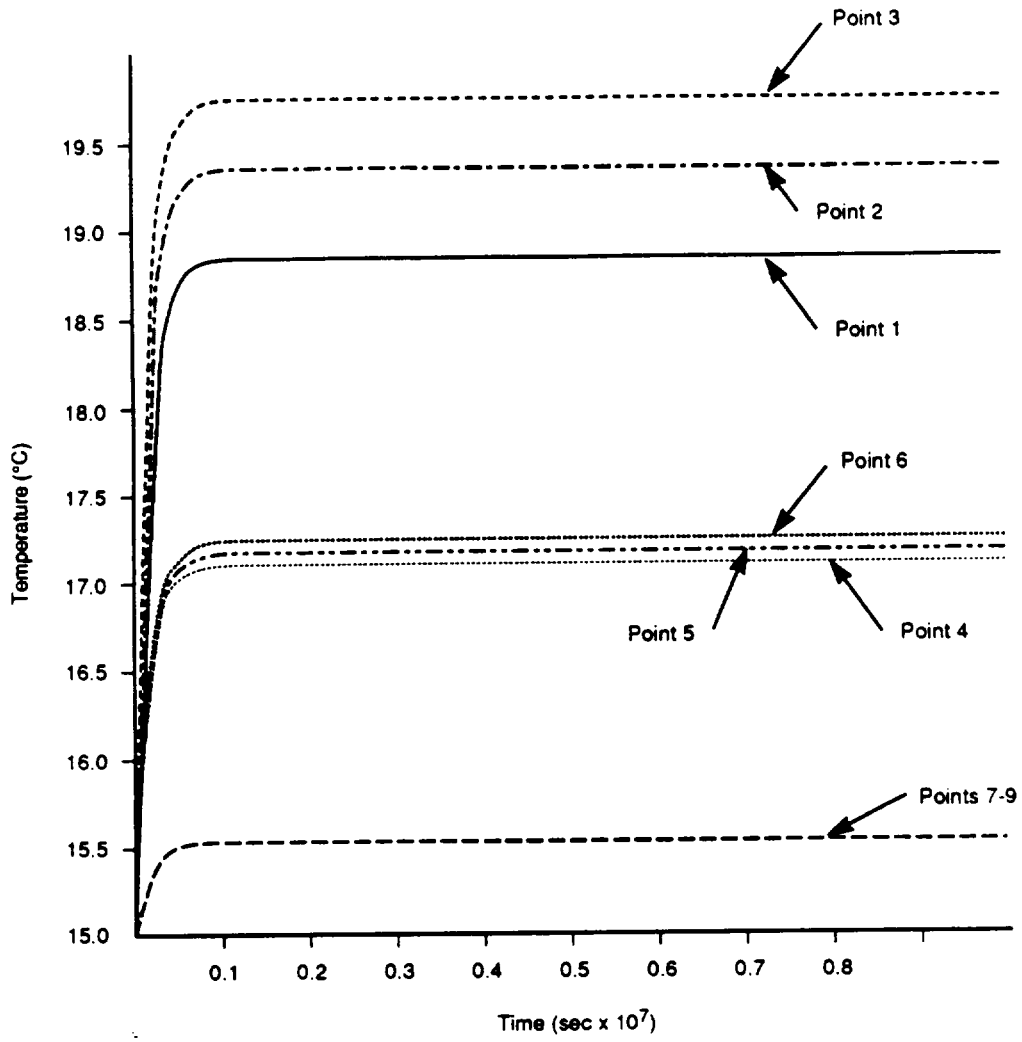

Figure 9. Temperature histories of points 1-9 located at the block centroids for BMT2

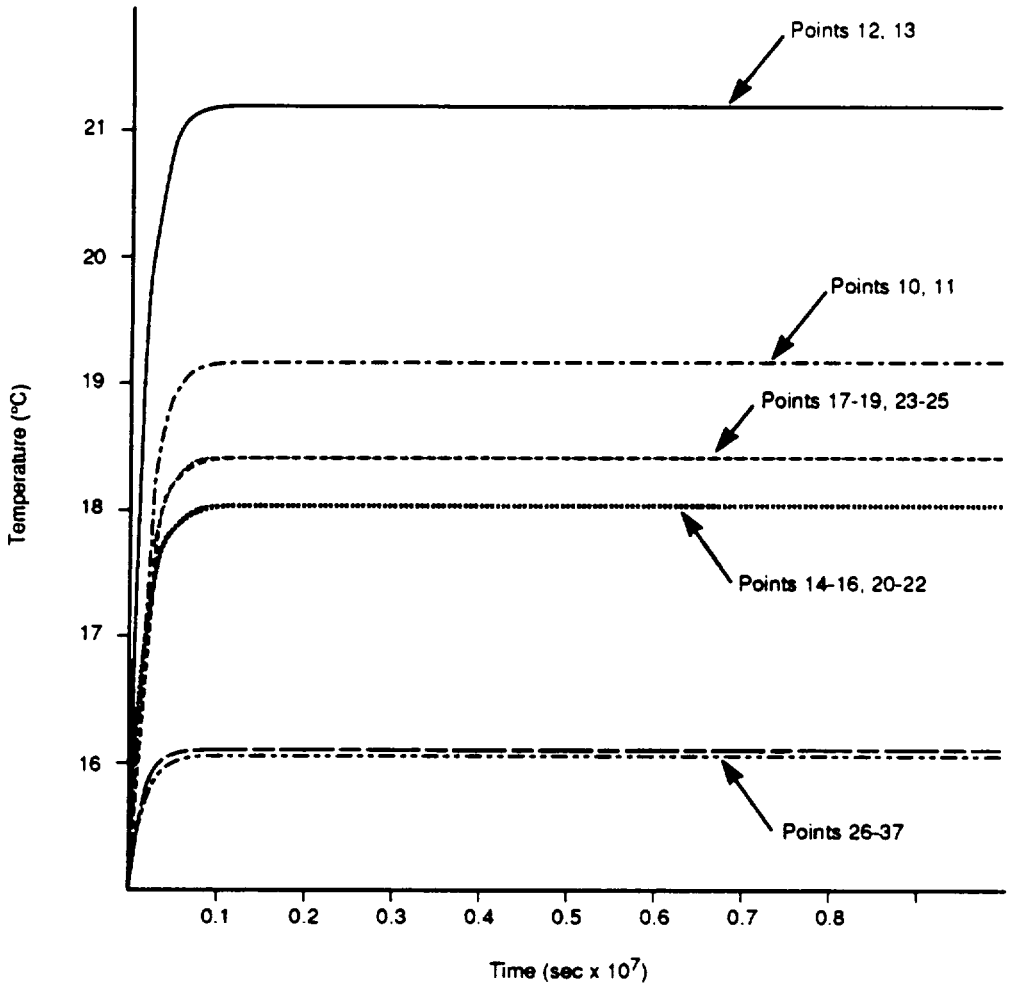

Figure 10. Temperature histories for points 10-41 located at the block corners for BMT2

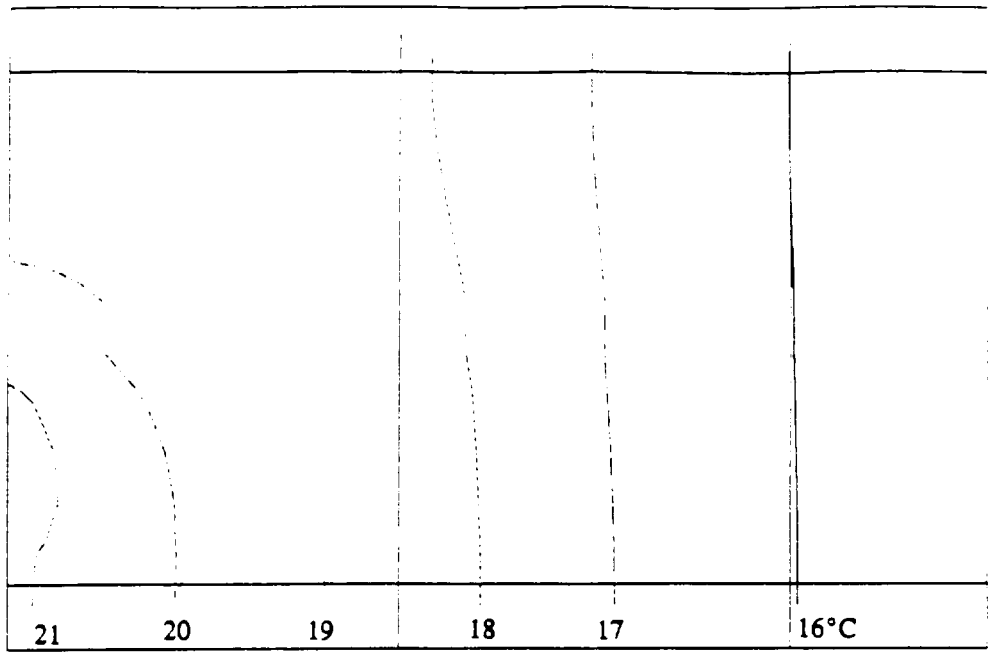

(a)

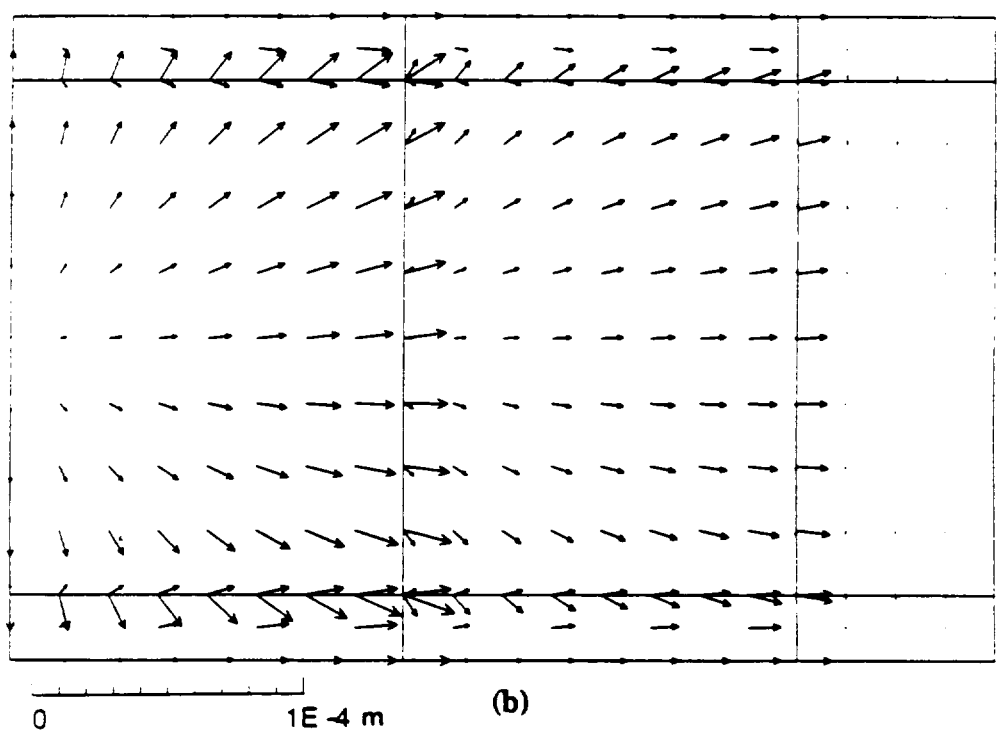

(b)

Figure 11 (a) Temperature contours at time 10^7 seconds for BMT2; (b) Gridpoint displacement vectors at time 10^7 seconds for BMT2

As a result of this, one would expect the temperature distribution shown in Table A.1.1 to be slightly higher than the actual temperature distribution. Section 7.1, containing the discussion of the results of BMT2, further addresses the effect that convective heat transfer in the joints would have on the temperature distribution.

6.2 COUPLED STRESS-FLOW MODEL, TC1

A two-dimensional plane stress analysis of the Coupled Stress-Flow Model was also performed using UDEC. Figure 12 shows the block geometry, monitoring points, and boundary conditions for the model. For this model, the rounding length for the blocks was set to 3 mm, mainly to try to eliminate the formation of new contacts during shear deformation along the joint. The formation of new contacts was not desired, since they would start out with zero normal load. Discretization of the blocks into triangular constant strain finite difference elements is shown in Figure 13. Within the rock, the maximum zone edge length was set to 15 mm, while a slightly larger maximum edge length was used for the epoxy as well as the steel loading plates. All materials were assumed to behave linearly elastic. The Barton-Bandis model was chosen to simulate the behavior of the rock joint. This model assumes a nonlinear stress-displacement relation for the rock joint. It also allows for dilation of the joint during shear deformation. All other interfaces were specified to have a linear stress-displacement relation. Material properties for the rock, steel, and epoxy, as well as rock joint and interface properties are specified in DECOVALEX Doc 91/105 (1991). Fluid flow was allowed only in the rock joint, with all other joints were assumed to be impermeable. The initial conducting aperture along the rock joint was specified at 80 microns. The fluid pressure was fixed at zero at the outlet (point E), while a constant head of 5 meters, or equivalent fluid pressure of 0.05 MPa, was fixed at the inlet (point I) as shown in Figure 12.

The two loading sequences specified for this test case problem are described in detail in DECOVALEX Doc 91/105 (1991). Loading sequence A required applying boundary stresses of equal magnitude to the left and top steel loading plates, to simulate only normal compression on the rock joint. These stresses were applied in increments of 5 MPa up to a maximum stress of 25 MPa, followed by unloading in the same stress increments back to zero. In using the Barton-Bandis model in UDEC, the rock joint is automatically pre-cycled three times in both loading and unloading. Thus, sequence A simulated the fourth loading and unloading cycle for the rock joint. After the first three cycles, much of the hysteresis between the normal loading and unloading versus closure curves for the rock joint is eliminated. Also, very little additional permanent joint closure occurs. At the start of the fourth normal loading cycle, the initial unstressed aperture for the rock joint was 51 microns. After each normal loading or unloading increment, the fluid flow was allowed to reach steady-state within the joint. During the simulation, it was found that in order to apply a normal stress of 25 MPa to the steel plates, the normal stiffnesses along the steel-epoxy and epoxy-epoxy interfaces had to be increased two orders of magnitude over the specified values given by DECOVALEX for this problem, to eliminate large overlaps between the blocks. A small overlap still occurred along the epoxy-epoxy interface, but it was judged to be acceptable.

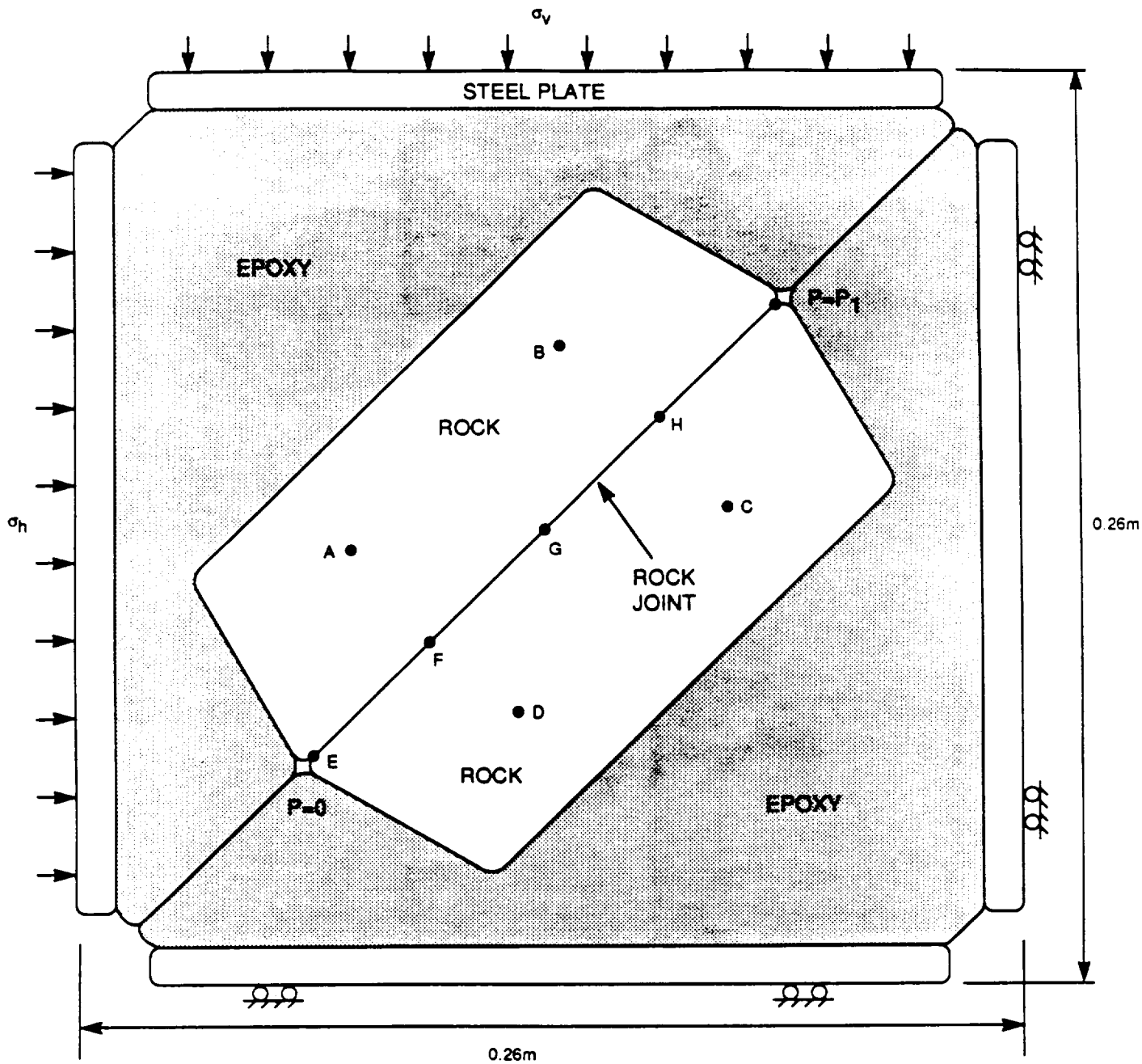

Figure 12. Block geometry for the coupled stress flow model (TC1) showing location of monitoring points

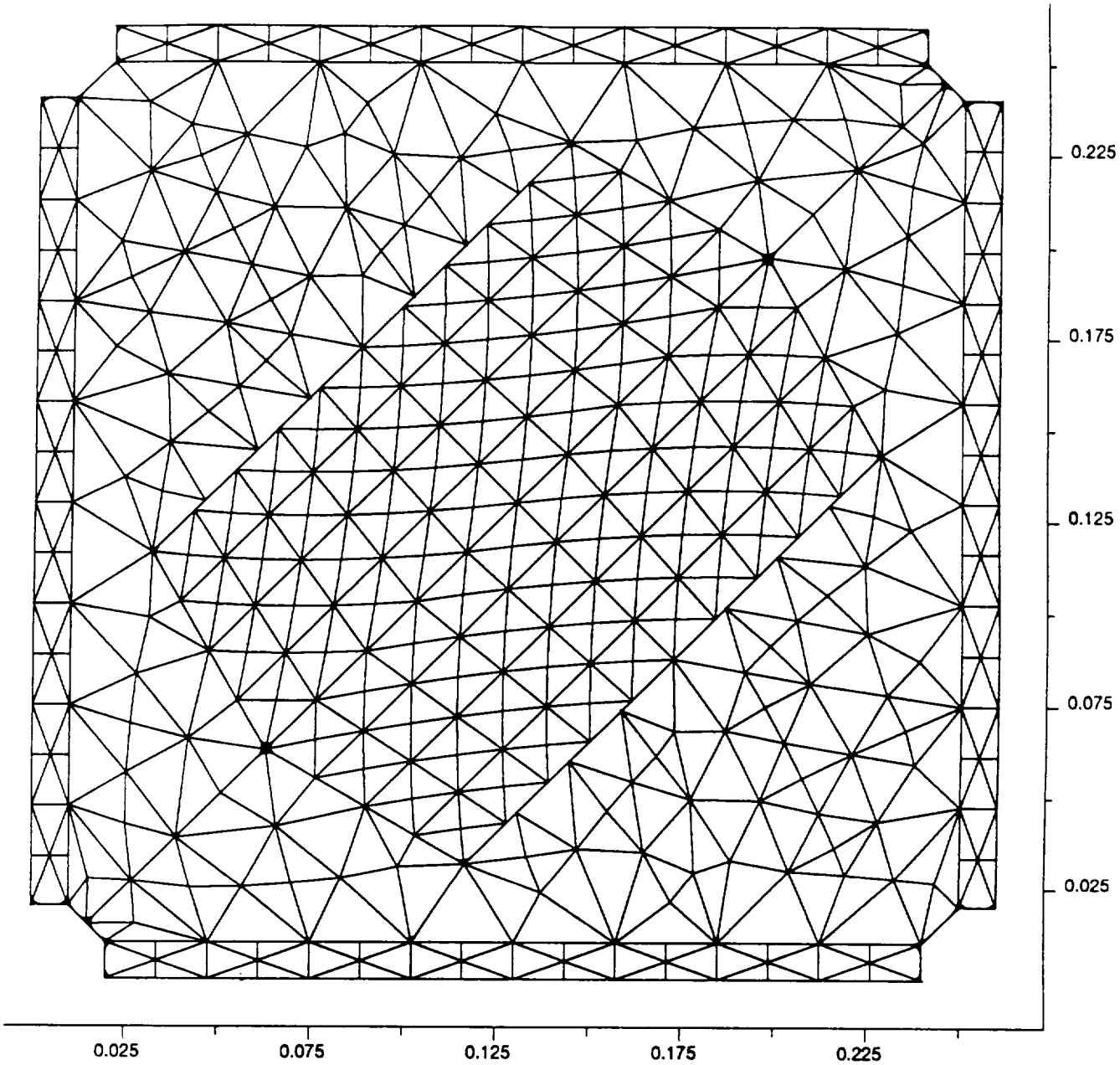

Figure 13. Zone discretization for fully deformable blocks for the coupled stress flow model (TC1)

During the loading increments, some tensile stresses develop in the steel platens, most likely due to the low stiffness of the epoxy in comparison to the modulus of the rock. Also, it was not possible to generate a uniform normal stress distribution along the rock joint by applying stresses of equal magnitude on the left and top loading plates. This is due to stress concentrations that develop at the edges of the rock specimen. For applied boundary loads of 25 MPa, the stress at the center of the joint was approximately 25 MPa. However, at the edges, the stress is approximately 70 MPa. The average normal stress along the joint is therefore somewhat higher than the desired 25 MPa.

Tables A.2.1.-A.2.6. show the numerical results at loading increments 5, 15, 25, 15, 5, and 0 MPa. These tables contain values of stresses and displacements at points within the rock, as well as stresses, displacements, apertures, fluid pressures, and flow rates along the rock joint. Figure 14 shows the average normal stress versus normal displacement at points E through I along the rock joint. The figure shows the normal stiffness increasing nonlinearly with increasing normal stress. It appears uncharacteristic that the unloading path is above the loading path during this fourth compression cycle, based on laboratory observations at the CNWRA. The first three cycles, as observed from using a joint exerciser spreadsheet program for the Barton-Bandis model, appear to correctly show the unloading path below the loading path. Figure 15 shows a similar plot except in this case, the average joint normal stress is plotted against the average normal displacement between points A-D and B-E located within the rock. In this case, both the elastic deformation of the rock as well as joint displacement between these points are considered. Figures 16 and 17 show the average joint normal stress as functions of the average joint aperture and flow rate. The aperture for this fourth cycle begins at 51 microns and decreases nonlinearly with increasing normal stress. After unloading, the final aperture reaches a value of approximately 60 microns. Several small jumps occur in Figures 15-17 during the unloading cycle. They happen when the boundary stresses during unloading reaches a value of around 5 MPa, and it could be attributed to small joint shear displacements or releases of elastic energy stored in the system during the unloading cycle. These small jumps do not appear to have any significant impact on the final apertures, flow rates, etc.

Loading sequence B as described in DECOVALEX Doc 91/195 (1991) consisted of shearing the top block 4 mm downward, followed by shearing 4 mm in the reverse direction while maintaining a constant average normal stress across the joint. This was accomplished by restarting the state from sequence A in which a normal stress of 25 MPa was applied, and then changing from stress to displacement boundaries along the top and left steel plates. During UDEC simulation of sequence B, the shear displacement along the boundaries was not equal to the shear displacement calculated along the rock joint, especially prior to sliding. This is mainly due to the elastic deformation in the different materials, as well as the friction along the joint. Once the joint became mobilized, the boundary shear displacement was approximately equal to the joint displacement. Since the problem specifications appeared to require specific shear displacements along the joint, a trial-and-error approach was required to determine the boundary displacement necessary to get the specified joint displacements.

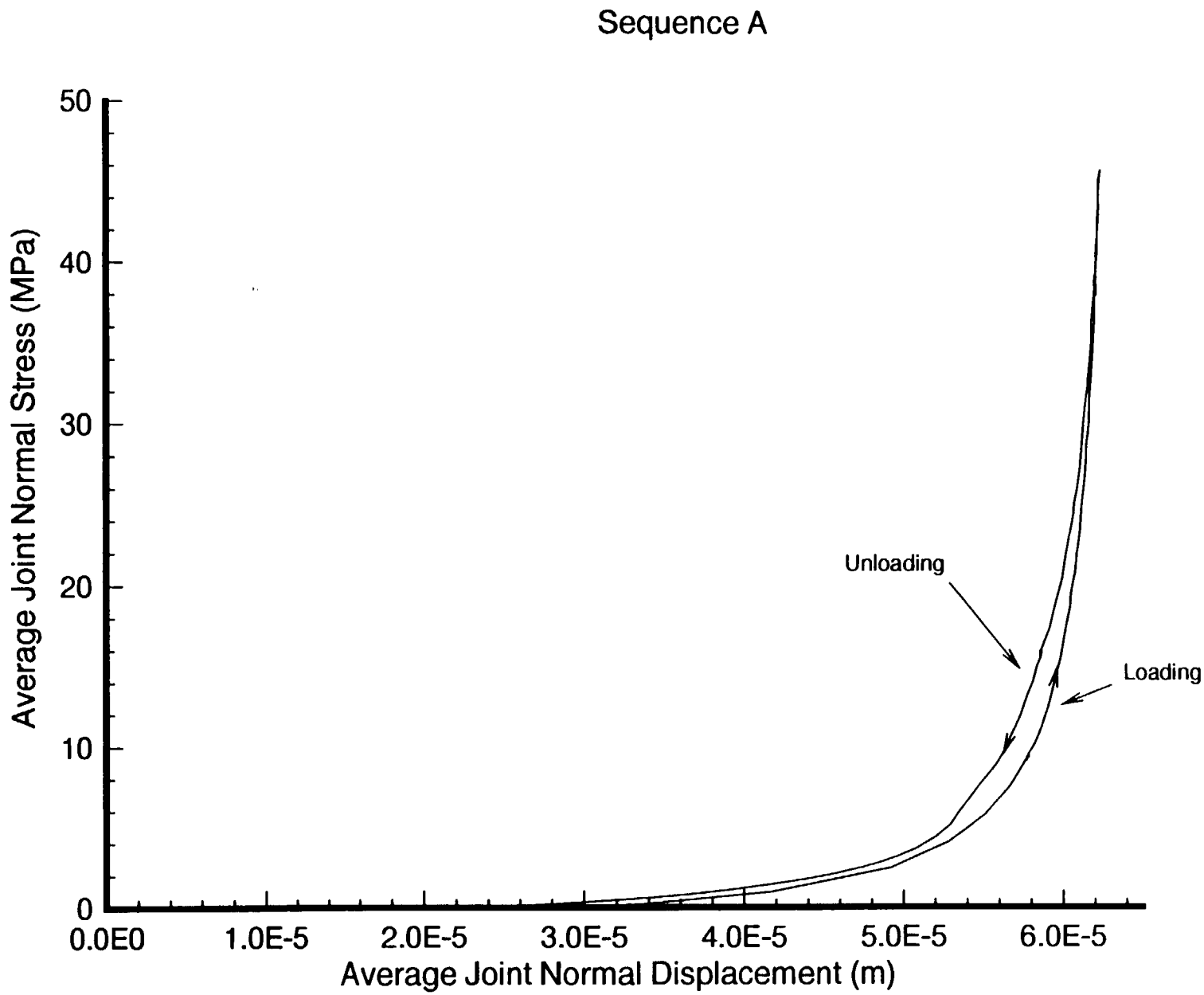

Figure 14. Average joint normal stress versus average normal displacement at points E-I for Sequence A

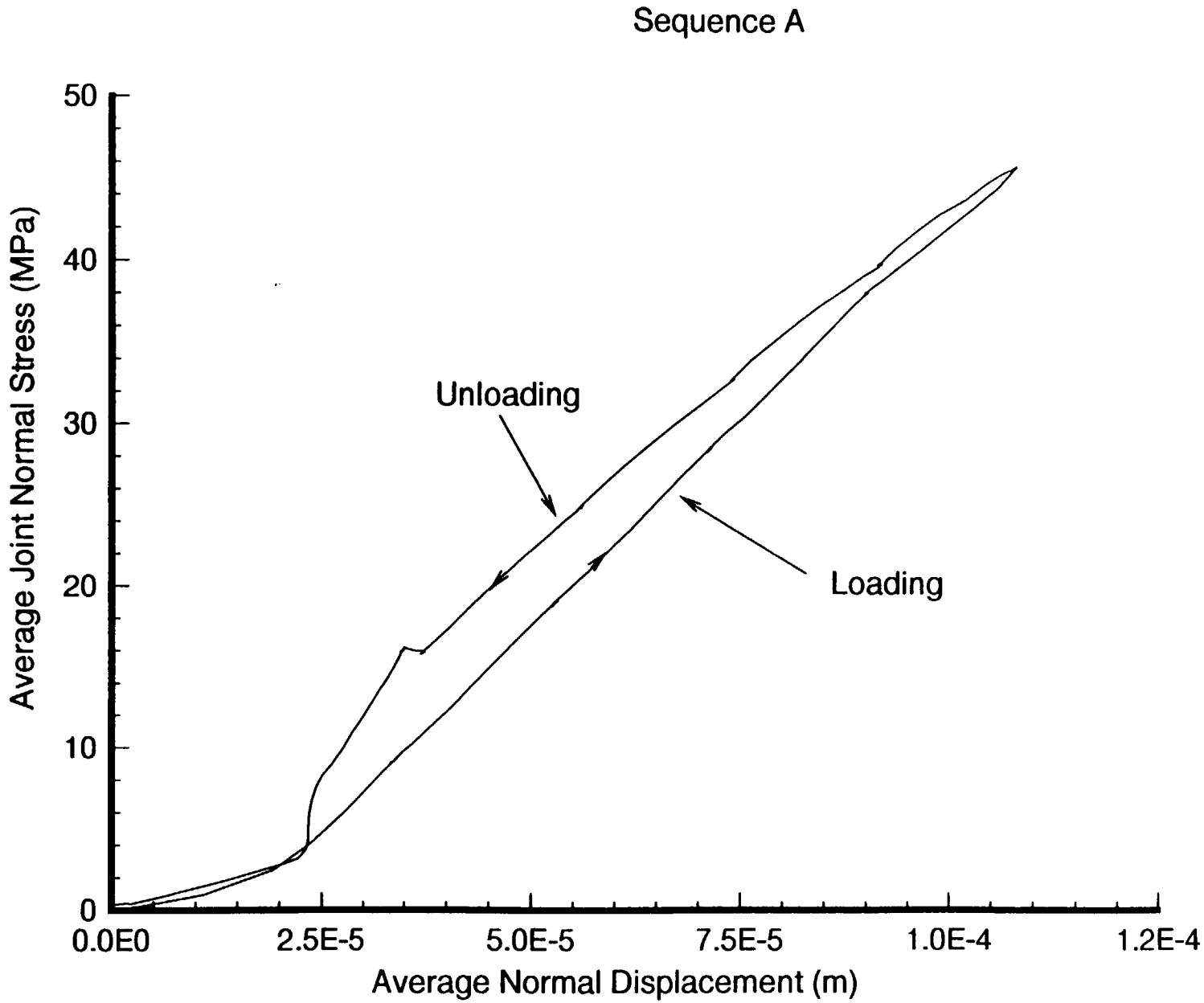

Figure 15. Average joint normal stress versus average normal displacement between points A-D and B-C for Sequence A

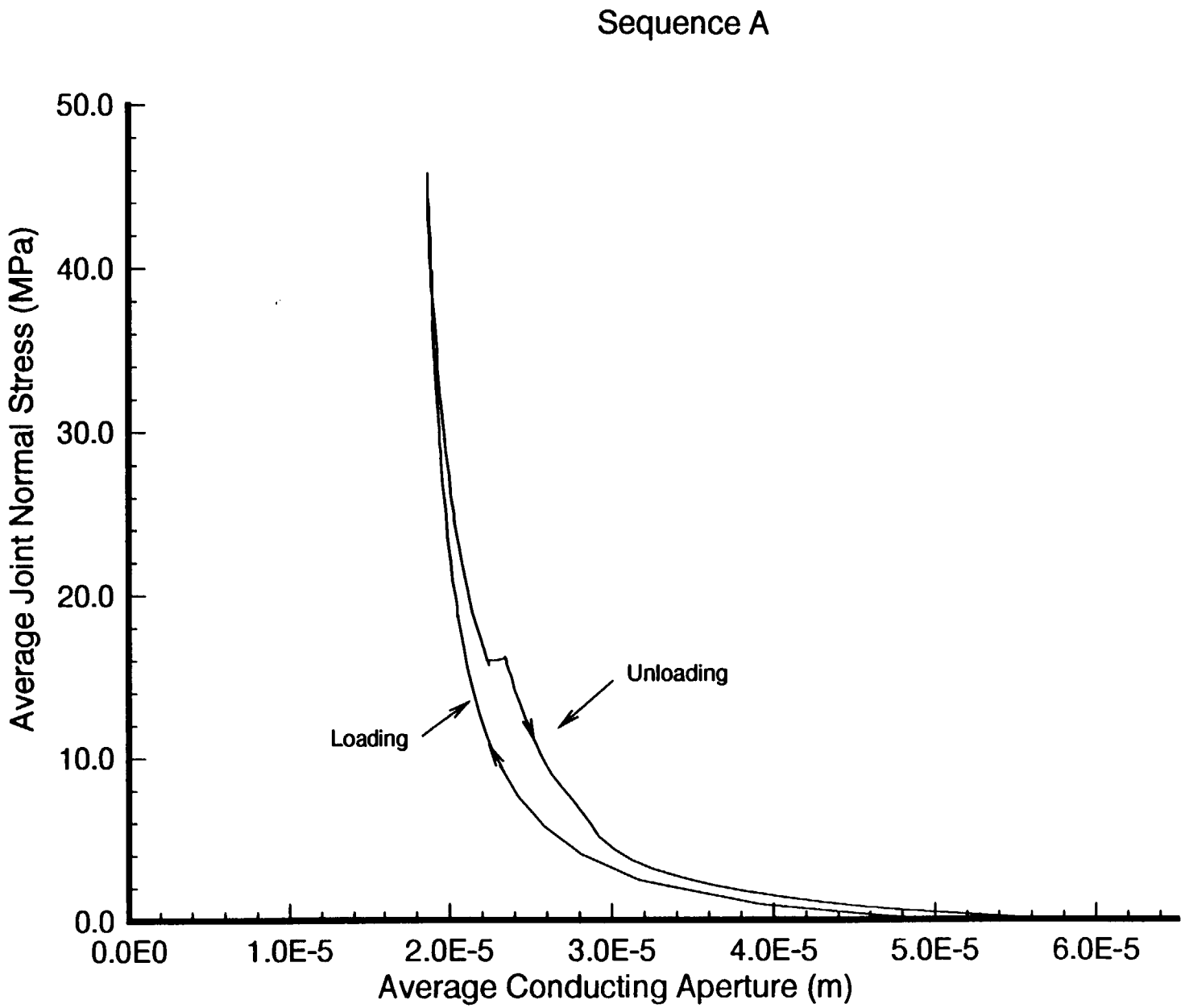

Figure 16. Average normal stress across the joint versus average aperture at points E-I for Sequence A

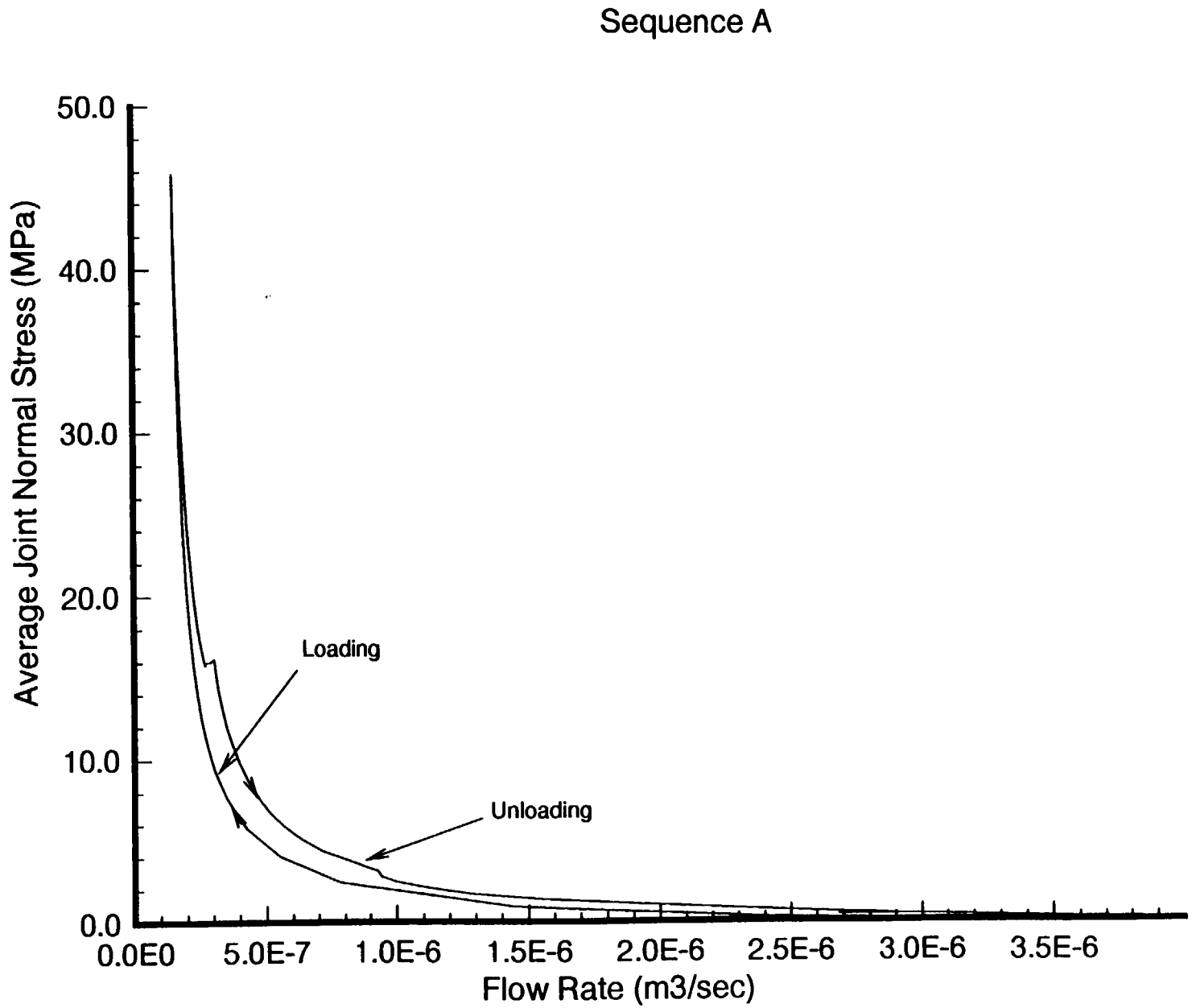

Figure 17. Average normal stress across the joint versus flow rate at the outlet (I) for Sequence A

During shearing, the Barton-Bandis joint model allows for dilation of the joint to take place. For the specified input parameters, the calculated dilation angle over the majority of the 4 mm of shear displacement averaged about 0.5 degrees. In order to account for the joint dilation, the boundary displacements were applied such that the top block was sheared downward at 44.5 degrees below horizontal rather than at 45 degrees. Figure 18 shows the initial normal stress distribution prior to any shear displacement. Tensile stresses are seen to develop in the left and top steel loading plates as a result of using boundary stresses to compress the joint. Even though the normal stiffness along the epoxy/epoxy interface was increased to orders of magnitude, Figure 18 still shows a small amount of overlap occurring along this interface. Even so, this small overlap is not considered to have much effect on the results along the rock joint. Figures 19 and 20 show plots of the principal stress vectors after joint shear displacements of 0.8 and 4 mm, respectively. Rotation of the principal stress vectors in the direction of shearing can be seen in these two figures. Figure 21 shows the average shear stress at points E-I along the joint versus the relative displacements parallel to the joint between points A-D and B-C. In addition, Figures 22 and 23 show the average flow rate and conducting aperture versus shear displacement along the joint. The initial flow rate and conducting aperture at the start of shearing were calculated to be 1.5E-7 m^3/sec and 19 microns, respectively. As a result of dilation, the flow rate and aperture are seen to increase upon shearing in the forward direction, as would be expected. During the reverse shearing, however, a sudden decrease in aperture initially occurs followed by a gradual increase in aperture to a value of 35 microns at the point where the top block is returned back to its original position. The flow rate responds in a similar fashion, and equilibrates to a final value of 9.5E-6 m^3/sec at the completion of shearing. The fact that the flow rate (and aperture) changes very little during the first 0.2 mm is related to the reversal tolerance specified by the user for the analysis. Tables A.2.7.-A.2.12. list the numerical values of stresses, displacements, etc. after joint shear displacement increments corresponding to 0.5, 0.8, 2.0, 4.0, 2.0, and 0 mm. Further discussion of the results from the analysis of TC1 are given in section 7.2.

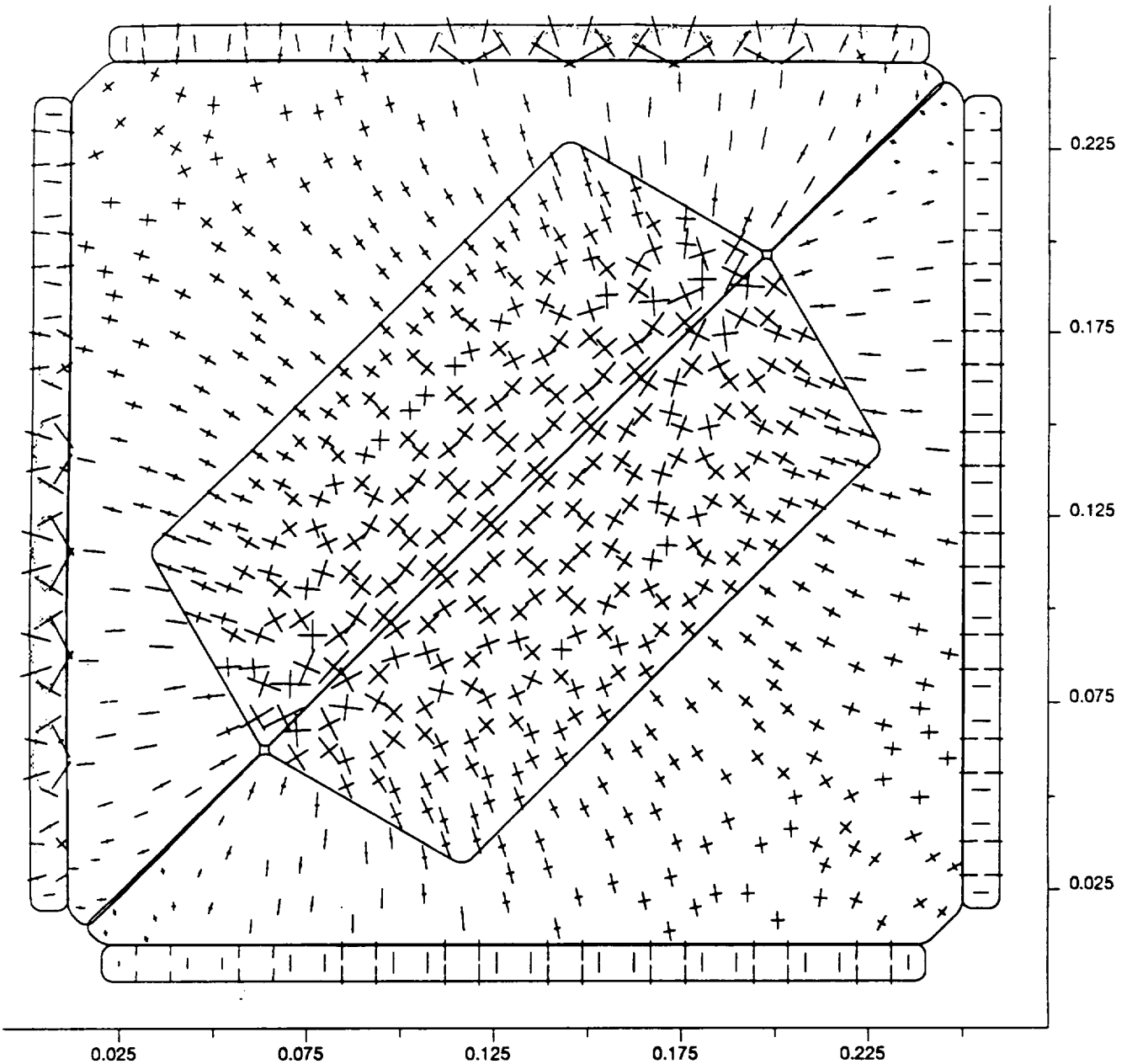

Figure 18. Principal stress vectors corresponding to a joint normal stress of 25 MPa and shear displacement of 0 mm for the coupled stress flow model (TC1)

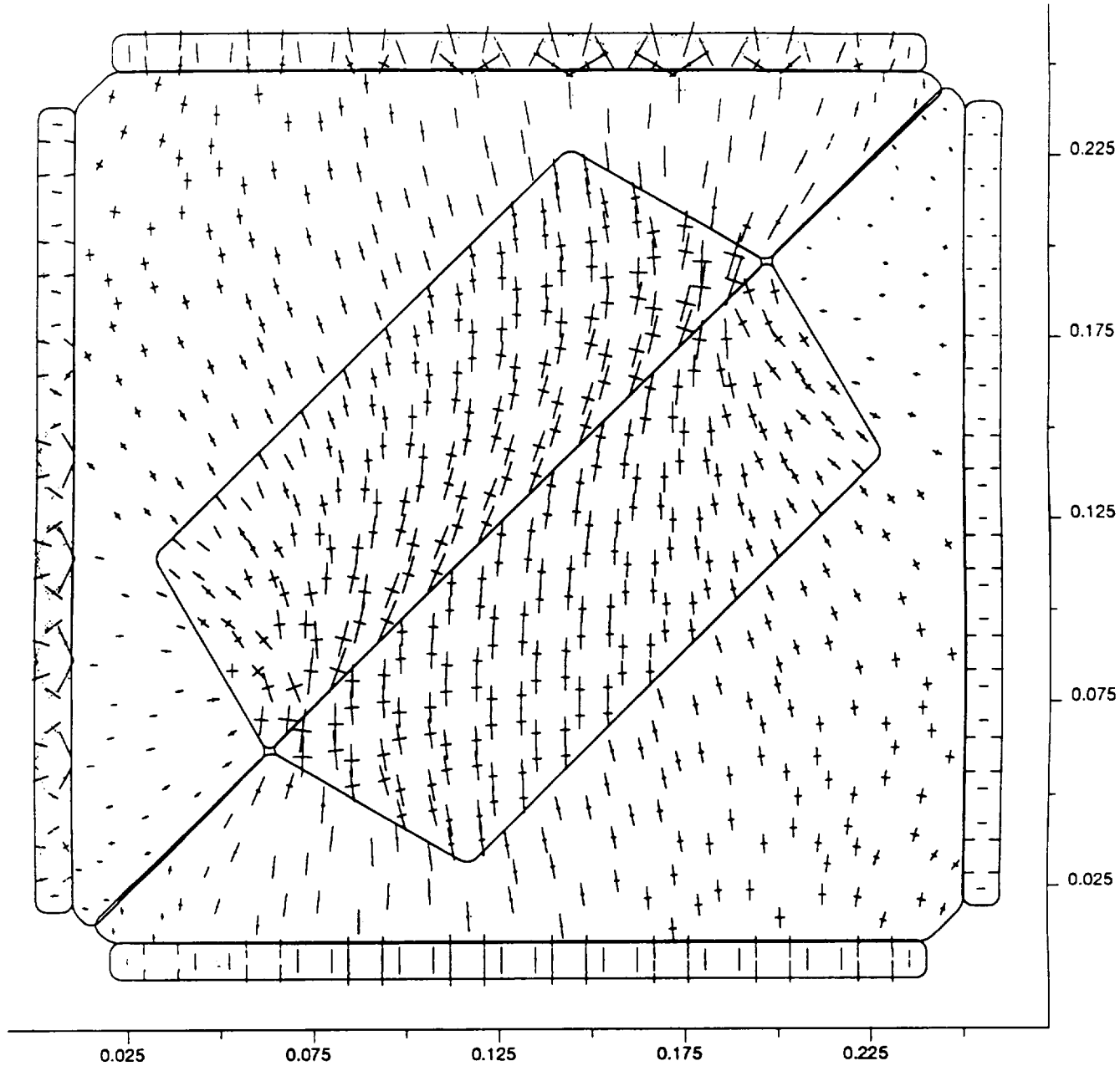

Figure 19. Principal stress vectors corresponding to a joint normal stress of 25 MPa and a shear displacement of 0.8 mm for the coupled stress flow model (TC1)

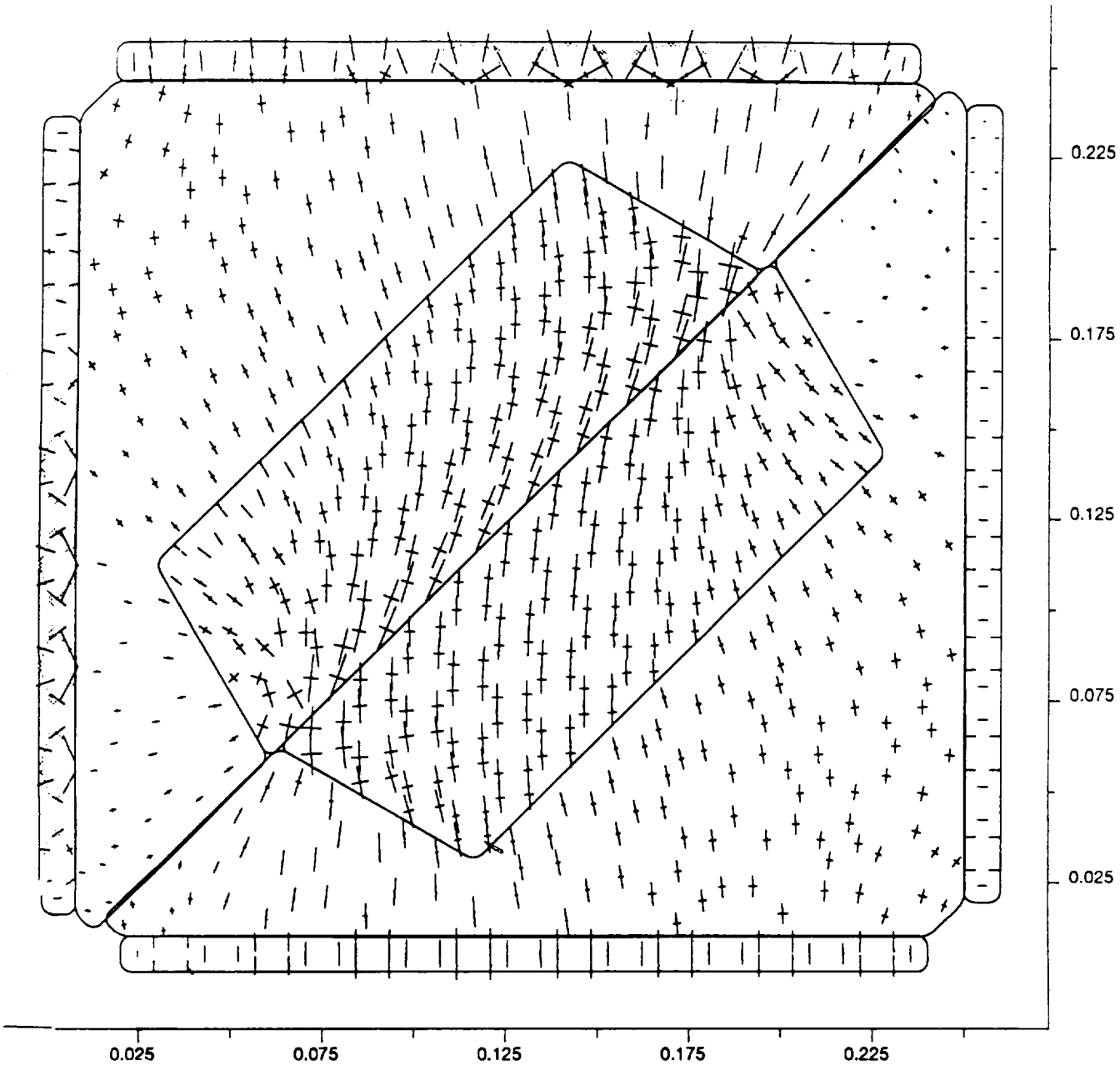

Figure 20. Principal stress vectors corresponding to a joint normal stress of 25 MPa and a joint shear displacement of 4 mm for the coupled stress flow model (TC1)

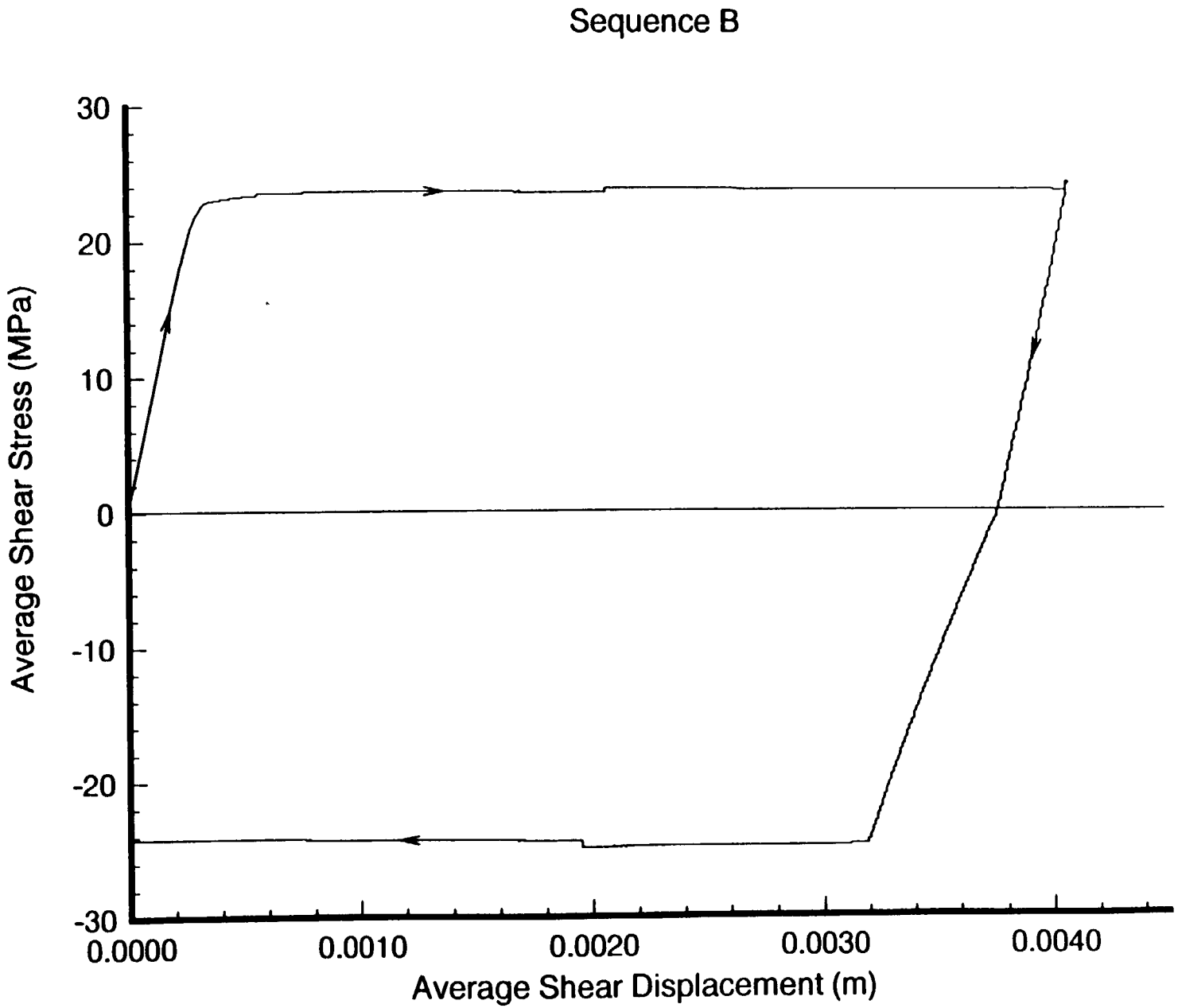

Figure 21. Average shear-stress along joint versus relative displacement of points A-D and B-C parallel to the joint

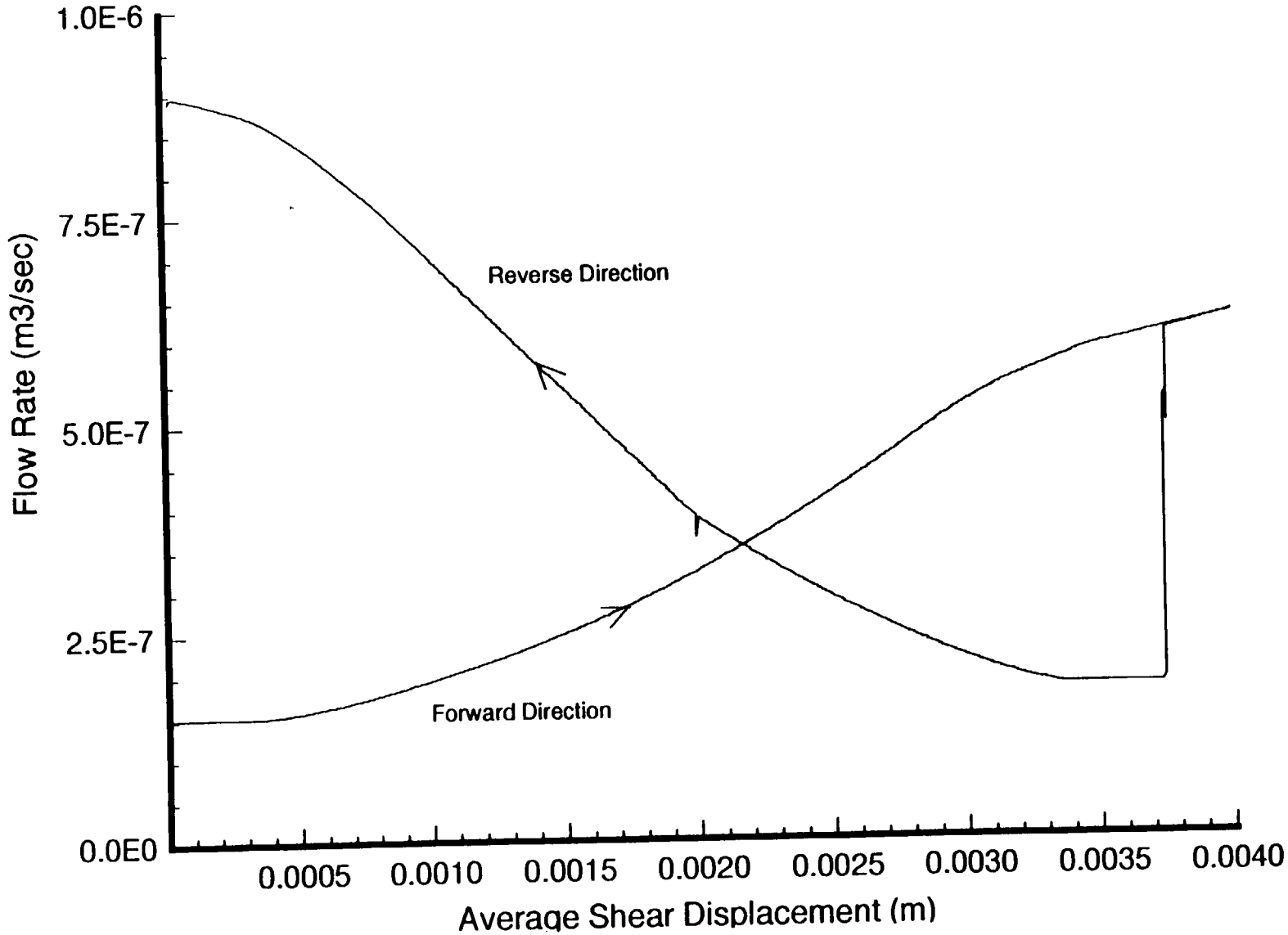

Figure 22. Flow rate at the outlet point (I) as a function of average shear displacement along the joint for Sequence B

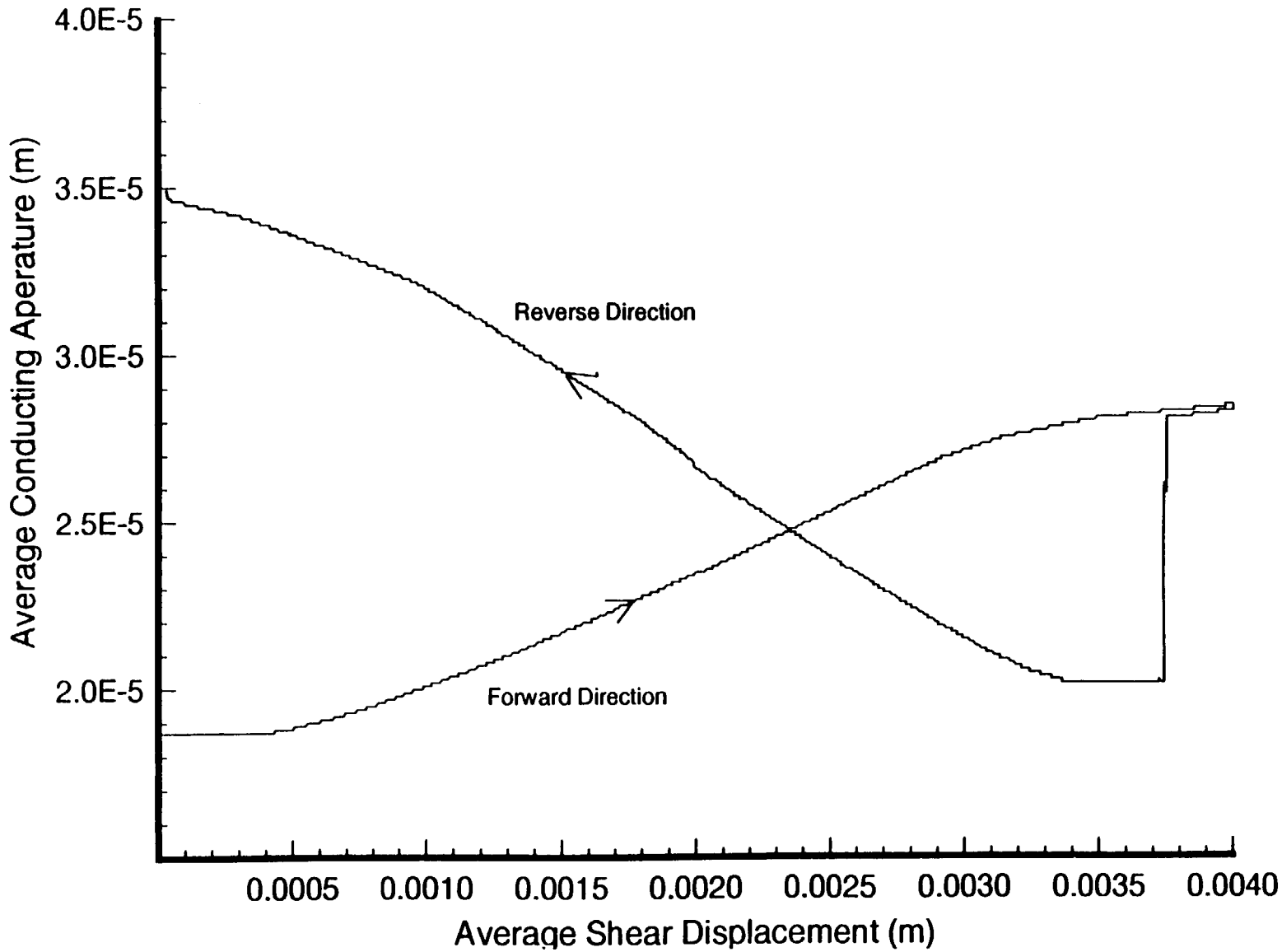

Figure 23. Average conducting aperture versus average shear displacement along the joint for Sequence B

7 DISCUSSION OF THE RESULTS

7.1 MULTIPLE FRACTURE MODEL, BMT2

The results of the BMT2 calculation may be summarized as follows.

- The analysis of Case A showed that throughout the period of thermal loading, the fluid flow remained only in the horizontal joints. The thermal loading did not create enough expansion and rotation in the blocks to initiate flow in the vertical fractures.

- The version of UDEC used for this analysis did not have the capability to input temperature-dependent fluid properties. The values for the fluid density and dynamic viscosity were calculated based on a temperature of 15°. Since the overall temperature changes were small, this approximation was judged acceptable.

The results presented in the previous section and in Tables A.1.1-A.1.6 should be viewed as an upper bound to the true solution for the temperature distribution.. This is because heat transfer caused by forced convection through the fractures is not accounted for in the present formulation of UDEC. If the effect of convection on the rock temperature distribution along the horizontal joints was known, one could then fix these gridpoint temperatures, and come up with a better estimate to the solution which would indirectly take into account the convective heat transfer effects. As a rough estimate of the effect that the convection may have on the maximum increase in the fluid temperature, as well as the maximum temperature increase for the rock along the joints, a simple energy balance and heat transfer relation can be applied.

Suppose, for instance, that all the heat applied to the left boundary was removed as a result of convection heat transfer in the lower horizontal fracture. The maximum temperature rise in the fluid ($\Delta T_{f,max}$) would be related to this thermal loading by:

$$Q = \dot{m} c_p \Delta T_{f,max} \tag{16}$$

where Q = total heat load applied to the boundary per unit depth (W/m)
$\dot{m}$ = mass flow rate through the fracture per unit depth (kg/m-sec)
c_p = specific heat at constant pressure for fluid (J/kg-°C)

The total heat load applied to the model is 12 W/m. The mass flow rate per unit depth can be calculated from the known density (ρ = 1000 Kg/m^3) and mean velocity of the fluid (v=8.902E-3 m/sec), as well as the joint aperture (δ = 300E-6 m). Assuming a value of 4186 J/kg-°C for the specific heat for water, $\Delta T_{f,max}$ for the fluid can be calculated to be approximately 1.07°C. Since the fluid temperature entering the right side of the model is initially at 15°C, the maximum temperature of the fluid exiting the left boundary of the model would be approximately 16.07°C. However, since there is flow in the upper horizontal joint as well as

some conduction through the right boundary, the maximum temperature rise of the fluid would be even less than 1.07°C.

Again assuming that all the heat is transferred out through flow in the lower joint, we can write a simple differential equation relating the convection heat transfer from the rock joint surface with the increase in energy of the fluid. This equation can be expressed as

$$\dot{m}c_p \frac{dT_f(x)}{dx} = h\left[T_r(x) - T_f(x)\right] \tag{17}$$

where h = convective heat transfer coefficient (W/m^2-°C)
T_r = temperature of the rock along the joint (°C)
T_f = temperature of the fluid along the joint (°C)

Both T_r and T_f will, in general, vary along the length of the joint. Writing Eq. (17) in approximate form and solving for the temperature difference between the rock and the fluid gives

$$\left[T_r(x) - T_f(x)\right]_{max} = \frac{\dot{m}c_p}{L} \frac{\Delta T_{f,max}}{h_{min}} \tag{18}$$

where L is the length of the model. Based on hand calculations, h was determined to be approximately 8000 W/m^2-°C for the present problem. This value was reduced to an estimated minimum so that (T_r-T_f) would be a maximum. Based on Table 6.1 of Rohsenow and Choi (1961), the heat transfer coefficient for flowing liquids ranges from 200-6000 W/m^2-°C. Choosing a value of h_{min}=200 W/m^2-°C, the maximum difference in the temperature of the rock at the joint interface and the fluid is calculated to be 0.08°C.

Since the upper bound on the fluid temperature itself was calculated to be 16.07°C, the result of Eq. (18) would indicate that an upper bound on the rock temperature at gridpoint 12 shown in Figure 8(a) would be 16.15°C. As shown in Figure 11a, the temperature at this gridpoint along the lower joint reaches a value of approximately 21°C when only conduction heat transfer through the rock is considered. This would indicate that based on the this particular model geometry and fluid flow rate that heat transfer by convection within the joints would be expected to reduce the temperatures along the joint and change the resultant thermally-induced stress field.

As a lower bound to the solution, a computer run was made in which, for simplicity, gridpoint temperatures along both the upper and lower horizontal joints were fixed to 15°C. Figures 24a and b show the results for the temperature contours and gridpoint displacement vectors, respectively. For this case, the maximum rock temperature is approximately 16.6°C at the left edge of the model, a rise of only 1.6°C. This temperature rise resulted in much less thermally induced stresses and gridpoint displacements.

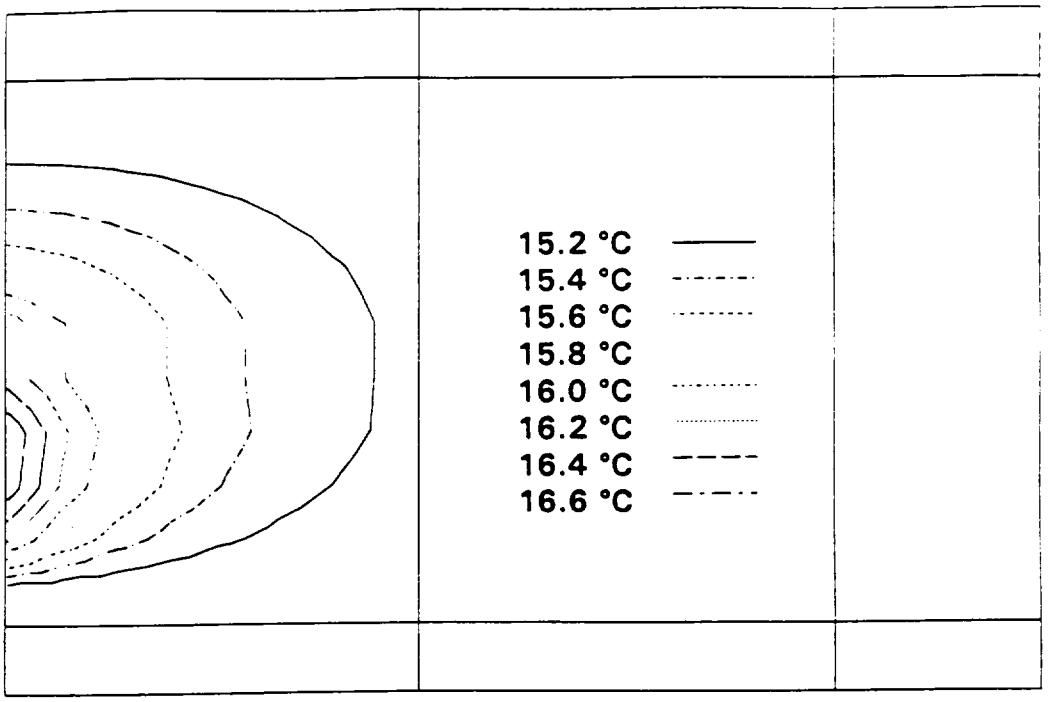

(a)

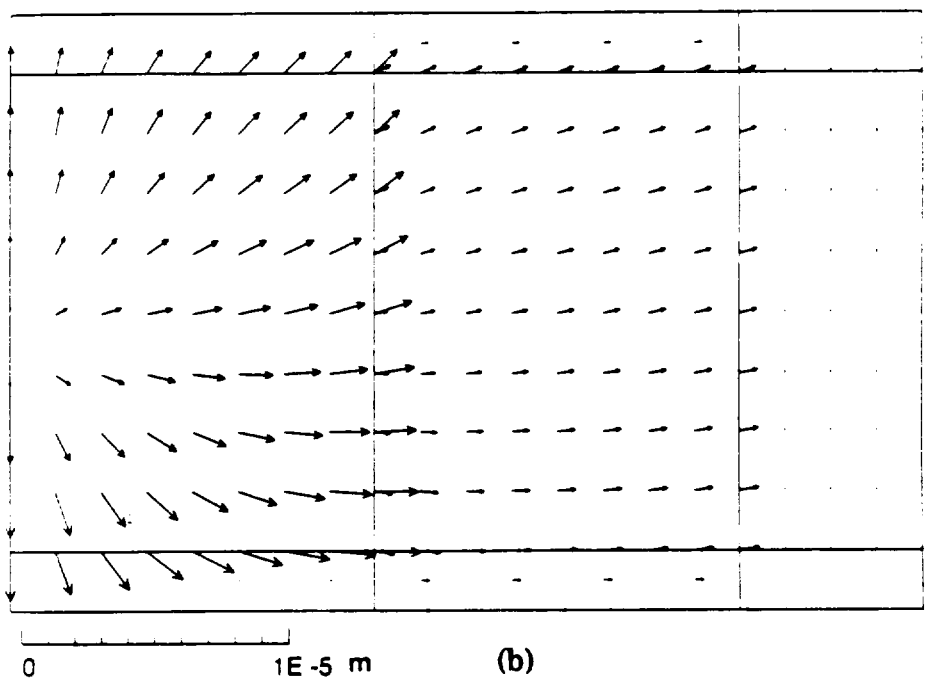

(b)

Figure 24. (a) Temperature contours at time 10^7 seconds as a result of fixing the gridpoint temperatures along the horizontal fractures to 15°C for BMT2 (b) Gridpoint displacement vectors at time 10^7 seconds as a result of fixing the gridpoint temperatures along horizontal fractures to 15°C for BMT2

7.2 COUPLED STRESS-FLOW MODEL, TC1

The results of the TC1 modeling effort raise the following points.

- Distribution of normal stresses across the joint for both load sequences (i.e., normal loading and shear loading) shows a great variation (i.e., a factor of 3). In all cases, the highest normal stresses occur at the ends of the joint, and the least normal stress occurs at the center of the joint. This variation is understandable from a mechanics viewpoint, but it makes interpretation of results (particularly, laboratory results) difficult. For example, average flow rates cannot be related to average normal stresses because flow rates for a single joint are governed by the minimum aperture along the joint length.

- Boundary conditions specified during shearing may influence interpretation of the results (particularly, laboratory results). In the numerical model, displacement boundary conditions were specified such that the normal stress remained constant during shearing. This may not accurately represent actual laboratory conditions, where shear stresses along the joint may lead to block rotation and a change in normal stress distribution along the joint. For example, in constant stress direct shear tests, a higher normal stress is predicted at the leading edge of a sample being sheared.

- Problem geometry involves low stiffness material in this model (or no material in the laboratory test) at the ends of the joint sample, as well as an angular geometry for each half of the rock specimen. In the calculation, the problem geometry leads to bending in the steel nearest the corners of the rock sample. Accurate modeling of the bending in the steel requires a finer discretization in the steel than might be otherwise anticipated.

- Computed changes in joint aperture during reverse shearing do not appear correct. During reverse shearing, the aperture initially decreases and then increases such that the aperture at the end of the reverse shearing is nearly the same as the aperture at the end of the initial 4 mm shear rather than the aperture before shearing. A problem could exist in the joint reversal logic for the Barton-Bandis model.

- The shape of the normal displacement-normal stress curve during unloading appears uncharacteristic for natural rock joint behavior (see Figure 14). During unloading, the normal displacement-normal stress curve is above the loading curve. These results are difficult to understand and do not agree with test results obtained at CNWRA.

- In reviewing various joint consitutive models, Kana et al. (1991) suggested that the piece-wise linear form of the mobilization and attrition of surface roughness

was an unsatisfactory feature of the Barton-Bandis model for practical application. However, results obtained in this study revealed no significant adverse effects of the piece-wise linear formulation. This is most likely due to the fact that the joint roughness coefficient was low (i.e., in essence, the modelled joint was smooth). One place in which the piece-wise linear nature of the Barton-Bandis model is evident is in the reverse shearing shown in Figure 21. This figure clearly shows a change in slope at the point where the shear stress changes sign.

8 RECOMMENDATIONS

8.1 MULTIPLE FRACTURE MODEL, BMT2

The following are recommendations for DECOVALEX regarding the BMT2 problem.

- The applied thermal loading for this model is low, and would appear to represent more of a far-field repository loading. The coupling of thermo-hydro-mechanical processes is primarily a factor associated with the near-field repository environment where the thermal loading would be substantially higher. It would therefore be useful to conduct a similar analysis for higher thermal loadings. A higher thermal loading would induce larger shear displacements along the joints and thermal expansion within the blocks, and may result in flow in the vertical joints.

- Detailed evaluations should be made of the types of coupling required for this test. If these couplings are shown to be relevant, they should be incorporated into UDEC. In particular, the ability to model matrix flow is an important feature to include for further studies of a proposed high-level waste repository at Yucca Mountain.

8.2 COUPLED STRESS-FLOW MODEL, TC1

The following are recommendations for DECOVALEX regarding the TC1 problem.

- Experimental tests such as the coupled-stress flow tests provide invaluable sources of information about the coupled behavior of rock joints. However, the results of such tests cannot be interpreted in terms of average behavior for reasons explained previously in Section 7.2. Tests such as the coupled-stress flow tests should be continued and their results used to continuously improve joint constitutive models. Future tests should include joints of varying roughness so that the effects of roughness (and dilatancy) can be more thoroughly investigated.

- The results of TC1 have raised several questions or inconsistencies about the Barton-Bandis model. An attempt should be made to understand whether the model itself, or its incorporation into UDEC, may be in error.

- Alternative joint models should be considered. One model which could be considered is the continuously-yielding model (Cundall and Lemos, 1990). According to Kana et al. (1991), this model is designed to be a coherent and unified joint model, taking account of nonlinear compression, nonlinearity and dilation in shear, and a nonlinear limiting shear strength criterion.

- It would be beneficial in this model to explicitly model all components of the physical test using best estimates for their properties. In particular, the gaps at the ends of the rock joint in the physical test, should be explicitly represented.

As a general recommendation for all bench-mark and test case problems, consideration should be given to conducting future calculations for the DECOVALEX project in a two-phase process. In the initial phase, parties should submit preliminary results of a few key parameters as well as an explanation of assumptions made. The Secretariat could then quickly review the submittals and provide updated final specifications prior to submittal of final detailed results. The goal of this procedure is to reduce irrelevant difference between parties and permit more meaningful comparison of results.

9 REFERENCES

Barton, N., S. Bandis, and K. Bakhtar. 1985. Strength, deformation and conductivity coupling of rock joints. *Int. J. Rock Mech., Min. Sci., and Geomech. Abstr.* 22(3): 121-140

Barton, N. 1982. *Modeling Rock Joint Behavior from In Situ Block Tests: Implications for Nuclear Waste Repository Design.* ONWI-308. Columbus, Ohio: Office of Nuclear Waste Isolation: 96.

Board, M. 1989. *UDEC (Universal Distinct Element Code) Version ICG1.5.* Vols. 1-3. NUREG/CR-5429. Washington, D.C.: Nuclear Regulatory Commission (NRC).

Brady, B. H. G., M. L. Cramer, and R. D. Hart. 1985. Preliminary analysis of a loading test on a large basalt block. *Int. J. Rock Mech.* 22(5): 345-348.

Brady, B. H. G., S. M. Hsiung, and A. H. Chowdhury. 1990a. Qualification studies on the distinct element code UDEC against some benchmark analytical problems. CNWRA 90-004. San Antonio, Texas: Center for Nuclear Waste Regulatory Analyses (CNWRA).

Brady, B. H., S. H. Hsiung, A. H. Chowdhury, and J. Philip. 1990b. Verification studies on the UDEC computational model of jointed rock. *Mechanics of Jointed and Faulted Rock.* 551-558. Rotterdam: A. A. Balkema.

Christianson, M. 1989. *Sensitivity of the Stability of a Waste Emplacement Drift to Variation in Assumed Rock Joint Parameters in Welded Tuff.* NUREG/CR-5336. Washington, D.C.: NRC.

Cundall, P. A. 1971. *A Computer Model for Simulating Progressive Large Scale Movements in Blocky Rock Systems.* Proceedings of the Symposium of the International Society for Rock Mechanics (Nancy, France, 1971), Vol. 1, Paper No. II-8.

Cundall, P. A. 1980. UDEC - A Generalized Distinct Element Program for Modelling Jointed Rock. Peter Cundall Associates. PCAR-1-80. U.S. Army, European Research Office, Contract DAJA37-79-C-0548.

Cundall, P. A. 1988. Formulation of a three-dimensional distinct element model - part I: A scheme to detect and represent contacts in a system composed of many polyhedral blocks. *Int. J. Rock Mech., Min. Sci. & Geomech. Abstr.* 25: 107-116.

Cundall, P. A., and J. V. Lemos. 1990. Numerical Simulation of Fault Instabilities with the Continuously-Yielding Joint Model. Rockbursts and Seismicity in Mines. 147-152. C. Fairhurst, ed. Rotterdam: A. A. Balkema.

Cundall, P. A., and J. Marti. 1979. *Some New Developments in Discrete Numerical Methods for Dynamic Modelling of Jointed Rock Masses*. Proceedings of the Rapid Excavation and Tunnelling Conference, 1979 (Atlanta, June 1979), Vol. 2: 1466-1477. Baltimore: Port City Press.

Cundall, P. A., and O. D. L. Strack. 1983. Modeling of Microscopic Mechanisms in Granular Material. in Mechanics of Granular Materials: New Models and Constitutive Relations. J. T. Jenkins and M. Satake, eds. Amsterdam: Elsevier Scientific Publications, B.V.

Cundall, P. A., J. Marti, P. Beresford, N. Last, and M. Asgian. 1978. *Computer Modeling of Jointed Rock Masses*. WES-TR-N-78-4. U.S. Army, Engineer Waterways Experiment Station.

DECOVALEX. 1991. Bench-Mark Test 1: Far Field TMH Model. DECOVALEX Doc 91/103. DECOVALEX Secretariat. Stockholm, Sweden:Royal Institute of Technology.

DECOVALEX. 1991. Bench-Mark Test 2: Multiple Fracture Model. DECOVALEX Doc 91/104. DECOVALEX Secretariat. Stockholm, Sweden:Royal Institute of Technology.

DECOVALEX. 1991. Test Case 1: Coupled Stress-Flow Model. DECOVALEX Doc 91/105. DECOVALEX Secretariat. Stockholm, Sweden:Royal Institute of Technology.

Halonen, O. 1989. Stability Calculation in Jointed Rock Mass. Publication No. 57. Helsinki, Finland. Technical Research Center of Finland.

Hart, R. D. 1991. *An Introduction to Distinct Element Modelling for Rock Engineering*. Proceedings of the 7th International Congress on Rock Mechanics (Aachen, Germany, September 1991). Vol. 3; to be published in Comprehensive Rock Engineering, 1992.

Hart, R. D., P. A. Cundall, and M. L. Cramer. 1985. Analysis of a Loading Test on a Large Basalt Block. in Research and Engineering - Applications in Rock Masses. Vol. 2: 759-768. E. Ashworth, ed. Boston: A. A. Balkema.

Hart, R., P. Cundall, and J. Lemos. 1988. Formulation of a three-dimensional distinct element model - part II: Mechanical calculations for motion and interaction of

a system composed of many polyhedral blocks. *Int. J. Rock Mech., Min. Sci. & Geomech. Abstr.* 25: 117-126.

Itasca Consulting Group, Inc. 1991. *UDEC Version 1.7.* Minneapolis, Minnesota: Itasca Consulting Group (ICG).

Johansson, E., M. Hakala, and L. J. Lorig. 1991a. *Rock Mechanical, Thermomechanical and Hydraulic Behavior of the Near Field for Spent Nuclear Fuel.* YJT-91-21. Nuclear Waste Commission of Finnish Power Companies.

Johansson, E., M. Hakala, E. Peltonen, J.-P. Aslo, and L. Lorig. 1991b. *Comparisons of Computed Two- and Three-Dimensional Thermomechanical Response of Jointed Rock.* Proceedings of the 7th International Congress on Rock Mechanics. Rotterdam: A. A. Balkema: 115-119.

Kana, D. D., B. H. G. Brady, B. W. Vanzant, and P. K. Nair. 1990. *Critical Assessment of Seismic and Geomechanics Literature Related to a High-Level Nuclear Waste Underground Repository.* NUREG/CR-5440. Washington, D. C.: NRC.

Karlekar, B. V., and R. M. Desmond. 1982. *Heat Transfer.* 2nd Ed. St. Paul, Minnesota: West Publishing Co.

Kelkar, S., and G. A. Zyvoloski. 1990. An Efficient, Three Dimensional, Fully-Coupled Hydro-Thermo-Mechanical Simulator: FEHMS. LA-UR-90-3750. Los Alamos, New Mexico. Los Alamos National Laboratory (LANL).

Lemos, J. V., and L. J. Lorig. 1990. Hydromechanical modelling of jointed rock masses using the distinct element method. *Mechanics of Jointed and Faulted Rock.* 605-612. Rotterdam: A. A. Balkema.

Lemos, J. V., R. D. Hart, and P. A. Cundall. 1985. *A Generalized Distinct Element Program for Modelling Jointed Rock Mass: A Keynote Lecture.* Proceedings of the International Symposium on Fundamentals of Rock Joints. Lulea, Sweden: Centek Publishers: 335-343.

Lorig, L. J.; and P. A. Cundall. 1987. Modeling of Reinforced Concrete Using the Distinct Element Method. Fracture of Concrete and Rock. 459-471. S. P. Shah and S. E. Swartz, Eds. Bethel, Conn.: SEM.

Lorig, L. J., and B. Dasgupta. 1989. *Analysis of Emplacement Borehole Rock and Liner Behavior for a Repository at Yucca Mountain.* NUREG/CR-5427. Washington, D.C.: NRC.

Mangold, D. C., and C. F. Tsang. 1991. A Summary of Subsurface Hydrological and Hydrochemical Models. Reviews of Geophysics. 29(1): 51-70.

Noorishad, J. and C. F. Tsang. 1989. Recent Enhancement of the Coupled Hydro-Mechanical Code: ROCMASII. Technical Report 89:4. Stockholm, Sweden. Swedish Nuclear Power Inspectorate.

Noorishad, J., C. F. Tsang, and P. A. Witherspoon. 1984. Coupled thermal-hydraulic-mechanical phenomena in saturated fractured porous rock: Numerical approach. *Journal of Geophysical Research*. 89(B12): 10365-10373.

Ohnishi, Y., M. Nishigaki, A. Kobayashi, and S. Akiyama. 1990. Three Dimensional Coupled Thermo-Hydraulic-Mechanical Analysis Code with PCG Method. Proceedings International Symposium. GEOVAL-90. Stockholm, Sweden.

Plesha, M. E., and E. C. Aifantis. 1983. *On the Modeling of Rocks with Microstructure*. Rock Mechanics - Theory-Experiment-Practice Proceedings of the 24th U.S. Symposium on Rock Mechanics, Texas A&M University. New York: Association of Engineering Geologists: 27-35

Rohsenow, W., and H. Choi. 1961. Heat, Mass, and Momentum Transfer. Prentice-Hall Inc.

Shi, G. H. 1990. Forward and Backward Discontinuous Deformation Analyses of Rock Block. Rock Joints. 731-743. Rotterdam: A. A. Balkema.

Stille, H., T. Groth, and A. Fredriksson. 1982. FEM-Analysis of Rock Mechanical Problems with JOBFEM. BeFo and KTH Techncial Report No. 307. Stockholm, Sweden. Swedish Rock Engineering Research Foundation.

Tsang, C. F. 1991. Coupled Hydromechanical-Thermomechanical Process in Rock Fractures. Reviews of Geophysics. 29(4): 537-551.

Voegele, M., E. Hardin, D. Lingle, M. Board, and N. Barton. 1981. *Site Characterization of Joint Permeability Using the Heated Block Test*. Rock Mechanics from Research to Application Proceedings of the 22nd U.S. Symposium on Rock Mechanics (MIT, 1981). Cambridge: Massachusetts Institute of Technology (MIT): 120-127.

Walton, O. R. 1980. *Particle Dynamic Modeling of Geologic Materials*. UCRL-52915. Livermore, California. Lawrence Livermore National Laboratory (LLNL).

Wijesinghe, A. M. 1989. Hydrothermoechanical Simulator Development Task. J. Yow Jr., et al. eds. Repository Technology Program Activities: FY1988. UC1D-2160. Livermore, California. LLNL.

Zimmerman, Roger M., Robert L. Schuch, Donald S. Mason, Michael L. Wilson, Michael E. Hall, Mark P. Board, Robert P. Bellman and Mark L. Blanford. 1986. *Final Report: G-Tunnel Heated Block Experiment*. SAND84-2620. Albuquerque, New Mexico: Sandia National Laboratory (SANDIA).

APPENDIX A: TABULAR OUTPUT FROM UDEC FOR THE BMT2 AND TC1 PROBLEMS

Table A.1.1. TEMPERATURE AT MONITORING POINTS 1-41 FOR BMT2 (Unit: °C)*

Time (sec)	Monitoring Points										
	1	2	3	4	5	6	7	8	9	10,11	12,13
$t = 0$	15.0	15.0	15.0	15.0	15.0	15.0	15.0	15.0	15.0	15.0	15.0
$t = 10$	15.0	15.0	15.0	15.0	15.0	15.0	15.0	15.0	15.0	15.0	15.0
$t = 10^2$	15.0	15.0	15.0	15.0	15.0	15.0	15.0	15.0	15.0	15.0	15.1
$t = 10^3$	15.0	15.0	15.0	15.0	15.0	15.0	15.0	15.0	15.0	15.0	15.4
$t = 10^4$	15.1	15.3	15.5	15.0	15.0	15.0	15.0	15.0	15.0	15.1	16.5
$t = 10^5$	16.7	17.2	17.6	15.8	15.8	15.9	15.2	15.2	15.2	16.9	19.0
$t = 10^6$	18.8	19.3	19.7	17.1	17.2	17.2	15.5	15.5	15.6	19.2	21.2
$t = 10^7$	18.8	19.3	19.7	17.1	17.2	17.2	15.5	15.5	15.6	19.2	21.2

*Note: Since UDEC only takes into account conduction through the rock, the temperatures at points on either side of a joint (i.e., points 10 and 11) will be identical.

The coordinates of points 1-9 are taken at the gridpoint nearest the block centroid. The locations are:

1: (0.15, 0.45)
2: (0.15, 0.25)
3: (0.15, 0.00)
4: (0.45, 0.45)
6: (0.45, 0.0)
7: (0.675, 0.45)
8: (0.675, 0.25)
9: (0.675, 0.00)

Table A.1.1. TEMPERATURE AT MONITORING POINTS 1-41 FOR BMT2 (Unit: °C) (cont'd)

Time (sec)	Monitoring Points									
	14,20	15,16 21,22	17,18 23,24	19,25	26,32	27,28 33,34	29,30 35,36	31,37	38,39	40,41
t = 0	15.0	15.0	15.0	15.0	15.0	15.0	15.0	15.0	15.0	15.0
t = 10	15.0	15.0	15.0	15.0	15.0	15.0	15.0	15.0	15.0	15.0
$t = 10^2$	15.0	15.0	15.0	15.0	15.0	15.0	15.0	15.0	15.0	15.0
$t = 10^3$	15.0	15.0	15.0	15.0	15.0	15.0	15.0	15.0	15.0	15.0
$t = 10^4$	15.0	15.0	15.1	15.1	15.0	15.0	15.0	15.0	15.0	15.0
$t = 10^5$	16.2	16.3	16.6	16.6	15.4	15.4	15.4	15.4	15.0	15.0
$t = 10^6$	18.0	18.0	18.4	18.4	16.1	16.1	16.1	16.1	15.0	15.0
$t = 10^7$	18.0	18.0	18.4	18.4	16.1	16.1	16.1	16.1	15.0	15.0

Table A.1.2. NORMAL STRESSES AT ROCK BLOCK CENTERS FOR BMT2 (POINT 1-9), (* Compressive Stress Negative)

Time	Normal Stress* (MPa)	Monitoring Points								
		1	2	3	4	5	6	7	8	9
t = 0	σ_x	-4.00	-4.00	-4.00	-4.00	-4.00	-4.00	-4.00	-4.00	-4.00
	σ_y	-4.00	-4.00	-4.00	-4.00	-4.00	-4.00	-4.00	-4.00	-4.00
t = 10	σ_x	-3.99	-4.00	-3.99	-3.99	-4.00	-3.99	-3.99	-4.00	-3.99
	σ_y	-4.00	-4.00	-4.00	-4.00	-4.00	-4.00	-4.00	-4.00	-4.00
$t = 10^2$	σ_x	-3.99	-3.99	-3.99	-3.99	-4.00	-3.99	-3.98	-4.00	-3.98
	σ_y	-4.00	-4.00	-4.00	-4.00	-4.00	-4.00	-4.00	-4.00	-4.00
$t = 10^3$	σ_x	-3.99	-4.00	-3.99	-3.99	-4.00	-3.99	-3.98	-4.00	-3.99
	σ_y	-4.00	-3.98	-4.00	-4.00	-4.00	-4.00	-4.00	-4.00	-4.00
$t = 10^4$	σ_x	-3.99	-4.03	-4.01	-3.99	-4.01	-4.00	-3.99	-4.01	-3.99
	σ_y	-4.00	-3.95	-3.98	-4.00	-4.00	-4.00	-4.00	-4.00	-4.00
$t = 10^5$	σ_x	-4.04	-4.12	-4.08	-4.02	-4.06	-4.03	-4.05	-4.04	-4.06
	σ_y	-4.05	-4.02	-4.02	-4.05	-4.00	-4.05	-3.99	-3.97	-3.99
$t = 10^6$	σ_x	-4.11	-4.20	-4.15	-4.07	-4.15	-4.08	-4.13	-4.07	-4.15
	σ_y	-4.11	-4.10	-4.08	-4.12	-4.03	-4.12	-3.98	-3.94	-3.97
$t = 10^7$	σ_x	-4.11	-4.20	-4.15	-4.07	-4.15	-4.08	-4.13	-4.07	-4.15
	σ_y	-4.11	-4.10	-4.08	-4.12	-4.04	-4.12	-3.98	-3.94	-3.97

Table A.1.3. HYDRAULIC HEAD AT MONITORING POINTS 1-41 FOR BMT2 (Unit: m)*

Time (sec)	Monitoring Points								
	A 10,11	B 12,13	C 14,20	D 15,16 21,22	E 17,18 23,24	F 19,25	G 26,32	H 27,28 33,34	I 29,30, 35,36
$t = 0$	1.019	1.019	1.058	1.058	1.058	1.058	1.099	1.099	1.099
$t = 10$	1.019	1.019	1.058	1.058	1.058	1.058	1.099	1.099	1.099
$t = 10^2$	1.019	1.019	1.058	1.058	1.058	1.058	1.099	1.099	1.099
$t = 10^3$	1.019	1.020	1.058	1.058	1.058	1.058	1.099	1.099	1.099
$t = 10^4$	1.020	1.020	1.058	1.058	1.058	1.058	1.099	1.099	1.099
$t = 10^5$	1.020	1.020	1.059	1.059	1.059	1.059	1.100	1.100	1.100
$t = 10^6$	1.020	1.020	1.060	1.060	1.060	1.060	1.100	1.100	1.100
$t = 10^7$	1.020	1.020	1.060	1.060	1.060	1.060	1.100	1.100	1.100

*Note: UDEC assumes flow only in the fractures, thus, no fluid pressures are given at points 1-9 within the blocks. Fluid pressures with the fractures are calculated in domains defined between two contacts. Domain centroids located nearest the specified output locations are given below:

A: (0.002, 0.45)
B: (0.02, 0.05)
C: (0.30, 0.47)
D: (0.30, 0.45)
E: (0.30, 0.05)
F: (0.30, 0.03)
G: (0.60, 0.47)
H: (0.60, 0.45)
I: (0.60, 0.05)
J: (0.60, 0.03)
K: (0.73, 0.45)
L: (0.73, 0.05)

Table A.1.3. HYDRAULIC HEAD AT MONITORING POINTS 1-41 FOR BMT2 (UNIT: m) (cont'd)

Time (sec)	Monitoring Points		
	J 31,37	K 38,37	L 40,41
t = 0	1.099	1.117	1.117
t = 10	1.099	1.117	1.117
$t = 10^2$	1.099	1.117	1.117
$t = 10^3$	1.099	1.117	1.117
$t = 10^4$	1.099	1.117	1.117
$t = 10^5$	1.100	1.117	1.117
$t = 10^6$	1.100	1.117	1.117
$t = 10^7$	1.100	1.117	1.117

Table A.1.4. FLUID VELOCITY AT MONITORING POINTS 42-48 FOR BMT2

Time (sec)	Velocity Components $x10^{-3}$(m/s)	Monitoring Points						
		42	43	44	45	46	47	48
t = 0	V_x	-8.899	-8.898	-8.901	-8.902	-0.905	-8.904	-8.906
	V_y	0.0	0.0	0.0	0.0	0.0	0.0	0.0
t = 10	V_x	-8.898	-8.898	-8.901	-8.901	-8.904	-8.904	-8.906
	V_y	0.0	0.0	0.0	0.0	0.0	0.0	0.0
$t = 10^2$	V_x	-8.897	-8.897	-8.899	-8.899	-8.903	-8.902	-8.904
	V_y	0.0	0.0	0.0	0.0	0.0	0.0	0.0
$t = 10^3$	V_x	-8.898	-8.896	-8.899	-8.895	-8.897	-8.897	-8.898
	V_y	0.0	0.0	0.0	0.0	0.0	0.0	0.0
$t = 10^4$	V_x	-8.891	-8.890	-8.899	-8.859	-8.863	-8.856	-8.857
	V_y	0.0	0.0	0.0	0.0	0.0	0.0	0.0
$t = 10^5$	V_x	-8.768	-8.753	-8.742	-8.625	-8.598	-8.563	-8.556
	V_y	0.0	0.0	0.0	0.0	0.0	0.0	0.0
$t = 10^6$	V_x	-8.578	-8.554	-8.521	-8.358	-8.287	-8.215	-8.196
	V_y	0.0	0.0	0.0	0.0	0.0	0.0	0.0
$t = 10^7$	V_x	-8.576	-8.553	-8.520	-8.358	-8.286	-8.216	-8.197
	V_y	0.0	0.0	0.0	0.0	0.0	0.0	0.0

Table A.1.5. FLUID VELOCITY AT MONITORING POINTS 49-55 FOR BMT2

Time (sec)	Velocity Components $x10^{-3}$(m/s)	Monitoring Points						
		49	50	51	52	53	54	55
t = 0	V_x	-8.899	-8.898	-8.901	-8.902	-8.905	-8.904	-8.906
	V_y	0.0	0.0	0.0	0.0	0.0	0.0	0.0
t = 10	V_x	-8.900	-8.900	-8.902	-8.902	-8.904	-8.905	-8.906
	V_y	0.0	0.0	0.0	0.0	0.0	0.0	0.0
$t = 10^2$	V_x	-8.903	-8.900	-8.902	-8.902	-8.904	-8.904	-8.906
	V_y	0.0	0.0	0.0	0.0	0.0	0.0	0.0
$t = 10^3$	V_x	-8.918	-8.899	-8.894	-8.900	-8.901	-8.901	-8.903
	V_y	0.0	0.0	0.0	0.0	0.0	0.0	0.0
$t = 10^4$	V_x	-8.962	-8.890	-8.834	-8.865	-8.861	-8.868	-8.868
	V_y	0.0	0.0	0.0	0.0	0.0	0.0	0.0
$t = 10^5$	V_x	-8.855	-8.753	-8.638	-8.633	-8.583	-8.579	-8.571
	V_y	0.0	0.0	0.0	0.0	0.0	0.0	0.0
$t = 10^6$	V_x	-8.665	-8.553	-8.417	-8.364	-8.270	-8.231	-8.210
	V_y	0.0	0.0	0.0	0.0	0.0	0.0	0.0
$t = 10^7$	V_x	-8.661	-8.549	-8.414	-8.362	-8.268	-8.230	-8.209
	V_y	0.0	0.0	0.0	0.0	0.0	0.0	0.0

Table A.1.6. DISPLACEMENT COMPONENTS AT MONITORING POINTS 1-41 FOR BMT2

Time (sec)	Displ. Components (m)	Monitoring Points						
		1	2	3	4	5	6	7
t = 0	u_x	0.00	0.00	0.00	0.00	0.00	0.00	0.00
	u_y	0.00	0.00	0.00	0.00	0.00	0.00	0.00
t = 10	u_x	1.477E-11	1.275E-9	7.871E-10	1.49E-8	6.932E-9	-9.53E-10	1.109E-13
	u_y	4.511E-12	1.594E-8	-3.350E-11	6.405E-13	9.222E-9	-2.107E-12	-5.180E-12
$t = 10^2$	u_x	7.848E-11	1.287E-8	8.470E-9	2.393E-8	1.891E-8	1.491E-8	-1.056E-11
	u_y	4.319E-11	3.470E-8	-2.782E-10	1.072E-11	2.351E-8	1.105E-11	6.413E-12
$t = 10^3$	u_x	1.011E-9	1.287E-7	1.309E-7	4.031E-8	7.539E-8	7.680E-8	2.302E-10
	u_y	3.461E-10	9.286E-8	2.770E-9	6.459E-11	6.058E-8	1.540E-10	2.360E-11
$t = 10^4$	u_x	1.278E-7	1.032E-6	1.393E-6	2.859E-7	6.802E-7	1.021E-6	4.904E-9
	u_y	-1.623E-8	4.594E-7	1.962E-7	-3.321E-10	2.088E-7	7.530E-9	-2.433E-11
$t = 10^5$	u_x	2.611E-6	4.750E-6	4.708E-6	3.482E-6	4.187E-6	4.934E-6	-8.824E-8
	u_y	-5.330E-7	8.324E-7	8.875E-7	-2.721E-7	4.261E-7	3.349E-7	-8.688E-8
$t = 10^6$	u_x	5.611E-6	8.665E-6	7.709E-6	7.130E-6	7.932E-6	8.8574E-6	-3.203E-7
	u_y	-1.182E-6	8.342E-7	1.536E-6	-7.088E-7	4.278E-7	7.717E-7	-2.479E-7
$t = 10^7$	u_x	5.628E-6	8.689E-6	7.724E-6	7.165E-6	7.970E-6	8.616E-6	-3.220E-7
	u_y	-1.184E-6	8.152E-7	1.538E-6	-7.110E-7	4.101E-7	7.722E-7	-2.481E-7

Table A.1.6. DISPLACEMENT COMPONENTS AT MONITORING POINTS 1-41 FOR BMT2 (cont'd)

Time (sec)	Displ. Components (m)	Monitoring Points						
		8	9	10	11	12	13	14
t = 0	u_x	0.00	0.00	0.00	0.00	0.00	0.00	0.00
	u_y	0.00	0.00	0.00	0.00	0.00	0.00	0.00
t = 10	u_x	1.287E-11	-1.029E-13	0.00	0.00	0.00	0.00	1.235E-11
	u_y	2.821E-9	4.318E-13	5.882E-12	1.596E-8	7.387E-9	9.900E-10	0.00
$t = 10^2$	u_x	1.299E-10	8.543E-11	0.00	0.00	0.00	0.00	1.495E-10
	u_y	1.385E-8	1.251E-11	7.551E-11	3.496E-8	-4.631E-8	1.029E-8	0.00
$t = 10^3$	u_x	9.414E-10	1.701E-9	0.00	0.00	0.00	0.00	2.670E-9
	u_y	4.107E-8	1.631E-10	6.279E-10	1.050E-7	-5.247E-7	1.055E-7	0.00
$t = 10^4$	u_x	9.289E-9	2.118E-8	0.00	0.00	0.00	0.00	2.276E-7
	u_y	1.279E-7	1.975E-9	-4.621E-8	8.897E-7	-2.635E-6	7.365E-7	0.00
$t = 10^5$	u_x	-1.398E-8	-7.497E-8	0.00	0.00	0.00	0.00	6.135E-6
	u_y	2.434E-7	1.018E-7	-1.144E-6	5.798E-6	-8.090E-6	2.229E-6	0.00
$t = 10^6$	u_x	-9.754E-8	-3.073E-7	0.00	0.00	0.00	0.00	1.365E-5
	u_y	2.450E-7	2.629E-7	-2.481E-6	1.115E-5	-1.344E-5	3.567E-6	0.00
$t = 10^7$	u_x	-9.924E-8	-3.073E-7	0.00	0.00	0.00	0.00	1.368E-5
	u_y	2.272E-7	2.637E-7	-2.490E-6	1.117E-5	-1.349E-5	3.573E-6	0.00

Table A.1.6. DISPLACEMENT COMPONENTS AT MONITORING POINTS 1-41 FOR BMT2 (cont'd)

Time (sec)	Displ. Components (m)	Monitoring Points						
		15	16	17	18	19	20	21
t = 0	u_x	0.00	0.00	0.00	0.00	0.00	0.00	0.00
	u_y	0.00	0.00	0.00	0.00	0.00	0.00	0.00
t = 10	u_x	1.225E-11	-1.390E-11	3.813E-9	8.576E-10	8.474E-10	1.490E-8	1.490E-8
	u_y	-4.310E-13	1.699E-8	1.743E-8	-6.775E-12	0.00	0.00	-2.799E-12
$t = 10^2$	u_x	1.647E-10	2.052E-10	3.655E-8	8.885E-9	8.821E-9	2.392E-8	2.391E-8
	u_y	9.571E-11	4.464E-8	4.836E-8	1.006E-10	0.00	0.00	2.660E-11
$t = 10^3$	u_x	2.807E-9	1.133E-8	3.475E-7	1.377E-7	1.373E-7	4.006E-8	4.013E-8
	u_y	1.294E-9	1.819E-7	2.161E-7	1.362E-9	0.00	0.00	7.007E-11
$t = 10^4$	u_x	2.322E-7	4.620E-7	2.806E-6	2.087E-6	2.063E-6	2.765E-7	2.783E-7
	u_y	2.787E-9	1.147E-6	9.920E-7	6.782E-8	0.00	0.00	-5.864E-9
$t = 10^5$	u_x	6.178E-6	6.795E-6	1.097E-5	9.827E-6	9.752E-6	2.028E-6	2.067E-6
	u_y	-7.562E-7	5.373E-6	-2.067E-6	1.039E-6	0.00	0.00	-7.328E-7
$t = 10^6$	u_x	1.372E-5	1.455E-5	1.873E-5	1.737E-5	1.727E-5	3.481E-6	3.558E-6
	u_y	-1.859E-6	9.909E-6	-6.599E-6	2.142E-6	0.00	0.00	-1.800E-6
$t = 10^7$	u_x	1.375E-5	1.460E-5	1.878E-5	1.740E-5	1.730E-5	3.504E-6	3.583E-6
	u_y	-1.860E-6	9.924E-6	-6.650E-6	2.150E-6	0.00	0.00	-1.808E-6

Table A.1.6. DISPLACEMENT COMPONENTS AT MONITORING POINTS 1-41 FOR BMT2 (cont'd)

Time (sec)	Displ. Components (m)	Monitoring Points						
		22	23	24	25	26	27	28
t = 0	u_x	0.00	0.00	0.00	0.00	0.00	0.00	0.00
	u_y	0.00	0.00	0.00	0.00	0.00	0.00	0.00
t = 10	u_x	1.496E-8	-1.077E-9	-9.473E-10	-9.526E-10	1.490E-8	1.490E-8	1.494E-8
	u_y	1.526E-8	1.527E-8	7.069E-12	0.00	0.00	4.446E-12	3.189E-9
$t = 10^2$	u_x	2.328E-8	1.577E-8	1.500E-8	1.499E-8	2.395E-8	2.395E-8	2.319E-8
	u_y	2.691E-8	2.638E-8	4.586E-11	0.00	0.00	1.124E-11	2.014E-8
$t = 10^3$	u_x	5.803E-8	9.861E-8	7.816E-8	7.808E-8	4.038E-8	4.049E-8	5.751E-8
	u_y	4.967E-8	4.745E-8	2.833E-10	0.00	0.00	4.041E-10	7.128E-8
$t = 10^4$	u_x	4.821E-7	9.262E-7	9.884E-7	9.806E-7	2.842E-7	2.851E-7	4.703E-7
	u_y	1.127E-7	-5.661E-8	4.520E-8	0.00	0.00	2.471E-9	3.538E-7
$t = 10^5$	u_x	2.700E-6	3.267E-6	3.205E-6	3.144E-6	4.791E-6	4.826E-6	5.405E-6
	u_y	3.302E-6	-3.357E-6	9.526E-7	0.00	0.00	-2.440E-7	1.728E-5
$t = 10^6$	u_x	4.439E-6	5.010E-6	4.697E-6	4.598E-6	1.074E-5	1.082E-5	1.170E-5
	u_y	7.639E-6	-7.695E-6	2.021E-6	0.00	0.00	-7.001E-7	3.598E-6
$t = 10^7$	u_x	4.461E-6	5.027E-6	4.730E-6	4.629E-6	1.078E-5	1.087E-5	1.175E-5
	u_y	7.644E-6	-7.730E-6	2.023E-6	0.00	0.00	-7.017E-7	3.602E-6

Table A.1.6. DISPLACEMENT COMPONENTS AT MONITORING POINTS 1-41 FOR BMT2 (cont'd)

Time (sec)	Displ. Components (m)	Monitoring Points						
		29	30	31	32	33	34	35
t = 0	u_x	0.00	0.00	0.00	0.00	0.00	0.00	0.00
	u_y	0.00	0.00	0.00	0.00	0.00	0.00	0.00
t = 10	u_x	-1.067E-9	-9.534E-10	-9.587E-10	3.885E-12	-3.162E-12	9.362E-13	-2.542E-12
	u_y	3.202E-9	-2.645E-12	0.00	0.00	-9.865E-14	2.816E-9	2.842E-9
$t = 10^2$	u_x	1.504E-8	1.473E-8	1.472E-8	-1.386E-11	-2.554E-11	6.595E-12	-7.307E-12
	u_y	2.031E-8	1.853E-11	0.00	0.00	2.486E-11	1.385E-8	1.389E-8
$t = 10^3$	u_x	9.007E-8	7.401E-8	7.397E-8	2.993E-10	2.921E-10	1.108E-9	2.220E-9
	u_y	6.988E-8	5.514E-10	0.00	0.00	5.866E-11	4.160E-8	4.017E-8
$t = 10^4$	u_x	9.043E-7	9.955E-7	9.956E-7	6.466E-9	6.575E-9	1.374E-8	2.308E-8
	u_y	3.525E-7	6.616E-9	0.00	0.00	-6.593E-11	1.340E-7	1.172E-7
$t = 10^5$	u_x	6.437E-6	6.447E-6	6.410E-6	-2.196E-7	-6.885E-7	-7.732E-8	-8.676E-8
	u_y	-3.381E-7	2.960E-7	0.00	0.00	-2.177E-7	9.636E-7	-5.283E-7
$t = 10^6$	u_x	1.273E-5	1.245E-5	1.236E-5	-7.165E-7	-6.245E-7	-3.455E-7	-3.549E-7
	u_y	-2.202E-6	7.518E-7	0.00	0.00	-6.173E-7	2.249E-6	-1.811E-6
$t = 10^7$	u_x	1.279E-5	1.249E-5	1.240E-5	-7.196E-7	-6.320E-7	-3.495E-7	-3.587E-7
	u_y	-2.244E-6	7.561E-7	0.00	0.00	-6.195E-7	2.243E-6	-1.837E-6

Table A.1.6. DISPLACEMENT COMPONENTS AT MONITORING POINTS 1-41 FOR BMT2 (cont'd)

Time (sec)	Displ. Components (m)	Monitoring Points					
		36	37	38	39	40	41
t = 0	u_x	0.00	0.00	0.00	0.00	0.00	0.00
	u_y	0.00	0.00	0.00	0.00	0.00	0.00
t = 10	u_x	-6.613E-12	-1.159E-11	0.00	0.00	0.00	0.00
	u_y	6.689E-12	0.00	1.306E-11	2.846E-9	2.822E-9	-2.693E-12
$t = 10^2$	u_x	1.247E-10	1.163E-10	0.00	0.00	0.00	0.00
	u_y	3.614E-11	0.00	2.992E-11	1.385E-8	1.377E-8	3.137E-11
$t = 10^3$	u_x	2.275E-9	2.271E-9	0.00	0.00	0.00	0.00
	u_y	3.302E-10	0.00	5.075E-11	4.152E-8	4.008E-8	3.251E-10
$t = 10^4$	u_x	2.812E-8	2.806E-8	0.00	0.00	0.00	0.00
	u_y	4.051E-9	0.00	-3.879E-11	1.330E-7	1.171E-7	3.738E-9
$t = 10^5$	u_x	-1.801E-7	-2.156E-7	0.00	0.00	0.00	0.00
	u_y	2.529E-7	0.00	-3.397E-8	5.694E-7	-1.123E-7	4.523E-8
$t = 10^6$	u_x	-6.210E-7	-7.127E-7	0.00	0.00	0.00	0.00
	u_y	6.533E-7	0.00	-9.322E-8	1.143E-6	-6.833E-7	1.046E-7
$t = 10^7$	u_x	-6.233E-7	-7.150E-7	0.00	0.00	0.00	0.00
	u_y	6.571E-7	0.00	-9.377E-8	1.133E-6	-7.078E-7	1.038E-7

Table A.2.1. UDEC RESULTS FOR NORMAL LOADING INCREMENT #1 CORRESPONDING TO A NORMAL STRESS OF 5.0 MPa FOR TC1

Point	σ_x (MPa)	σ_y (MPa)	σ_{xy} (MPa)	σ_1 (MPa)	σ_2 (MPa)	u_x (m)	u_y (m)
A	-5.37	-5.20	1.06	-6.35	-4.22	1.14E-4	-1.10E-4
B	-5.21	-5.38	1.06	-6.36	-4.23	1.10E-4	-1.14E-4
C	-5.72	-5.64	0.60	-6.28	-5.08	8.54E-5	-9.02E-5
D	-5.65	-5.72	0.60	-6.29	-5.08	9.02E-5	-8.54E-5

Point	σ_n (MPa)	σ_s (MPa)	u_n (μm)	u_s (μm)	b (μm)	e (μm)	P (MPa)	Q (m^3/s)
E	14.32	-0.26	-60.05	8.76	20.87	20.87	0.00	3.055E-7
F	7.26	-0.08	-57.21	5.35	23.72	23.72	1.415E-2	3.055E-7
G	5.19	0.00	-55.26	-0.02	25.67	25.67	2.296E-2	3.055E-7
H	5.99	0.04	-56.14	-3.57	24.79	24.79	3.589E-2	3.055E-7
I	14.26	0.26	-60.03	-8.79	20.88	20.88	5.00E-2	3.055E-7

Table A.2.2. UDEC RESULTS FOR NORMAL LOADING INCREMENT #2 CORRESPONDING TO A NORMAL STRESS OF 15.0 MPa FOR TC1

Point	σ_x (MPa)	σ_y (MPa)	σ_{xy} (MPa)	σ_1 (MPa)	σ_2 (MPa)	u_x (m)	u_y (m)
A	-15.98	-15.48	3.27	-19.01	-12.45	3.22E-4	-3.08E-4
B	-15.51	-15.98	3.26	-19.01	-12.48	3.08E-4	-3.22E-4
C	-17.28	-17.06	1.92	-19.09	-15.25	2.57E-4	-2.72E-4
D	-17.09	-17.28	1.91	-19.10	-15.27	2.72E-4	-2.57E-4

Point	σ_n (MPa)	σ_s (MPa)	u_n (μm)	u_s (μm)	b (μm)	e (μm)	P (MPa)	Q (m^3/s)
E	43.48	-2.04	-62.38	22.71	18.52	18.53	0.00	1.758E-7
F	21.95	-0.61	-61.24	13.44	19.70	19.70	1.315E-2	1.758E-7
G	15.63	0.00	-60.34	-0.01	20.59	20.59	2.271E-2	1.758E-7
H	18.12	0.33	-60.76	-8.90	20.17	20.17	3.685E-2	1.758E-7
I	43.43	2.04	-62.38	-22.74	18.53	18.53	5.00E-2	1.758E-7

Table A.2.3. UDEC RESULTS FOR NORMAL LOADING INCREMENT #3 CORRESPONDING TO A NORMAL STRESS OF 25.0 MPA FOR TC1

Point	σ_x (MPa)	σ_y (MPa)	σ_{xy} (MPa)	σ_1 (MPa)	σ_2 (MPa)	u_x (m)	u_y (m)
A	-26.39	-24.90	5.27	-30.97	-20.32	5.11E-4	-4.96E-4
B	-25.28	-26.37	5.34	-31.19	-20.46	4.94E-4	-5.23E-4
C	-27.98	-27.45	3.77	-31.49	-23.94	4.15E-4	-4.49E-4
D	-26.69	-28.62	3.55	-31.33	-23.98	4.33E-4	-4.21E-4

Point	σ_n (MPa)	σ_s (MPa)	u_n (μm)	u_s (μm)	b (μm)	e (μm)	P (MPa)	Q (m^3/s)
E	67.91	-2.81	-62.82	20.03	18.07	18.07	0.00	1.519E-7
F	35.54	-0.75	-62.14	10.19	18.80	18.80	1.272E-2	1.519E-7
G	26.16	0.18	-61.61	-3.27	19.33	19.33	2.256E-2	1.519E-7
H	30.13	0.75	-61.87	-12.10	19.06	19.06	3.723E-2	1.519E-7
I	69.74	3.91	-62.84	-27.14	18.05	18.05	5.0E-2	1.519E-7

Table A.2.4. UDEC RESULTS FOR NORMAL UNLOADING INCREMENT #4 CORRESPONDING TO A NORMAL STRESS OF 15.0 MPa FOR TC1

Point	σ_x (MPa)	σ_y (MPa)	σ_{xy} (MPa)	σ_1 (MPa)	σ_2 (MPa)	u_x (m)	u_y (m)
A	-17.38	-16.66	3.20	-20.24	-13.80	3.40E-4	-3.43E-4
B	-17.19	-17.52	3.30	-20.66	-14.05	3.33E-4	-3.71E-4
C	-18.35	-21.04	1.50	-21.71	-17.68	2.80E-4	-3.18E-4
D	-19.55	-19.59	1.09	-20.66	-18.48	2.89E-4	-2.92E-4

Point	σ_n (MPa)	σ_s (MPa)	u_n (μm)	u_s (μm)	b (μm)	e (μm)	P (MPa)	Q (m^3/s)
E	50.44	-2.95	-62.50	31.91	18.39	18.39	0.00	1.741E-7
F	23.73	-0.67	-61.32	15.40	19.63	19.63	1.323E-2	1.741E-7
G	15.95	0.32	-60.23	-10.85	20.70	20.70	2.262E-2	1.741E-7
H	19.49	1.01	-60.83	-28.17	20.11	20.11	3.658E-2	1.741E-7
I	53.82	5.33	-62.58	-53.82	18.32	18.32	5.00E-2	1.741E-7

Table A.2.5. UDEC RESULTS FOR NORMAL UNLOADING INCREMENT #5 CORRESPONDING TO A NORMAL STRESS OF 5.0 MPa FOR TC1

Point	σ_x (MPa)	σ_y (MPa)	σ_{xy} (MPa)	σ_1 (MPa)	σ_2 (MPa)	u_x (m)	u_y (m)
A	-7.21	-6.77	1.17	-8.18	-5.80	1.20E-4	-1.70E-4
B	-7.86	-6.90	1.47	-8.93	-5.83	1.26E-4	-1.97E-4
C	-7.01	-11.47	-0.13	-11.47	-7.00	1.16E-4	-1.58E-4
D	-8.99	-8.91	-0.80	-9.75	-8.15	1.10E-4	-1.33E-4

Point	σ_n (MPa)	σ_s (MPa)	u_n (μm)	u_s (μm)	b (μm)	e (μm)	P (MPa)	Q (m^3/s)
E	24.02	-0.48	-61.20	6.60	21.01	21.01	0.00	3.291E-7
F	9.31	0.13	-57.86	-9.71	24.24	24.24	1.473E-2	3.291E-7
G	5.42	0.38	-54.52	-38.04	27.98	27.98	2.244E-2	3.291E-7
H	7.81	0.81	-56.90	-56.65	25.76	25.76	3.396E-2	3.291E-7
I	29.36	4.51	-61.64	-83.14	19.91	19.91	5.00E-2	3.291E-7

Table A.2.6. UDEC RESULTS FOR NORMAL UNLOADING INCREMENT #6 CORRESPONDING TO A NORMAL STRESS OF 0.0 MPa FOR TC1

Point	σ_x (MPa)	σ_y (MPa)	σ_{xy} (MPa)	σ_1 (MPa)	σ_2 (MPa)	u_x (m)	u_y (m)
A	0.00	0.00	0.00	0.00	0.00	-9.75E-5	-7.69E-5
B	0.00	0.00	0.00	0.00	0.00	-9.79E-5	-7.64E-5
C	0.00	0.00	0.00	0.00	0.00	-1.08E-6	8.63E-7
D	0.00	0.00	0.00	0.00	0.00	-1.07E-6	8.53E-7

Point	σ_n (MPa)	σ_s (MPa)	u_n (μm)	u_s (μm)	b (μm)	e (μm)	P (MPa)	Q (m^3/s)
E	0.00	0.00	-22.2	-122.8	62.57	62.57	0.00	0.00
F	0.00	0.00	-23.67	-122.8	59.97	59.97	0.00	0.00
G	0.00	0.00	-23.57	-122.8	59.62	59.62	0.00	0.00
H	0.00	0.00	-23.80	-122.8	60.44	60.44	0.00	0.00
I	0.00	0.00	-20.80	-122.9	63.66	63.66	0.00	0.00

Table A.2.7. UDEC RESULTS FOR SHEAR LOADING INCREMENT #1 CORRESPONDING TO A JOINT SHEAR DISPLACEMENT OF 0.5 MM IN THE FORWARD DIRECTION FOR TC1

Point	σ_x (MPa)	σ_y (MPa)	σ_{xy} (MPa)	σ_1 (MPa)	σ_2 (MPa)	u_x (m)	u_y (m)
A	-10.14	-34.59	8.15	-37.-6	-7.67	-6.28E-4	-6.14E-4
B	-15.75	-43.03	2.57	-43.27	-15.51	-6.25E-4	-6.18E-4
C	-10.99	-36.34	6.36	-37.85	-9.48	-2.23E-4	-2.17E-4
D	-16.57	-44.64	0.96	-44.67	-16.54	-2.28E-4	-2.14E-4

Point	σ_n (MPa)	σ_s (MPa)	u_n (μm)	u_s (μm)	b (μm)	e (μm)	P (MPa)	Q (m^3/s)
E	68.55	34.86	-62.82	-503.6	18.15	18.15	0.00	1.58E-7
F	35.65	18.44	-62.15	-501.2	18.97	18.97	1.289E-2	1.58E-7
G	25.95	13.57	-61.59	-520.0	19.64	19.64	2.275E-2	1.58E-7
H	29.86	15.56	-61.85	-519.0	19.37	19.37	3.728E-2	1.58E-7
I	69.41	35.36	-62.83	-523.7	18.21	18.21	5.00E-2	1.58E-7

Table A.2.8. UDEC RESULTS FOR SHEAR LOADING INCREMENT #2 CORRESPONDING TO A JOINT SHEAR DISPLACEMENT OF 0.8 MM IN THE FORWARD DIRECTION FOR TC1

Point	σ_x (MPa)	σ_y (MPa)	σ_{xy} (MPa)	σ_1 (MPa)	σ_2 (MPa)	u_x (m)	u_y (m)
A	-10.03	-34.52	8.23	-37.03	-7.52	-8.18E-4	-8.03E-4
B	-15.63	-43.13	2.57	-43.37	-15.39	-8.16E-4	-8.06E-4
C	-10.88	-36.26	6.45	-37.81	-9.33	-2.25E-4	-2.17E-4
D	-16.45	-44.72	0.98	-44.75	-16.42	-2.29E-4	-2.15E-4

Point	σ_n (MPa)	σ_s (MPa)	u_n (μm)	u_s (μm)	b (μm)	e (μm)	P (MPa)	Q (m^3/s)
E	68.62	35.09	-62.81	-768.9	18.47	18.47	0.00	1.758E-7
F	35.69	18.64	-62.15	-766.5	19.62	19.62	1.314E-2	1.758E-7
G	25.93	13.69	-61.59	-785.4	20.52	20.52	2.285E-2	1.758E-7
H	29.88	15.71	-61.86	-784.4	20.17	20.17	3.709E-2	1.758E-7
I	69.47	35.54	-62.82	-789.3	18.55	18.55	5.00E-2	1.758E-7

Table A.2.9. UDEC RESULTS FOR SHEAR LOADING INCREMENT #3 CORRESPONDING TO A JOINT SHEAR DISPLACEMENT OF 2.0 MM IN THE FORWARD DIRECTION FOR TC1

Point	σ_x (MPa)	σ_y (MPa)	σ_{xy} (MPa)	σ_1 (MPa)	σ_2 (MPa)	u_x (m)	u_y (m)
A	-10.20	-33.77	8.51	-36.52	-7.45	-1.69E-3	-1.67E-3
B	-15.43	-42.95	2.70	-43.21	-15.17	-1.70E-3	-1.67E-3
C	-11.06	-35.47	6.79	-37.23	-9.30	-2.25E-4	-2.09E-4
D	-16.16	-44.57	1.15	-44.62	-16.11	-2.27E-4	-2.11E-4

Point	σ_n (MPa)	σ_s (MPa)	u_n (μm)	u_s (μm)	b (μm)	e (μm)	P (MPa)	Q (m^3/s)
E	69.01	35.35	-62.78	-2003.0	20.61	20.61	0.00	3.269E-7
F	35.77	18.74	-62.15	-2000.0	24.15	24.15	1.438E-2	3.269E-7
G	25.95	13.75	-61.60	-2019.0	26.47	26.47	2.317E-2	3.269E-7
H	30.04	15.84	-61.87	-2018.0	25.47	25.47	3.59E-2	3.269E-7
I	69.99	35.83	-62.78	-2024.0	2.67	20.67	5.00E-2	3.269E-7

Table A.2.10. UDEC RESULTS FOR SHEAR LOADING INCREMENT #4 CORRESPONDING TO A JOINT SHEAR DISPLACEMENT OF 4.0 MM IN THE FORWARD DIRECTION FOR TC1

Point	σ_x (MPa)	σ_y (MPa)	σ_{xy} (MPa)	σ_1 (MPa)	σ_2 (MPa)	u_x (m)	u_y (m)
A	-10.44	-32.63	8.67	-35.62	-7.45	-3.10E-3	-3.07E-3
B	-15.26	-42.17	2.60	-42.42	-15.01	-3.11E-3	-3.07E-3
C	-11.39	-34.20	7.00	36.18	-9.41	-2.26E-4	-1.91E-4
D	-15.95	-43.77	1.12	-43.82	-15.91	-2.23E-4	1.98-E-4

Point	σ_n (MPa)	σ_s (MPa)	u_n (μm)	u_s (μm)	b (μm)	e (μm)	P (MPa)	Q (m^3/s)
E	71.61	36.54	-62.75	-3993.0	24.28	24.28	0.00	6.29E-7
F	35.68	18.60	-62.15	-3991.0	30.78	30.78	1.342E-2	6.29E-7
G	25.48	13.42	-61.55	-4010.0	31.63	31.63	2.279E-2	6.29E-7
H	29.90	15.67	-61.86	-4009.0	31.20	31.20	3.673E-2	6.29E-7
I	72.69	37.07	-62.75	-4014.0	24.25	24.25	5.00E-2	6.29E-7

Table A.2.11. UDEC RESULTS FOR SHEAR LOADING INCREMENT #5 CORRESPONDING TO A JOINT SHEAR DISPLACEMENT OF 2.0 MM IN THE REVERSE DIRECTION FOR TC1

Point	σ_x (MPa)	σ_y (MPa)	σ_{xy} (MPa)	σ_1 (MPa)	σ_2 (MPa)	u_x (m)	u_y (m)
A	-44.43	-14.78	3.14	-44.76	-14.45	-1.15E-3	-1.14E-3
B	-35.56	-9.95	8.30	-38.01	-7.50	-1.16E-3	-1.13E-3
C	-45.09	-16.55	1.77	-45.20	-16.44	2.27E-4	2.42E-4
D	-35.87	-11.37	6.40	-37.44	-9.80	2.36E-4	2.31E-4

Point	σ_n (MPa)	σ_s (MPa)	u_n (μm)	u_s (μm)	b (μm)	e (μm)	P (MPa)	Q (m^3/s)
E	70.09	-35.66	-62.79	-1980.0	26.78	26.78	0.00	3.875E-7
F	35.45	-18.37	-62.18	-1990.0	32.75	32.75	7.413E-3	3.875E-7
G	25.84	-13.50	-61.61	-1990.0	30.39	30.39	1.989E-2	3.875E-7
H	32.39	-16.82	-60.84	-2003.0	23.23	23.23	3.377E-2	3.875E-7
I	73.84	-37.52	-62.81	-2007.0	20.84	20.84	5.00E-2	3.875E-7

Table A.2.12. UDEC RESULTS FOR SHEAR LOADING INCREMENT #6 CORRESPONDING TO A JOINT SHEAR DISPLACEMENT IN THE REVERSE DIRECTION BACK TO THE INITIAL STARTING LOCATION FOR TC1

Point	σ_x (MPa)	σ_y (MPa)	σ_{xy} (MPa)	σ_1 (MPa)	σ_2 (MPa)	u_x (m)	u_y (m)
A	-44.93	-15.72	2.83	-45.20	-15.45	2.47E-4	2.56E-4
B	-36.71	-9.91	8.68	-39.28	-7.34	2.41E-4	2.58E-4
C	-45.42	-17.69	1.23	-45.47	-17.64	2.39E-4	2.31E-4
D	-36.89	-11.50	6.74	-38.57	-9.82	2.44E-4	2.24E-4

Point	σ_n (MPa)	σ_s (MPa)	u_n (μm)	u_s (μm)	b (μm)	e (μm)	P (MPa)	Q (m^3/s)
E	67.37	-34.23	-62.81	-20.87	38.00	38.00	0.00	8.956E-7
F	36.18	-18.66	-62.21	-27.96	42.65	42.65	6.453E-3	8.956E-7
G	24.73	-12.87	-61.46	-24.54	31.72	31.72	2.011E-2	8.956E-7
H	33.06	-17.08	-60.89	-39.25	30.95	30.95	3.978E-2	8.956E-7
I	70.95	-36.00	-62.82	-48.57	31.36	31.26	5.0E-2	8.956E-7

APPENDIX B: UDEC INPUT FILES FOR THE BMT2 AND TC1 PROBLEMS

B.1 INPUT FILE FOR MULTIPLE FRACTURE MODEL, BMT2

```
set log on
set plot po
start
* Bench Mark Test #2 - AECL
head
BMT #2 - Multiple Fracture Model - DECOVALEX
thermal
* Input block and joint geometry
round 0.0001
bl 0.0,0.0 0.0,0.5 0.75,0.5 0.75,0.0
split 0.0,0.45 0.75,0.45
split 0.0,0.05 0.75,0.05
split 0.3,0.0 0.3,0.5
split 0.6,0.0 0.6,0.5
* Generate fully-deformable triangular elements within blocks
gen 0.0,0.75 0.0,0.50 edge = 0.07
* apply boundary stresses for initial mechanical state
insitu stress -4.0, 0.0, -4.0 nodis
insitu -0.01,0.76  0.045,0.055 stress -3.99, 0.0, -3.99 nodis
insitu -0.01,0.76  0.445,0.455 stress -3.99, 0.0, -3.99 nodis
insitu  0.29,0.31 -0.010,0.510 stress -3.99, 0.0, -3.99 nodis
insitu  0.59,0.61 -0.010,0.510 stress -3.99, 0.0, -3.99 nodis
damp auto
* define mechanical and thermal properties for matrix and joints
prop mat=1 k=3.333e+04 g=2.0e+04 d=.0026
prop mat=1 cond=3.34 thexp=1.0E-05 spec=9.0E+08
prop jmat=1 jkn=1.03E+04 jks=2.43E+03 jfric=0.5774 jdil=0.0 azero=3.0E-4 &
  ares=7.0E-5 jperm=7.412E7
* replace mechanical boundaries with rollers and and apply hydr. boundaries
bound  0.74,0.76 -0.01,0.51  xvel = 0.0  pp = 0.011  pgrad = 0.0
bound -0.01,0.76  0.49,0.51  yvel = 0.0  imperm
bound -0.01,0.01 -0.01,0.51  xvel = 0.0  pp = 0.010  pgrad = 0.0
bound -0.01,0.76 -0.01,0.01  yvel = 0.0  imperm
* initialize domain pressures to 0.010 MPa (10 KPa)
pfix -0.1,0.76 -0.1,0.51 pressure 0.01
prop mat=1 jfric=0.0
cycle 500
prop mat=1 jfric=0.5774
* define fluid properties
fluid dens=0.001 bulk=2000.0
pfree 0
set ptol 0.00001
set sflow on
set capratio=200
* cycle until steady state flow is reached before applying thermal load
cycle 2500
pr domain
pr con
pr max
pr flow
save bmt2a.sav
* reset time as well as joint and block displacements and rotations to zero
reset disp jdisp time rota
* Define thermal boundary and initial conditions
hist ncyc=25
initem 15.0 -0.01,0.76 -0.01,0.51
tfix 15.0 0.74,0.76 -0.01,0.51
thapp -0.01,0.01  0.0495,0.25 flux 60.0 0.0
* Define history locations for normal stresses near midpoints of blocks
hist sxx 0.15,0.475 syy 0.15,0.475 sxx 0.15,0.25 syy 0.15,0.25 &
```

```
 sxx 0.15,0.025 syy 0.15,0.025 sxx 0.45,0.475 syy 0.45,0.475 &
 sxx 0.45,0.25 syy 0.45,0.25 sxx 0.45,0.025 syy 0.45,0.025 sxx 0.675,0.475 &
 syy 0.675,0.475 sxx 0.675,0.25 syy 0.675,0.25 sxx 0.675,0.025 &
 syy 0.675,0.025
* Define history addresses for domain fluid pressures in joints
hist add 9546 4  add 16427 4  add 10979 4  add 16609 4  add 1162 4 &
  add 1862 4  add 986 4  add 1686 4  add 672 4 add 1381 4 add 767 4 &
  add 1467 4
* monitor temperatures at selected points
thist tem 0.0,0.05 tem 0.0,0.45 tem 0.3,0.0 tem 0.3,0.05 tem 0.3,0.45 &
 tem 0.3,0.50 tem 0.6,0.0 tem 0.6,0.05 tem 0.6,0.45 tem 0.6,0.50      &
 tem 0.75,0.05 tem 0.75,0.45  tem 0.0,0.15 type=1 ntcyc=50
thist tem 0.15,0.475 tem 0.15,0.25 tem 0.15,0.025 tem 0.45,0.475   &
 tem 0.45,0.25 tem 0.45,0.025 tem 0.675,0.475 tem 0.675,0.25      &
 tem 0.675,0.025
run age=10.0 delt=0.01 step=1000000 tol=0.005
reset damp
cycle 2000
pr dom
pr con
pr flow
pr grid dis
pr grid tem
save bmt2b.sav
run age=1.0e2 delt=0.1 step=1000000 tol=0.005
reset damp
cycle 2000
pr dom
pr con
pr flow
pr grid disp
pr grid tem
save bmt2c.sav
run age=1.0e3 delt=1.0 step=1000000 tol=0.005
reset damp
cycle 2000
pr dom
pr con
pr flow
pr grid disp
pr grid tem
save bmt2d.sav
run age=1.0e4 delt=5.0 step=1000000 tol=0.005
reset damp
cycle 2000
pr dom
pr con
pr flow
pr grid disp
pr grid tem
save bmt2e.sav
run age=1.0e5 delt=9.0 step=1000000 tol=0.005
reset damp
cycle 2000
pr dom
pr con
pr flow
pr grid disp
pr grid tem
save bmt2f.sav
```

```
run age=1.0e6 delt=500.0 step=1000000 impl tol=0.005
reset damp
cycle 2000
pr dom
pr con
pr flow
pr grid disp
pr grid tem
save bmt2g.sav
run age=1.0e7 delt=500.0 step=1000000 impl tol=0.005
reset damp
cycle 2000
pr dom
pr con
pr flow
pr grid disp
pr grid tem
save bmt2h.sav
stop
end
```

B.2 INPUT FILE FOR COUPLED STRESS-FLOW MODEL, TC1

```
*set log on
set plot po
start
head
* DECOVALEX Test Case 1 - Coupled Stress Flow Test
round 0.003
set ovtol 0.01
* plane stress problem
set p-stress
bl 0.0,0.0 0.0,0.26 0.26,0.26 0.26,0.0
split 0.01,0.0 0.01,0.26
split 0.0,0.01 0.26,0.01
split 0.25,0.0 0.25,0.26
split 0.0,0.25 0.26,0.25
*
split 0.01,0.02 0.02,0.01
split 0.01,0.24 0.02 0.25
split 0.24,0.01 0.25,0.02
split 0.24,0.25 0.25,0.24
*
split 0.0,0.02 0.01,0.02
split 0.02,0.0 0.02,0.01
split 0.24,0.0,0.24,0.01
split 0.25,0.02 0.26,0.02
split 0.0,0.24 0.01,0.24
split 0.02,0.25 0.02,0.26
split 0.24,0.25 0.24,0.26
split 0.25,0.24 0.26,0.24
*
del area=0.002
* create joint surface
split 0.0,0.0 0.26,0.26
* create top rock block
crack 0.06282,0.06282 0.03177,0.11662
crack 0.03177,0.11662 0.14339,0.22824
crack 0.14339,0.22824 0.19718,0.19718
* create bottom rock block
crack 0.06282,0.06282 0.11662,0.03177
crack 0.11662,0.03177 0.22824,0.14339
crack 0.22824,0.14339 0.19718,0.19718
* generate fully deformable zones
gen 0.10,0.12 0.14,0.16 quad 0.015 * upper rock block
gen 0.14,0.16 0.10,0.12 quad 0.015 * lower rock block
gen 0.00,0.01 0.12,0.14 edge 0.02  * steel
gen 0.12,0.14 0.00,0.01 edge 0.02
gen 0.25,0.26 0.12,0.14 edge 0.02
gen 0.12,0.14 0.25,0.26 edge 0.02
gen 0.07,0.09 0.17,0.19 edge 0.03  * upper epoxy block
gen 0.17,0.19 0.07,0.09 edge 0.03  * lower epoxy block
* define material property 1 (steel)
change 0.00,0.01 0.12,0.14 mat=1
change 0.12,0.14 0.00,0.01 mat=1
change 0.25,0.26 0.12,0.14 mat=1
change 0.12,0.14 0.25,0.26 mat=1
* define material property 2 (epoxy)
change 0.07,0.09 0.17,0.19 mat=2 * upper half
change 0.17,0.19 0.07,0.09 mat=2 * lower half
* define material property 3 (rock)
change 0.10,0.12 0.14,0.16 mat=3 * upper half
change 0.14,0.16 0.10,0.12 mat=3 * lower half
```

```
*define elastic properties for materials 1-3
prop mat=1 k=1.449e5 g=7.874e4 dens=0.007            * steel
prop mat=2 k=8.333e3 g=3.846e3 dens=0.00225          * epoxy
prop mat=3 k=3.667e4 g=2.20e4 dens=0.0026            * rock
* define interface joint properties change jcon=2
change int 3 3 jmat=1 jcon=7    * rock-rock
change int 2 3 jmat=2           * rock-epoxy (No deformation - no flow)
change int 1 2 jmat=3           * steel-epoxy (No flow)
change int 2 2 jmat=4           * epoxy-epoxy (No flow)
* Barton-Bandis model assumed for rock joint interface (jmat=1)
prop jmat=1 jkn=5.0e5 jks=15.8e3 JRCo=1.95212 JCSo=156.207 jperm=8.333e7 &
 Ln=0.20 Lo=0.10 Phir=26.5 sig=240
prop jmat=2 jkn=1.0e6 jks=1.0e6 jc=100.0 jf=10.0 jperm=0.0
* joint normal stiffness on steel/epoxy interface increased from 1.e3 to 1.e5
prop jmat=3 jkn=1.0e5 jks=1.0e3 jc=0.0 jf=0.1763 jperm=0.0
* joint normal stiffness on epoxy/epoxy interface increased from 1e2 to 1e4
prop jmat=4 jkn=1.0e4 jks=1.0e2 jc=0.0 jf=0.0175 jperm=0.0
* define properties for newly formed contacts (jmat=10)
prop jmat=10 jkn=1.e4 jks=1.e3 jperm=8.333e7 ares=8.e-5 azero=8.e-5
*
damp auto
mscale on
*
* apply roller boundary conditions to bottom and right sides
bound  0.259,0.261 -0.001,0.261 xvel=0.0
bound -0.001,0.261 -0.001,0.001 yvel=0.0
*
* Sequence A - apply normal load to 25.0 MPa in increments of 5.0 MPa
*
bound -0.001,0.001 -0.001,0.261 stress -5.0 0.0 -5.0
bound -0.001,0.261  0.259,0.261 stress -5.0 0.0 -5.0
* stress and displacement history at points A-D
hist sxx 0.07343,0.13 syy 0.07343,0.13 sxy 0.07343,0.13 xdis 0.07343,0.13 &
 ydis 0.07343,0.13
hist  sxx 0.13,0.18656 syy 0.13,0.18656 sxy 0.13,0.18656 xdis 0.13,0.18656 &
  ydis 0.13,0.18656
hist sxx 0.18656,0.13 syy 0.18656,0.13 sxy 0.18656,0.13 &
  xdis 0.18656,0.13 ydis 0.18656,0.13
hist sxx 0.13,0.07343 syy 0.13,0.07343 &
  sxy 0.13,0.07343 xdis 0.13,0.07343 ydis 0.13,0.07343
* monitor fluid pressures at points F, G, and H  along the rock joint
hist add 2757 4 add 471 4 add 1206 4
* monitor normal stresses & disp, aperature, and flow rates at pts E-I
hist nstr 345 nstr 2444 nstr 2045 nstr 2691 nstr 388
hist ndis 345 ndis 2444 ndis 2045 ndis 2691 ndis 388
hist sstr 345 sstr 2444 sstr 2045 sstr 2691 sstr 388
hist sdis 345 sdis 2444 sdis 2045 sdis 2691 sdis 388
hist add 345 20 add 2444 20 add 2045 20 add 2691 20 add 388 20
hist add 345 21 add 2444 21 add 2045 21 add 2691 21 add 388 21 ncyc 100
set ptol 0.00001
set capratio=8
set delc off
set jmatdf=10 jcondf=2
*cycle 4000
* define fluid properties
fluid dens=0.001 bulk=2000.0
set sflow on
pfix 0.0,0.0628 0.0,0.26 press 0.0
pfix 0.197,0.26 0.0,0.26 press 0.0
pfix  reg 0.00,-0.001 0.26,0.259 0.26,-0.001 0.01,-0.001 press 0.0
```

```
pfix  reg 0.00,0.001 0.0,0.261 0.01,0.261 0.26,0.261 press 0.0
pfix dom 3080 pressure 0.0
pfix dom 818 pressure 0.05
reset damp
cycle 5000
save tc315.sav
bound -0.001,0.001 -0.001,0.261 stress -5.0 0.0 -5.0
bound -0.001,0.261  0.259,0.261 stress -5.0 0.0 -5.0
reset damp
cycle 5000
save tc3110.sav
bound -0.001,0.001 -0.001,0.261 stress -5.0 0.0 -5.0
bound -0.001,0.261  0.259,0.261 stress -5.0 0.0 -5.0
reset damp
cycle 5000
save tc3115.sav
bound -0.001,0.001 -0.001,0.261 stress -5.0 0.0 -5.0
bound -0.001,0.261  0.259,0.261 stress -5.0 0.0 -5.0
reset damp
cycle 5000
save tc3120.sav
bound -0.001,0.001 -0.001,0.261 stress -5.0 0.0 -5.0
bound -0.001,0.261  0.259,0.261 stress -5.0 0.0 -5.0
reset damp
cycle 5000
save tc3125.sav
*
* Unload sample from 25 Mpa to 0. in increments of 5.0 MPa
*
* IMPORTANT !!!!!!!! must set jhist on for reversal
jhist on 0.01
bound -0.001,0.001 -0.001,0.261 stress 5.0 0.0 5.0
bound -0.001,0.261  0.259,0.261 stress 5.0 0.0 5.0
reset damp
cycle 5000
save tc3u20.sav
bound -0.001,0.001 -0.001,0.261 stress 5.0 0.0 5.0
bound -0.001,0.261  0.259,0.261 stress 5.0 0.0 5.0
reset damp
cycle 5000
save tc3u15.sav
bound -0.001,0.001 -0.001,0.261 stress 5.0 0.0 5.0
bound -0.001,0.261  0.259,0.261 stress 5.0 0.0 5.0
reset damp
cycle 5000
save tc3u10.sav
bound -0.001,0.001 -0.001,0.261 stress 5.0 0.0 5.0
bound -0.001,0.261  0.259,0.261 stress 5.0 0.0 5.0
reset damp
cycle 5000
save tc3u5.sav
bound cor 3001 3566 xfree yfree
bound cor 3743 3881 xfree yfree
reset damp
cycle 1000
pfix press 0
reset damp
cycle 1000
bound cor 3001 3566 stress -1.e-3 0 -1.e-3
bound cor 3743 3881 stress -1.e-3 0 -1.e-3
```

```
reset damp
cycle 1000
save tc3u0.sav
return
*
* Sequence B - Begin shearing top block downward 4.0 mm and then back to zero
*
res tc3125.sav
reset time damp disp jdis rot hist
* monitor stresses and displacements at points A-D within the rock
hist sxx 0.07343,0.13 syy 0.07343,0.13 sxy 0.07343,0.13 xdis 0.07343,0.13 &
 ydis 0.07343,0.13
hist sxx 0.13,0.18656 syy 0.13,0.18656 sxy 0.13,0.18656 &
 xdis 0.13,0.18656  ydis 0.13,0.18656
hist sxx 0.18656,0.13 syy 0.18656,0.13 sxy 0.18656,0.13 &
 xdis 0.18656,0.13 ydis 0.18656,0.13
hist sxx 0.13,0.07343 syy 0.13,0.07343 &
 sxy 0.13,0.07343 xdis 0.13,0.07343 ydis 0.13,0.07343
* monitor fluid pressures at points F, G, and H  along the rock joint
hist add 2757 4 add 471 4 add 1206 4
* monitor normal stresses & disp, aperature, and flow rates at pts E-I
hist nstr 345 nstr 2444 nstr 2045 nstr 2691 nstr 388
hist ndis 345 ndis 2444 ndis 2045 ndis 2691 ndis 388
hist sstr 345 sstr 2444 sstr 2045 sstr 2691 sstr 388
hist sdis 345 sdis 2444 sdis 2045 sdis 2691 sdis 388
hist add 345 20 add 2444 20 add 2045 20 add 2691 20 add 388 20
hist add 345 21 add 2444 21 add 2045 21 add 2691 21 add 388 21 ncyc 100
set ptol 0.00001
***  shear top block to 0.5 mm
bound cor 3001 3566 xvel=-3.56e-2 yvel=-3.5e-2
bound cor 3743 3881 xvel=-3.56e-2 yvel=-3.5e-2
reset damp
cycle time=0.0237
bound cor 3001 3566 xvel=0.0 yvel=0.0
bound cor 3743 3881 xvel=0.0 yvel=0.0
reset damp
cycle 1000
save tc3s05.sav
***  shear top block to 0.8 mm
bound cor 3001 3566 xvel=-3.56e-2 yvel=-3.5e-2
bound cor 3743 3881 xvel=-3.56e-2 yvel=-3.5e-2
reset damp
cycle time=0.0054
bound cor 3001 3566 xvel=0.0 yvel=0.0
bound cor 3743 3881 xvel=0.0 yvel=0.0
reset damp
cycle 1000
save tc3s08.sav
***  shear top block to 2.0 mm
bound cor 3001 3566 xvel=-3.56e-2 yvel=-3.5e-2
bound cor 3743 3881 xvel=-3.56e-2 yvel=-3.5e-2
reset damp
cycle time=0.0246
bound cor 3001 3566 xvel=0.0 yvel=0.0
bound cor 3743 3881 xvel=0.0 yvel=0.0
reset damp
cycle 1000
save tc3s2.sav
***  shear top block to 4.0 mm
bound cor 3001 3566 xvel=-3.56e-2 yvel=-3.5e-2
```

```
bound cor 3743 3881 xvel=-3.56e-2 yvel=-3.5e-2
reset damp
cycle time=0.0395
bound cor 3001 3566 xvel=0.0 yvel=0.0
bound cor 3743 3881 xvel=0.0 yvel=0.0
reset damp
cycle 1000
save tc3s4.sav
*
*  Shear top block in reverse direction 2.0 mm
*
jhist on 0.01
bound cor 3001 3566 xvel=3.56e-2 yvel=3.5e-2
bound cor 3743 3881 xvel=3.56e-2 yvel=3.5e-2
reset damp
cycle time=0.0673
bound cor 3001 3566 xvel=0.0 yvel=0.0
bound cor 3743 3881 xvel=0.0 yvel=0.0
reset damp
cycle 1000
save tc3r2.sav
***  shear top block in reverse direction to 0 mm
bound cor 3001 3566 xvel=3.56e-2 yvel=3.5e-2
bound cor 3743 3881 xvel=3.56e-2 yvel=3.5e-2
reset damp
cycle time=0.0395
bound cor 3001 3566 xvel=0.0 yvel=0.0
bound cor 3743 3881 xvel=0.0 yvel=0.0
reset damp
cycle 1000
save tc3r0.sav
return
```